CYCLIC CREEP AND RECOVERY BEHAVIOR OF NEXTEL™ 720/ALUMINA CERAMIC MATRIX COMPOSITE AT 1200°C IN AIR AND IN STEAM ENVIRONMENTS

THESIS

Bridgett A. Whiting, 2nd Lieutenant, USAF

AFIT/GAE/ENY/07-S05

DEPARTMENT OF THE AIR FORCE
AIR UNIVERSITY

AIR FORCE INSTITUTE OF TECHNOLOGY

Wright-Patterson Air Force Base, Ohio

The views expressed in this thesis are those of the author and do not reflect the official

policy or position of the United States Air Force, Department of Defense, or the United

States Government.

AFIT/GAE/ENY/07-S05

CYCLIC CREEP AND RECOVERY BEHAVIOR OF NEXTEL™ 720/ALUMINA CERAMIC MATRIX COMPOSITE AT 1200°C IN AIR AND IN STEAM ENVIRONMENT

THESIS

Presented to the Faculty

Department of Aeronautics and Astronautics

Graduate School of Engineering and Management

Air Force Institute of Technology

Air University

Air Education and Training Command

In Partial Fulfillment of the Requirements for the

Degree of Master of Science in Aeronautical Engineering

Bridgett A. Whiting, BS

2nd Lieutenant, USAF

September 2007

CYCLIC CREEP AND RECOVERY BEHAVIOR OF NEXTEL™ 720/ALUMINA

CERAMIC MATRIX COMPOSITE AT 1200°C IN AIR AND IN STEAM

ENVIRONMENTS

Bridgett A. Whiting, BS

2nd Lieutenant, USAF

Approved:

____//Signed//_____   _____
Dr. Marina Ruggles-Wrenn (Chairman)   date

____//Signed//_____   _____
Dr. Robert Canfield (Member)   date

____//Signed//_____   _____
Dr. Geoff Fair (Member)   date

Abstract

The cyclic creep and recovery behaviors of the $N720/Al_2O_3$ composite were investigated in this research. The ceramic matrix composite (CMC) contains a porous alumina matrix with laminated, woven mullite/alumina (Nextel[TM] 720) fibers. The composite does not have an interface between the fiber and matrix. The CMC relies on the porous nature for flaw tolerance.

The objective is to study the behaviors of monotonic creep and cyclic creep loading histories on the creep lifetime, creep strain rate, accumulated creep strain as well as on the recovery of creep strain at near zero stress. The cyclic creep and recovery tests were performed at 1200 °C with maximum creep stress levels of 100 and 125 MPa in air and in steam. The creep and recovery periods ranged from 3 min to 30 h.

The laboratory air tests significantly exceeded the life of the monotonic creep tests. Introduction of intermittent periods of unloading and recovery at near zero stress into the monotonic creep history resulted in one to two orders of magnitude improvement in the creep life and rate. The presence of steam greatly reduced the performance of the material. The results in steam were similar to those of the monotonic creep. The composite microstructure, damage and failure mechanisms were also explored.

Acknowledgments

I like to give my sincere appreciation to all of those people who made this thesis possible: Dr. Marina Ruggles-Wrenn, my advisor, whose knowledge and guidance helped me through;   Mr. Sean Miller and Mr. Barry Page, whose technical support ensured equipment was operating at its best; Mr. Jan LeValley and staff at the AFIT model fabrication shop, whose prompt and quality work allowed the specimens to be manufactured quickly so tests could begin; Dr. Ruth Sikorski and Dr. Charles Cross, whose sponsorship made this thesis possible; Dr. Robert Canfield and Dr. Geoff Fair for being a member of my board and feedback; Lt Amanda Devuono and Lt Stephen Koether for all their support and friendship; and finally, my family that gave constant support. Thank you everyone.

Bridgett A. Whiting

Table of Contents

List of Figures

List of Tables

CYCLIC CREEP AND RECOVERY BEHAVIOR OF NEXTEL™ 720/ALUMINA

CERAMIC MATRIX COMPOSITE AT 1200°C IN AIR AND IN STEAM

ENVIRONMENTS

I.   Introduction

Man for centuries has used one form or another of a composite material, from clay and straw to make strong bricks to reinforced cement.   Composites today are everyday items.   As technology advances so does the need for composites for advanced materials.

Aerospace has taken advantage of composites. Composites provide strength without the cost of weight. Other advantages include more aerodynamic forms, resistance to acoustic environment, crash resistance and improved stealth qualities [4].   The Lockheed Martin F-22 Raptor is comprised by weight of 24% composite materials [1]. While the brand new commercial Boeing 787 Dreamliner, has as much as 50% of the main structure constructed out of composites [2]. Rockets and the underside of reentry vehicles also make use of composites.

The knowledge of the turbine engine is forever expanding, but the greatest limitations are the physical qualities of the components. To get the most out of the engine, an engineer requires high temperatures but is limited to what the turbine materials can withstand.   Developing a composite that is stronger and can operate at higher temperatures than the metal alloy predecessors, allows advancements in the engine design.

The environment within the turbine engine is extremely harsh. Ceramic Matrix Composites (CMC) are the latest material type being studied that have the most potential of withstanding the environment. However, many CMCs experience oxidation that in turn leads to the strength degradation. The introduction of an all alumina (Al_2O_3) matrix reduced the effects of the oxidation. With oxidation reduced other problems still exist for the CMC such as creep and compressive strength.

A CMC with a new 3D fiber architecture was developed, which employs woven Nextel 610 fibers and Z-pin reinforcement placed through the thickness. The Z-pins added a third dimension to the strength to the woven material. The initial objective of this effort was to investigate the compressive strength of the Nextel 610/A CMC with Z-pins. However, results of a few preliminary tests revealed that the virgin specimens exhibited delamination, which rendered them useless. Material processing has to be significantly improved before that CMC would be ready for mechanically testing.

At this point the thesis objective shifted to an investigation of cyclic creep and recovery behavior of Nextel 720/A CMC at 1200° C. The Nextel 720/A CMCs have been extensively investigated in previous research at AFIT. Harlan [14; 33] investigated the creep responses at 1200° C and 1300° C in air and in steam, while Mehrman [25; 26] reported on the effect of hold times at maximum stress on the cyclic behavior. The goal of this effort is to determine if recovery at near zero stress was possible in a porous matrix CMC, and if so, would it serve to extend the creep lifetime. Knowing, that if a material is allowed time to recover at zero or near zero stress the service, life would be extended and could be directly useful in designing structural components with this

material. Furthermore, microstructural deformational failure mechanisms present in air and in steam environments are explored.

II. Background

2.1 Ceramic Matrix Composites

A composite is a material that is made up of a continuous and discontinuous phases.   By combining the two separate phases different mechanical properties can be obtained according to the objective. The matrix is the continuous portion, while the dispersed portion is usually known as reinforcement.   An everyday example of a composite is reinforced concrete. The mixture of sand and rock is the matrix while the steel bars within the mixture are the reinforcement.   The combination of the two, enhances the strengths of each component. In a composite material there are three forms the reinforcements: particles, whiskers or fibers. The fibers can be short, continuous, in a sheet, or woven. [6].
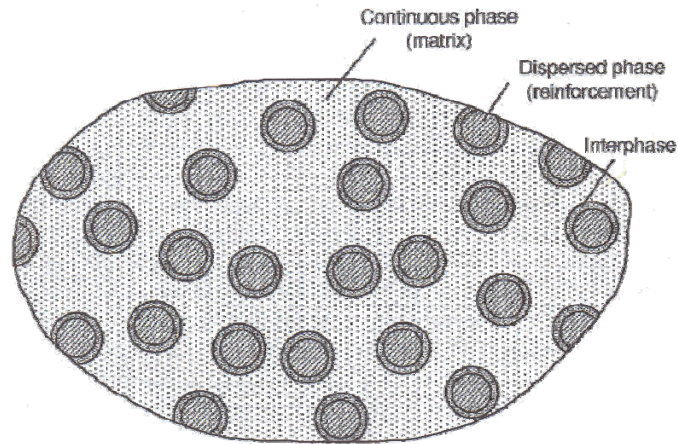
Figure 1. Different Phases of a Composite [8].

It is common practice to classify the composite by the type of matrix it is made up of. For instance, a composite with a polymer matrix is a polymer matrix composite (PMC) while a composite with a ceramic matrix is a ceramic matrix composite (CMC).

Ceramic matrix composites are the most recent addition to the composite family. A ceramic is commonly referred to as a non-metallic, inorganic material which is processed at high temperatures [6, 2]. Common types of ceramic matrix materials being studied are alumina, silicon nitride and silicon carbide. CMCs are designed to withstand higher temperatures than their metallic or polymer counterparts as seen in Figure 2.
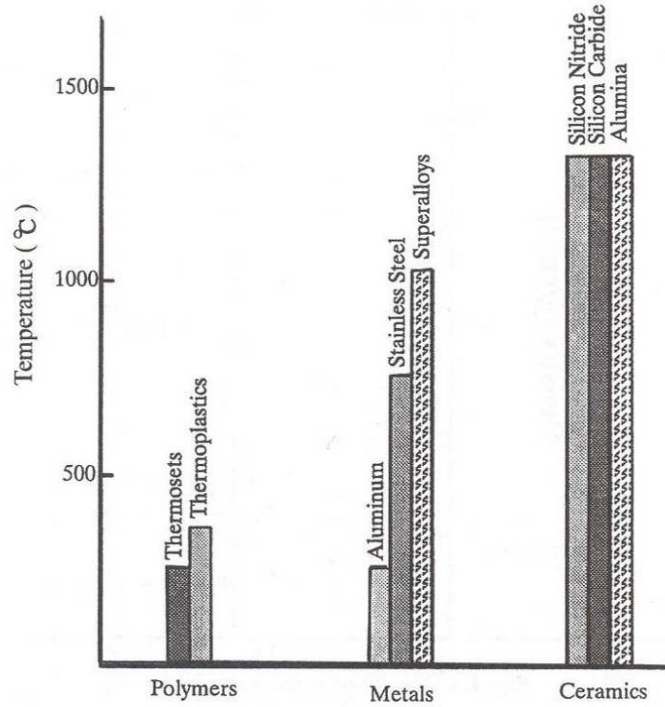
Figure 2. Comparison of types of composites and their max service temperatures [6,5].

The temperatures seen within a turbine engine are around 1400° C. CMCs are the only composite today that has the potential to withstand those temperatures with reduced cooling, making them the most sought after type of composite for this application.

2.1.1 Fiber Matrix Interface

The ceramic matrix is designed to carry the load, separate the fibers to prevent correlated failure of adjacent fibers and provide protection from the environment. The matrix material is designed for high temperatures, but it is brittle and exhibits low damage tolerance and low overall toughness.

The addition of fibers to the ceramic matrix increases the toughness of the composite. The fibers provide the strength and stiffness required and can maintain these attributes at high temperatures. Two categories of ceramic fibers exist: non-oxide and oxide. Common non-oxide fibers are silicon nitride or silicon carbide, while oxide fibers are alumina or silica-based. A CMC is classified as non-oxide if at least one of its constituents is a non-oxide material.

Studies have found that non-oxide CMCs have exceptional strength and superior performance at high temperatures, but when exposed to oxidation their performance degrades rapidly [13]. One way to counter the oxidation problems is to limit the temperature to below critical when oxidation degradation becomes a concern. However, this would greatly reduce the range of useful temperatures of the non-oxide composite.

Oxide CMCs on the other hand have proven to withstand oxidation, but do not exhibit the strength characteristics of the non-oxide CMCs. In the mid 1990s two oxide fibers, namely Nextel 610 and Nextel 720 were developed to compete with the non-oxide covalently bonded SiC fibers [37]. The Nextel 610 has a tensile strength of 1500 MPa at room temperature, while a single fiber of Nextel 720 possess a tensile strength of at least 1450 MPa at 1200 °C [38].

To exhibit damage tolerance a ceramic composite requires a weak interface between matrix and fibers. When a composite contains a strong fiber-matrix interface a strong bond exists between fibers and matrix. This causes a single crack front to propagate through both fibers and matrix, resulting in catastrophic failure. Such material exhibits low damage tolerance. In contrast, CMCs with a weak fiber-matrix interface allow the matrix cracks to be deflected around the fibers, thereby allowing fiber pull-out and "graceful" failure of the material.
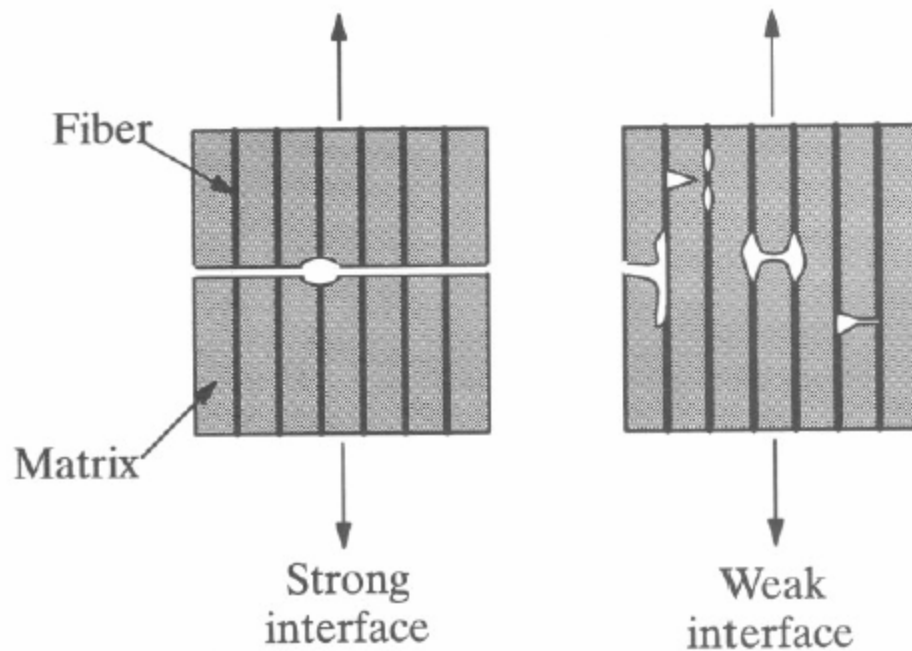
Figure 3. Damage in ceramic composites with propagation of strong and weak fiber-matrix interface [6:148].

In the case of a CMC with a weak fiber-matrix interface, failure proceeds in three stages. In the first stage, the matrix carries most of the load of the CMC exhibits linear stress-strain behaviors. As matrix weakens through microcracking in the second stage, the slope of the stress-strain curve decreases. As the microcracks coalesce the load is transferred from the matrix to the fibers. When the matrix microcracking becomes

saturated in the third stage, the load is carried mainly by the fibers. Finally, when the fibers fail, the specimen fails. The Figure 4 shows a typical stress-strain curve for a CMC with a weak fiber-matrix interface.
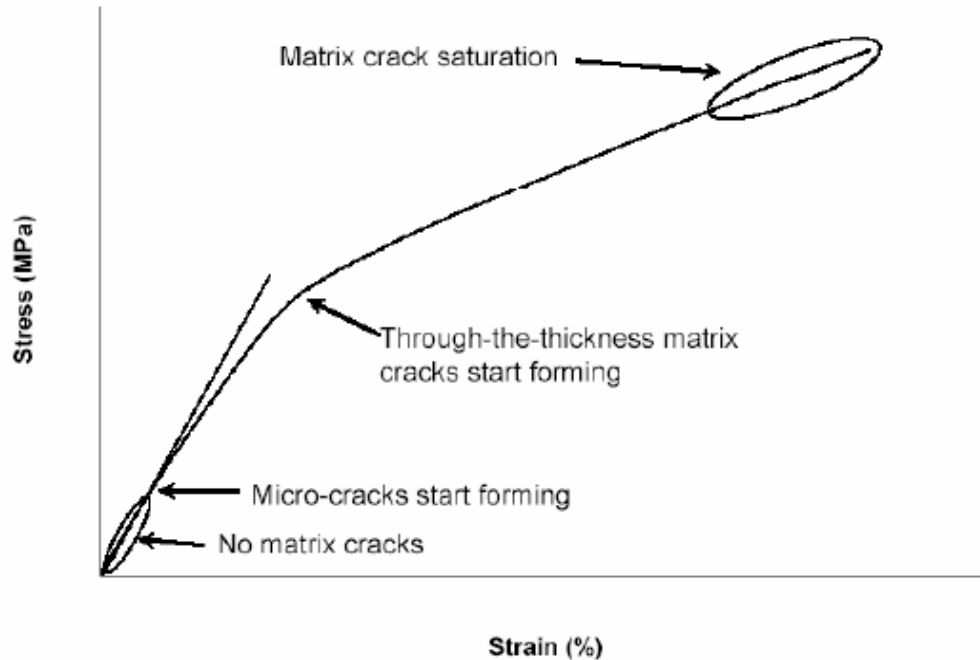
Figure 4. Typical stress-strain curve for a CMC with a weak fiber-matrix interface [42]

Recently it has been demonstrated that the desired damage tolerant behavior can be achieved by using a ceramic matrix with a finely distributed porosity [23; 35]. A porous matrix allows matrix cracks to be deflected around the fibers. The matrix porosity is controlled to maintain a balance between a low toughness for crack deflection and sufficient strength for off-axis and interlaminar properties [24]. The use of porous matrix provides for energy dissipation, as seen in crack deflection subsequent fiber pullout [6: 148].

The CMC with the weak fiber-matrix interface and porous matrix exhibit different failure mechanisms. A weak interface slowly transfers a crack along a front line, while

allowing fibers to slide. On the other hand a porous matrix diverts cracks around fibers allowing extensive cracking matrix before the load is transferred to the fibers, as seen in Figure 5. It should be also noted that tensile stress-strain behavior of a porous matrix CMC remains mainly linear to failure [15].

(a) Conventional (Weak Interface) Concept

(b) Porous Matrix Concept
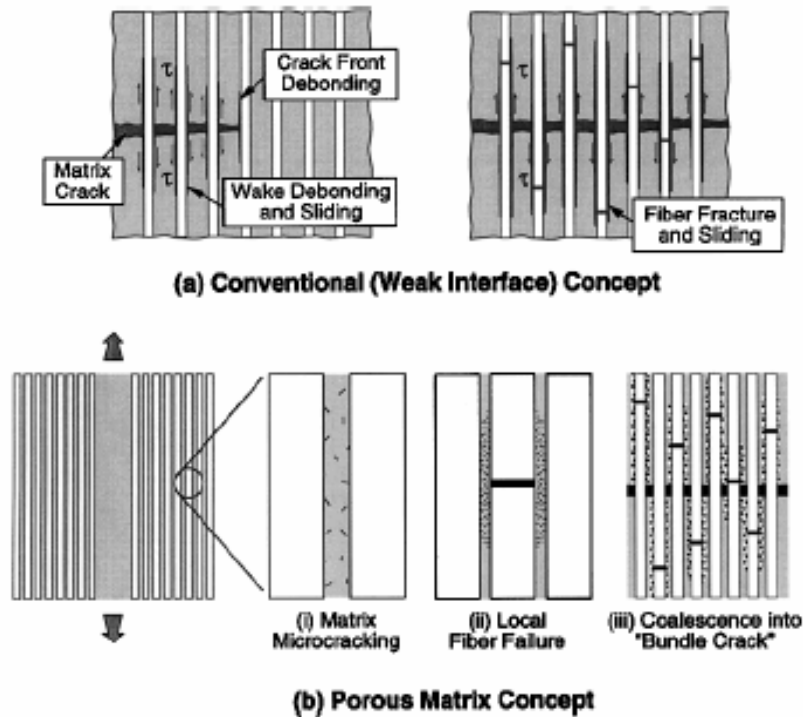
Figure 5. Damage Propagation a) Weak Interface b) Porous Matrix [15].

Determining the optimum matrix porosity has been the subject of the processing science and research. To-date a porosity of about 35-40%, result in a fracture surface dominated by fiber pullout, which represents high fracture toughness. This indicates that the fibers are breaking in different places and that the matrix is allowing the fibers to slide. A denser matrix would result in a fracture surface dominated coordinated fiber failure, reflecting low damage tolerance and low toughness [42].

2.2 Application of CMCs

As mentioned in Section 1 CMCs are prime candidate materials to be used in turbine engine components. Currently, the engine design philosophy is limited by the physical qualities of the components.   The use of CMCs instead of metallic superalloys increases the operating temperature range of an engine. The current goal is to develop a material that can withstand 1400° C without cooling [31].   The graph in Figure 6 demonstrates the need for high temperature materials to allow the engine to operate at higher levels of efficiency as the years progress.
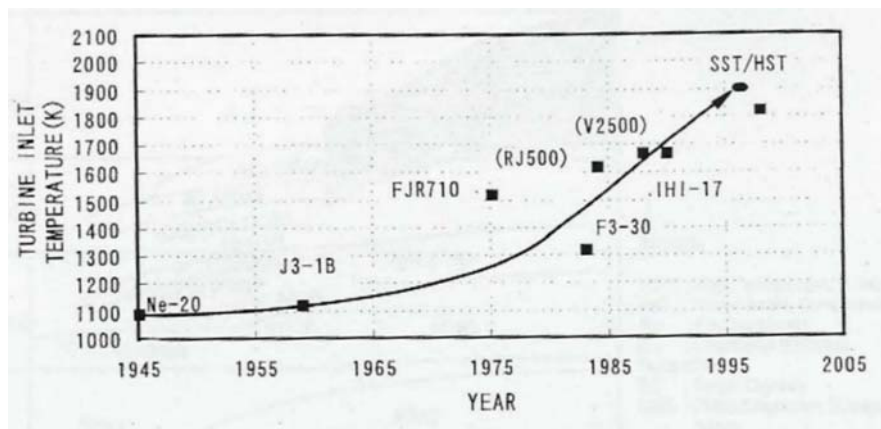
Figure 6. Turbine inlet temperatures vs. the years of development [30].

The turbine blade is not the only component where composites can be applied in the engine.   Ceramic composite materials can be used in combustor liners, transition ducts, turbine airfoil, and exhaust liners [30].

10
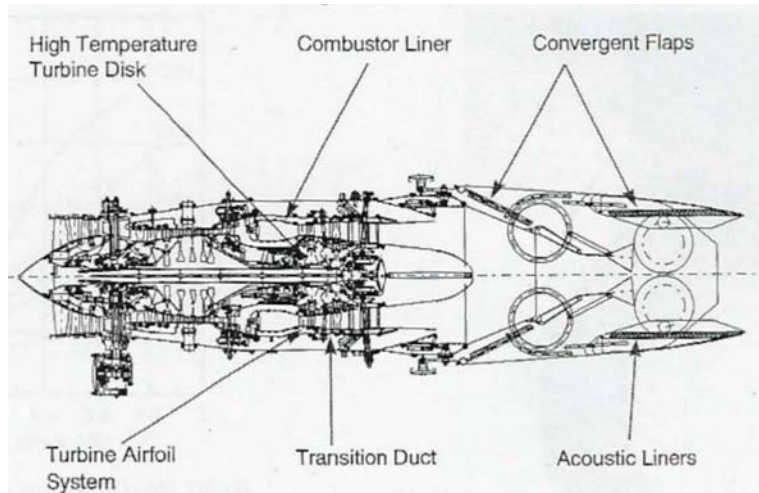
Figure 7. Turbine engine applications of CMCs [30].

Rocket engine components can also benefit from using CMCs, for example in construction of the thrust chambers of liquid-propellant rockets. The CMCs offer lower total weight and high resistance to extreme temperatures [34].

2.3 Previous Work

Recent research efforts at AFIT investigated creep performance of the Nextel 720/A CMC. Harlan [14] studied the effects of the air and steam environments at 1200 °C on the creep resistance. The presence of steam significantly degraded creep performance and dramatically reduced creep lifetimes [14].

Mehrman [25] explored effects of hold times at maximum stress on cyclic behavior of Nextel 720/A CMC at 1200° C in both air and in steam. Mehrman also reported that prior fatigue subsequently improved in air but creep performance but in steam creep performance remained poor. Mehrman conducted an Energy Dispersive X-ray Spectroscopy (EDS) analysis to determine whether leaching of Si species from Nextel

720 fibers took place, thereby degrading fiber performance. Results revealed some evidence of Si species migration from fiber to matrix.

Recently, Braun [5] investigated the creep behaviors of the Nextel 720/A CMC in the 1000-1100° C temperature range in air and in steam. The objective of that study was to determine the temperature at which degrading effects of the steam environment became significant.

2.4 Thesis Objective

The initial thesis objective was to characterize the compressive response of the Nextel 610/A composite with 3D fiber architecture (i.e. composite reinforced with 0/90 woven layers and through-thickness Z-pins).

However, the Z-pinned material exhibited extensive delamination in the as-processed condition and consequently produced extremely low compressive strength. Processing needs to be improved considerably before that material system can produce adequate mechanical properties. Therefore, the thesis objective was shifted to investigation of cyclic creep and recovery of Nextel 720/A CMC in air and in steam environments. This research aims to determine whether introducing periods of recovery at near zero stress levels would improve one or more of the following: the creep lifetime, creep strain rate, and accumulated creep strain of the material.

III. Material and Specimens

3.1 Materials

3.1.1 Nextel[TM] 610 Alumina Ceramic Matrix Composite

For the monotonic compressive tests the Nextel 610/A with Z-pin reinforcement developed at the North Carolina A and T University was used. The CMC was supplied in two panels that contained a 0°/90° plain weave. Throughout the panel, the Z-pins of Nextel 610 fibers were sewn through the 3mm thickness at a 2% density [3]. The 3D reinforcement's objective is to reduce the delamination within the CMC [19]. A density below 2% does not provide improvement in delamination [19]. An increase in compressive strength is expected due to the Z-pin reinforcement fibers. Nextel 610/A CMC is made up of alumina matrix and Nextel 610 fibers. The fibers are mainly alumina $(\alpha- Al_2O_3)$, 99% [27].

3.1.2 Nextel[TM] 720 Alumina Ceramic Matrix Composite

The study of cyclic creep and recovery focused on a CMC comprised of an alumina matrix with alumina/mullite Nextel 720 fibers manufactured by Composite Optics, Inc. (COI) Ceramics. The CMC was supplied in three separate 30.48 cm by 30.48 cm panels at 2.8 mm thick. The plates ranged in density from 2.54-2.7 g/cm^3 and had a fiber volume of 46.4-49.2% [7]. All panels consisted of 8-harness satin 0°/90° woven layers. The panel specifications can be seen in Table 1.

The Nextel 720 fibers are made by the Minnesota Mining and Manufacturing Company (3M^{TM}). The fibers consist of 85% alumina (Al$_2$O$_3$) and 15% mullite (SiO$_2$) [18]. Mullite is more creep resistant than alumina, therefore the combination of the two lowers the creep rate [38]. The fibers are infiltrated with the alumina matrix so that the fiber volume is approximately 45% [18].

Table 1. N720/A panel properties [7].

Panel	COI Serial #	Thickness (mm)	Fabric Volume (%)	Matrix Volume (%)	Porosity (%)	Density (g/cc)
1	6656-2	2.69	46.8	29.9	23.3	2.79
2	6656-1	2.54	49.2	28.3	22.5	2.80
3	4569	2.70	46.4	29.9	23.7	2.77

3.2 Specimen Machining

All Nextel 720/A specimens and the Nextel 610/A specimens were cut using a computer controlled water jet as the AFIT Machine Shop. The water jet uses a nozzle to spray a mixture of water and garnet particles at high velocities to precision cut the specimens. To insure an orthogonal cut to the panel and reduce fraying a plastic panel is attached to the top for extra support. The last six tensile specimens in the Nextel 610/A panel were cut using the diamond cut saw to verify processing delaminating.

After machining, all specimens were soaked in a deionized ultrasonic bath for twenty minutes to remove any residual debris, then soaked in ethanol for fifteen minutes to remove any moisture. Finally, all specimens were dried in an oven at 250° C for an hour.

3.2.1 Specimen Geometry

A rectangular specimen shown in Figure 8 was used for compressive testing. A dog bone shaped specimen shown in Figure 9 was used in tensile tests.
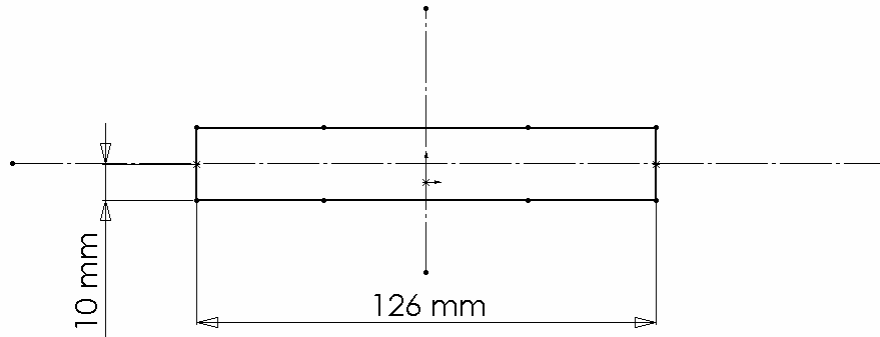
Figure 8. Compressive specimen [11].
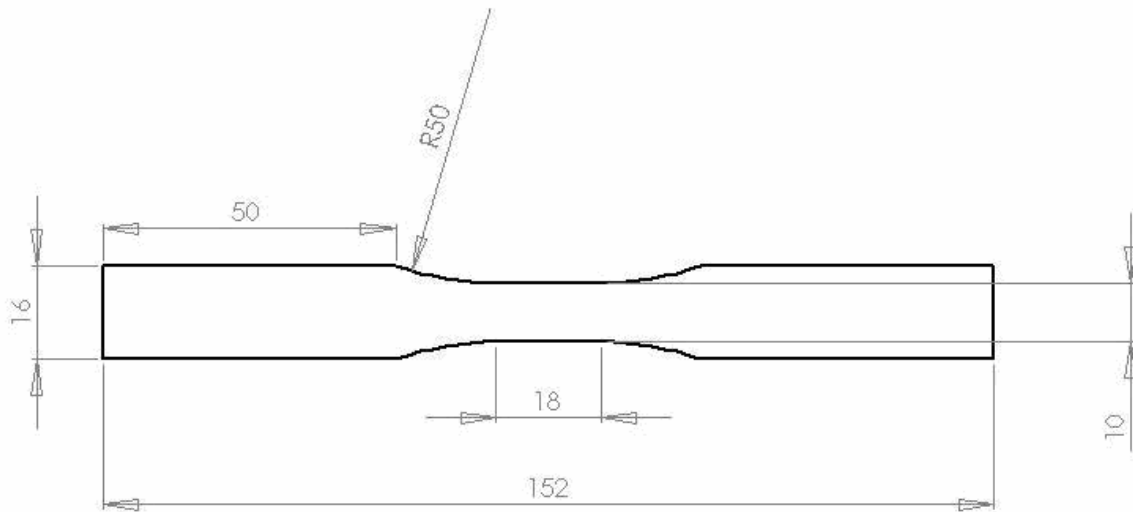
Figure 9. Tensile specimen[25].

3.2.2 Tabbing

The grips holding the specimens during the tensile and compressive tests apply a fairly high pressure to the specimen. To prevent grip failures, tabs were attached on the gripped portions of the specimens. The fiberglass/epoxy tabs were bonded to specimens with M-Bond 200 adhesive. A tabbed specimen is shown in Figure 10.

Figure 10. Example of a tabbed Nextel 720/A specimen.

IV. Experimental Set-Up and Testing Program

4.1 Testing Equipment

A servo hydraulic testing machine manufactured by Material Testing Corporation model Material Testing System (MTS) 810 was used in all tests. The load cell capacity was 5.5 kip (25kN). The testing machine was equipped MTS 647 (Model 661.19 E-04) hydraulic wedge grips. An 8 MPa grip pressure was used in all tests. Grips wedges were water-cooled using water chiller NESLAB model HX-75 Figure 11 to prevent grips from overheating when testing at high temperatures.
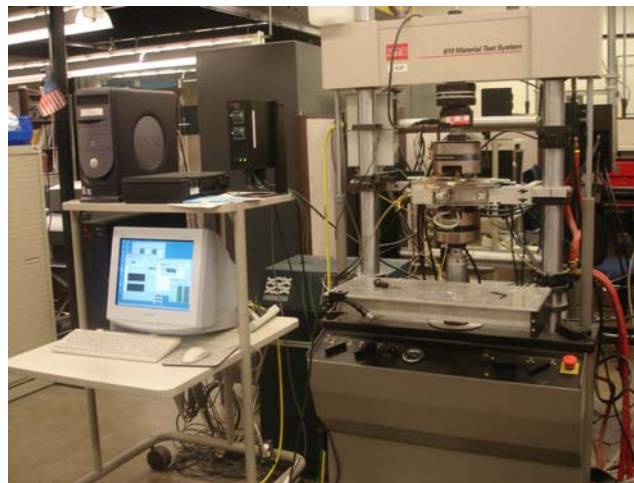
Figure 11. MTS work station.

The chilled water is pumped through 6.35 mm outer diameter tubes passing through the grip wedges. The average water temperature was 16-20° C. To prevent corrosion deionized water was used.

Figure 12. NESLAB model HX-75 cooler.

An AMTECO Hot-Rail Furnace System with two resistance elements ovens. The ovens were controlled by MTS Model 409.83B Temperature Controller.   The thermocouples connected the controller to the ovens were R-type in order to withstand the high temperatures.

The temperature was set according to TestStar II and sent to the temperature controller.   The controller can be seen in Figure 13. The temperature recorded by the thermocouples is not the temperature of the specimen but only the oven temperature. Therefore, temperature controller was calibrated to ensure specimen was at the desired temperature level.

Figure 13. Temperature controller.

The procedures for calibrating the controller were identical for the Nextel 610/A and Nextel 720/A specimens. One specimen of each material was fitted with two R-type thermocouples. The Nextel 610/A's thermocouples were attached with Omega CC, High Temperature Cement and piano wire to ensure contact. The Nextel 720/A utilized two pieces of scrape Nextel 720/A with groves cut out to hold the thermocouples to the specimen and held on with piano wire. An example of a specimen outfitted with thermocouples can be seen in Figure 14.
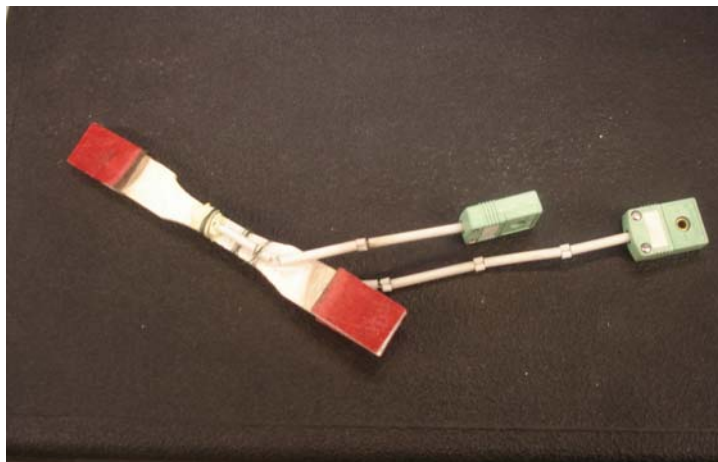
Figure 14. Nextel 610/A calibration specimen with mounted R-type thermocouples.

The specimen was mounted in the MTS machine. The temperature was raised

slowly to determine where the specimen reached 1200° C. Once the specimen reached

temperature on both sides, the temperature was maintained for one hour to ensure thermal

equilibrium. The results for the Nextel 610/A for 900 °C and 1000 °C specimen

temperatures can be seen in Table 2. Nextel 720/A air and steam calibrated temperatures

for 1200 °C are in

Table 3.

Table 2. Calibrated oven temperatures for both 900 °C and 1000 °C in air for Nextel 610/A.

Desired Temp of Specimen	Left Oven Setting	Right Oven Setting
900 C	775 °C	796 °C
1000 C	951 °C	978 °C

Table 3. Calibrated temperature for 1200 °C in air and steam for Nextel 720/A.

Desired Temp of Specimen	Left Oven Setting	Right Oven Setting
Air – 1200 C	1061 °C	1066 °C
Steam -1200 C	1167 °C	1185 °C

Strain measurement was accomplished with a MTS high temperature low contact

force extensometer with 12.5 mm gage length. The set up of the oven and extensometer is

seen in Figure 15 (a) and an operating system in Figure 15 (b).
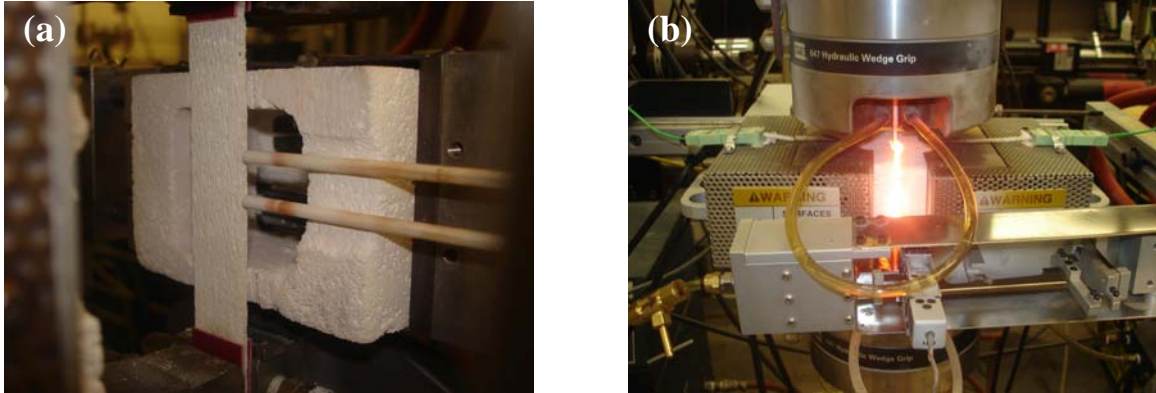
Figure 15. (a) Cross section mounting of air test and (b) MTS and ovens testing.

For those tests requiring steam, a continuous steam environment was provided by an AMTECO HRFS-STMGEN Steam Generation System seen in Figure 16. Steam was guided to the alumina susceptor through a ceramic feeding tube at a temperature of approximately 300° C. The steam was comprised of deionized water.
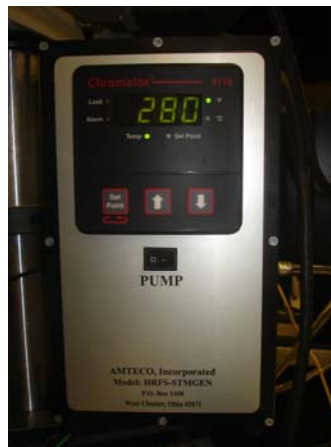
Figure 16. AMTECO, Inc steam pump.

An alumina susceptor was used to maintain a steam environment around the gage section of the specimen. One end of the susceptor had an opening allowing the steam tube to be applied, while the other end had two openings for the extensometer rods. Figure 17 shows the susceptor mounted and broken down.
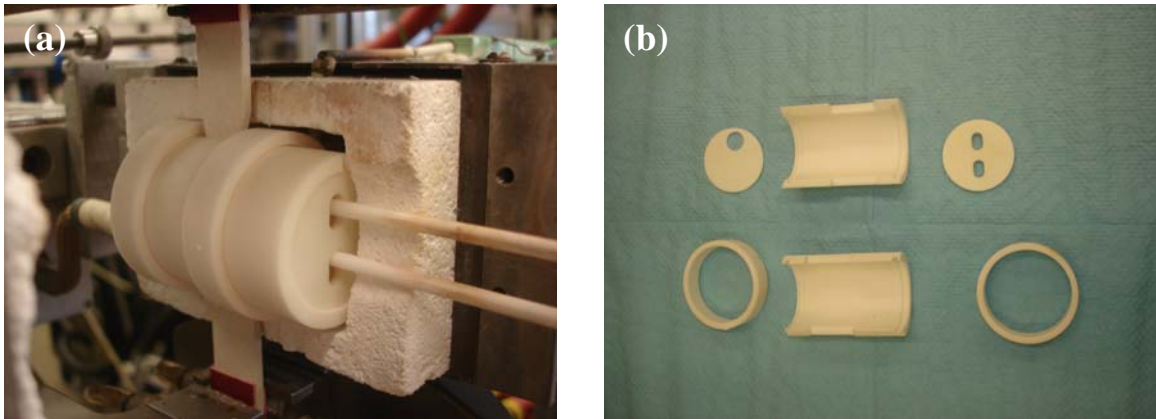
Figure 17. (a) Cross section of steam mounting and (b) susceptor pieces.

4.2 Test Procedures

Tests are programmed using the Multipurpose Testware (MPT) software. The first step in all tests specimens was to heat ovens to test temperature at the rate of 1° C/s and then held at test temperature for additional 30 min to allow for thermal equilibration.

Monotonic tensile and compression tests to failure were conducted in displacement control with the displacement rate magnitude of 0.05 mm/s. A typical procedure for compression to failure test is shown in Figure 18.

Figure 18. Procedure for compressive failure for Nextel 610/A Z-pin.

Cyclic creep and recovery tests were conducted in stress control. A schematic of the stress input is shown in Figure 19. In all cyclic creep and recovery tests, loading to maximum stress and unloading to minimum stress were performed at the stress rate magnitude of 20 MPa/s. Minimum stress load of 2 MPa was used in all tests.
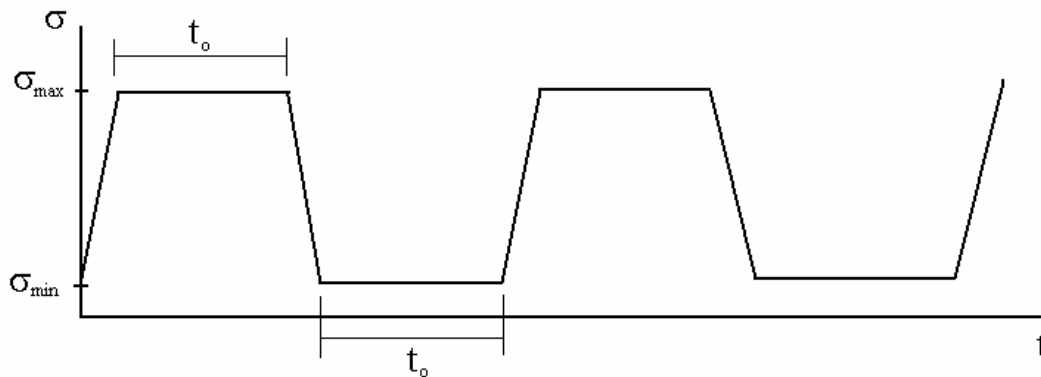
Figure 19. Loading schematic for Nextel 720/A cyclic creep-recovery tests.

Creep and recovery time varied from test to test as did the maximum stress, σ_{max}. The creep and recovery time will also be known as the hold time, t_o, throughout this investigation. Creep and recovery time and maximum stress values are summarized in Table 4. Cyclic creep and recovery test procedures in MTS are shown in Figure 20. The cyclic pattern for the creep and recovery tests were continuous until specimen reached failure or until the accumulated creep time reached 100 h, also known as run out. All specimens that survived the 100 h at σ_{max} were subjected to tensile test to failure to determine retained tensile properties.

Table 4. Summary of cyclic creep and recovery tests for Nextel 720/A CMC.

Specimen Number	Panel	Test Environment	Max Stress σ_{max}, (MPa)	Creep and Recovery Time, t_o (h)
P1	1-6656	Air	100	30
P2	2-6656	Air	100	1
P3	4569	Air	125	1
P4	2-6656	Steam	100	1
P5	1-6656	Steam	125	0.167
P6	1-6656	Steam	100	1
P7	2-6656	Steam	100	1
P8	4569	Steam	100	1
P9	4569	Steam	125	0.05
P10	1-6656	Steam	125	0.083

(a)

Type	Name	Start	Interrupt
	Safety Net	\<Procedure\>.Start	
	Monitor Thermal Rise	\<Procedure\>.Start	Thermal Rise -1200 Air.Done
	Thermal Rise -1200	\<Procedure\>.Start	
	Sample Pretest Conditi	Thermal Rise -1200 Air.Done	
	Timer	Sample Pretest Conditions.Do	Safety Net.Done
	Loop	Sample Pretest Conditions.Do	Timer.Done
	Return to Zero	Timer.Done	
	Monitor Load to Failure	Return to Zero.Done	Load to Failure.Done
	Load to Failure	Return to Zero.Done	Safety Net.Done
	End of Procedure	Load to Failure.Done	
	Turn off Ovens	End of Procedure.Done	

Procedure is done when | Turn off Ovens.Done

(b)

Type	Name	Start	Interrupt
	Monitor Ramp Up	Hold Low.Done \<Group\>.Start	Ramp Up.Done
	Ramp Up	Hold Low.Done \<Group\>.Start	
	Creep 0-8min	Ramp Up.Done	
	Creep 8-1hr	Creep 0-8min.Done	
	Hold High	Ramp Up.Done	
	Monitor Ramp Down	Hold High.Done	Ramp Down.Done
	Ramp Down	Hold High.Done	
	Recovery 0-8min	Ramp Down.Done	
	Recovery 8-1 hr	Recovery 0-8min.Done	
	Hold Low	Ramp Down.Done	

Group is done when |

Figure 20. Procedure for creep recovery a) main procedure b) infinite inner loop.

4.3 Microscopy

4.3.1   Optical Microscopy

A Zeiss Discovery.V12 optical microscope was used to examine the specimens' fractured surfaces. The microscope is equipped with a Zeiss AxioCam HRc digital camera and Axiovision version 4.4 software.
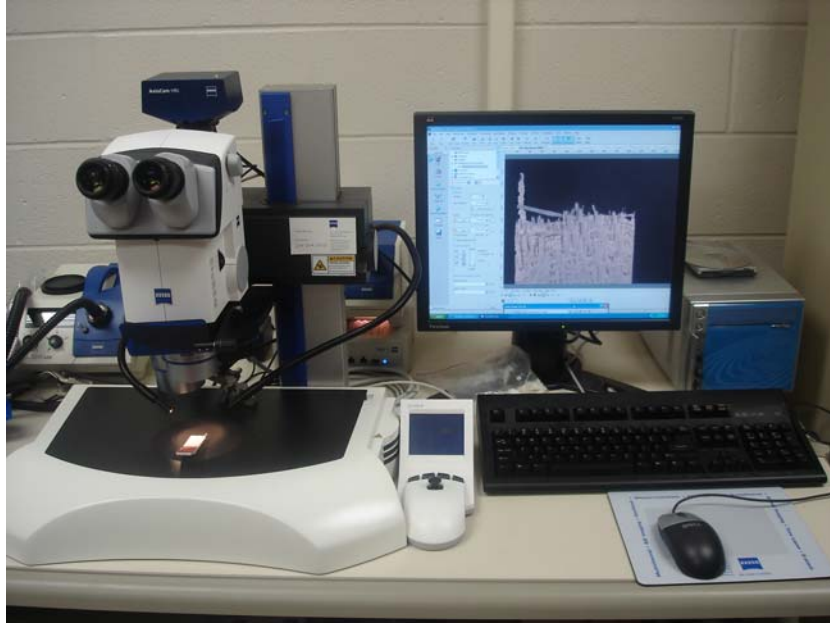
Figure 21. Zeiss Discovery.V12 optical microscope.

4.3.2   Scanning Electron Microscope Analysis

An FEI Quanta 200 HV Scanning Electron Microscope (SEM) was used to observe sample at higher magnifications. The SEM bombards the specimen with electrons and Gaseous Secondary Electron Detectors record the backscatter of the electrons from the specimen.

Figure 22. FEI Quanta 200 HV scanning electron microscope.

The SEM specimen must have a conductive surface, as a non conductive surface builds up charge and degrades the resolution and can be damaging to the equipment. Therefore, all SEM specimens were carbon coated using a SPI-MODULE Control and Carbon Coater. In preparation for SEM analysis, specimen fracture surface were cut using a MTI Corporation EC.400 CNC Dicing/Cutting unit with a 3.5 in diamond cutting blade. The specimen is then grounded with carbon tape to the mounting surface. Finally, the specimen is carbon coated. The pressure inside the chamber of the carbon coater varies from 10^{-1} ATM and 2^{-1} ATM. The voltage used was 7V.
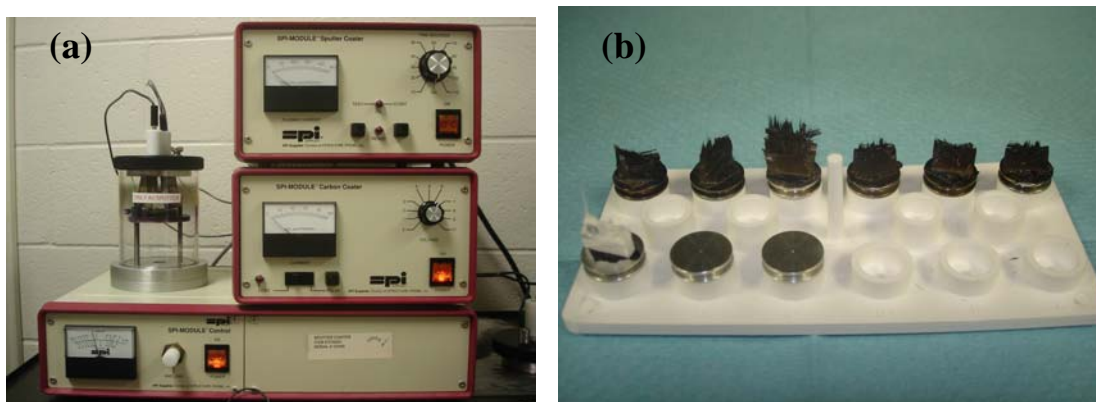
Figure 23 . (a) SPI-MODULE Control and Carbon Coater and (b) carbon and uncarbon coated specimens.

27

V.   Results and Discussion

5.1 Compressive Behavior of Nextel 610/A 3D Composite

Monotonic compression to failure tests were performed on Nextel 610/A specimens with the Z-pin architecture at 900° C. Compressive stress-strain response is typified in Figure 24. The average ultimate compressive strength was 14 MPa, which is significantly below the compressive strength of ~200 MPa exhibited by Nextel 610/A specimens without the Z-pin reinforcement at 1100° C.   The addition of Z-pin reinforcement was expected to increase compressive strength of the composite. Microstructure of the Nextel 610/A specimen with Z-pin reinforcement was examined to determine whether processing defects were the cause of the low compressive strength. An optical micrograph (side view) of the untested Nextel 610/A specimen with Z-pins shown in Figure 25 reveals extensive interlaminar cracking. Large interlaminar cracks seen in Figure 25 would lead to rapid delamination and failure of the specimen subjected to compressive loading. Clearly, the material processing must be considerably improved to insure proper matrix infiltration. The test material in its present form was deemed unsuitable for further investigation. Hence, the research focus was shifted to the experimental investigation of cyclic creep and recovery response of Nextel 720/A Composite at 1200° C.
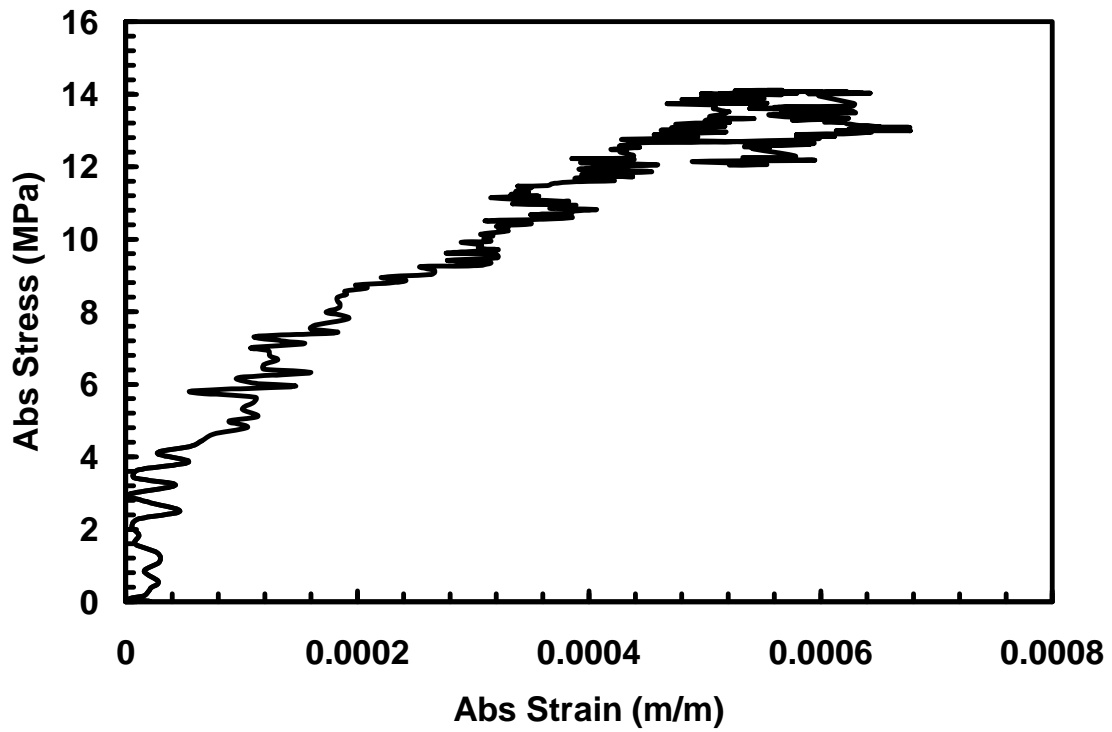
Figure 24. Compressive stress-strain curve of Nextel 610/A composite with Z-Pin reinforcement at 900 ° C in laboratory air.

3 mm
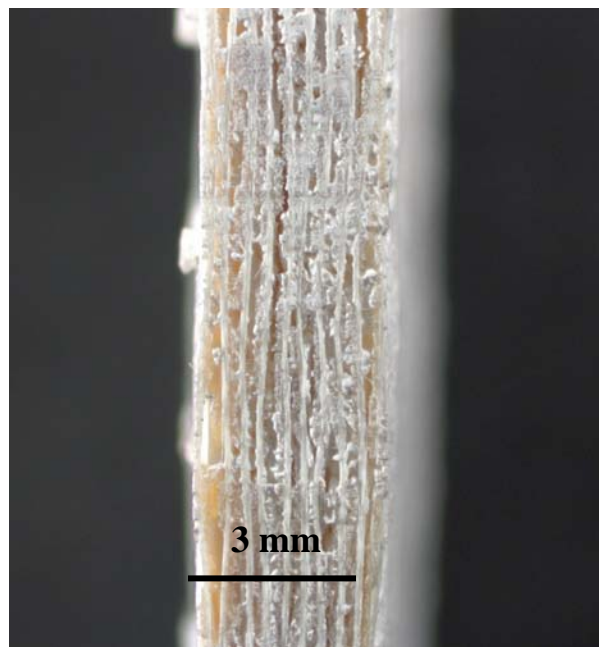
Figure 25. As-processed Nextel 610/A composite with Z-Pin reinforcement (side view). Interlaminar cracks are clearly visible.

5.2 Cyclic Creep and Recovery Behavior of Nextel 720/A Composite at Results 1200 °C in Air and Steam.

5.2.1 Thermal Expansion

All tests in this investigation were conducted at 1200 °C. Test temperature was verified by periodic calibration discussed in Section 4.1 above. In addition, temperature of each test was verified by comparing thermal strain produced in a particular test to those measured in previous tests on N720/A conducted at the same temperature. Thermal strains obtained for all specimens in this effort are listed in Table 5.

Table 5. Summary of coefficients of thermal expansion for Nextel 720/A.

Specimen	Panel	Test Environment	Thermal Strain (%)	Coefficient of Thermal Expansion (ppm/° C)
P1	6656-1	Air	0.74	6.3
P2	6656-2	Air	0.736	6.26
P3	4569	Air	0.82	7.14
P8	4569	Steam	0.84	7.15
P9	4569	Steam	0.88	7.45

Comparison of the thermal strain mean values and standard deviations produced in the present research and in prior studies of N720/A at 1200 °C are given in Table 6.

Table 6. Thermal strains produced by N720/A CMC due to temperature rise from 23 to 1200 °C and corresponding coefficients of linear thermal expansion. Results from prior studies are also included [5; 14; 16; 25]

Author	Specimens	Mean Thermal Strain (%)	Thermal Strain Standard Deviation (%)	Coefficient of Linear Thermal Expansion (10^{-6} C^{-1})
Harlan [14]	12	0.867	0.174	7.20
Mehrman [25]	16	0.902	0.0717	7.66
Hetrick [16]	7	0.891	0.0294	7.57
Current Research	5	0.783	0.0719	6.86

The results in Table 6 show that all the data collected in the current research is slightly below the previous efforts however, the steam results are more consistent. The specimens in the P3, P8 and P9 test were from the panel 4569, which resulted in coefficients similar to the previous work. The 6656 panels have a lower thermal expansion. In all tests, mechanical strain was calculated by subtracting out the thermal strain from the total strain.

5.2.2   Basic Tensile Properties

The initial load-up portion of the cyclic creep and recovery tests was used to evaluate the elastic modulus. The values obtained in the present research are summarized in Table 7. It is seen that these values are slightly below those values from prior work in Table 8 [7; 14; 16; 25].

Table 7. **Summary elastic modulus values obtained during initial load-up in cyclic creep and recovery tests conducted at 1200 °C in laboratory air.**

Specimen	Elastic Modulus (GPa)
P1	60.6
P2	60.8
P3	66.4
P8	61.3
P9	60.5
Average	63.1

Table 8. Ultimate tensile strength, elastic modulus, and failure strain for N720/A composite at 1200° C.

Source	UTS (MPa)	Elastic Modulus (GPa)	Failure Strain (%)
Harlan [14:45]	192	74.7	0.38
Mehrman [25:33]	186	77.7	0.37
COI [7]	219	76.1	0.43
Hetrick [32:28]	190	76	0.38
Average	199	76.2	0.39

It is seen that the average value of the elastic modulus was 61.9 GPa and is below the average values of 74.7, 77.7, 76.1 and 76 GPa reported by Harlan [14], Mehrman [25], and COI [7], and Hetrick [32], respectfully. However, the previous work results are averages and Hetrick [32], for instance, did experience a range of elastic modulus values throughout his testing. The current results fall within those bounds.

5.2.3 Cyclic Creep and Recovery Tests in Laboratory Air

5.2.3.1 Creep Curves

Cyclic creep and recovery tests were conducted at the creep stress levels of 100 and 125 MPa at 1200 °C in laboratory air and in steam. The summary of all cyclic creep and recovery tests conducted in air is given in Table 9. In addition, data from monotonic creep tests obtained by Harlan [14] are included for comparison.

Table 9. Nextel 720/A test results for air 1200 ° C.

Specimen	Max Stress σ_{max}(MPa)	Creep and Recovery Time t_o (h)	Creep strain (%)	Time to rupture (h)
P1[b]	100	30	0.6	>150
P2[b]	100	1	0.4	>100
H1[a]	100	N/A	3.04	41.0
P3[b]	125	1	0.8	>100
H2[a]	125	N/A	3.4	4.25

[a] data from Harlan 2005 [14]
[b] run-out

In this investigation the following definitions are adopted:

1. Mechanical or total strain is the strain produced after the test temperature has been reached and mechanical loading was applied.

2. Creep strain is the strain accumulated after the creep stress level has been reached and while the creep stress level is maintained constant.

Results obtained in cyclic creep and recovery tests with the creep stress of 100 MPa are presented in Figure 26, where results obtained in the 100 MPa monotonic creep test by Harlan [14] are included for comparison. Note that the cyclic creep data in Figure 26 have been compressed by removing the loading, unloading and recovery periods and plotting only strain accumulated during creep periods of each cycle. Plotting cyclic creep strain vs. compressed time permits a comparison of strain accumulated under maximum stress in cyclic creep test with that accumulated in the monotonic creep. The results in Figure 26 reveal that the introduction of the unloading and recovery at near zero stress into the creep cycle considerable reduced the amount of accumulated creep strain. Note that the creep strains accumulated during 100 h of creep in tests with creep and recovery time t_0 of 1 and 30 h remain at or below 0.5%. Furthermore, it is seen that less creep strain is accumulated in the test with t_0 of 1 h than in the test with a longer creep and

recovery time of 30 h. Apparently a shorter time spent under sustained load results in a lower permanent strain produced in the creep and recovery cycle. Additionally, a reduced amount of time is required to achieve recovery saturation.

Creep strain vs. time curves obtained in 100 MPa cyclic creep and recovery tests (Figure 26) exhibit primary and secondary creep regimes. In contrast, the creep curve obtained in 100 MPa monotonic creep test exhibits primary, secondary and tertiary creep regimes. Much larger creep strain accumulation (3.04% in 41 h) is also observed. Finally, while the 100 MPa cyclic creep and recovery tests achieved a run-out, the 100 MPa monotonic creep test survived only 41 h [14].

The discrepancy in the accumulated strain for the first one hour between the cyclic creep and recovery tests and the monotonic test in Figure 26 may be due to several factors. Depending on where within the panel the specimen was cut may result in slight variations in the behavior. Another speculation is that Harlan may have had a warped specimen and that would couple both tensile and bending stress and therefore resulting in faster creep rates and early failure times. Finally, the external factor of the precision of the extensometer may have influenced the initial hour. The strain being measured is around 0.001-0.005 m/m and the uncertainty is very large at these small values.

(a)

(b)
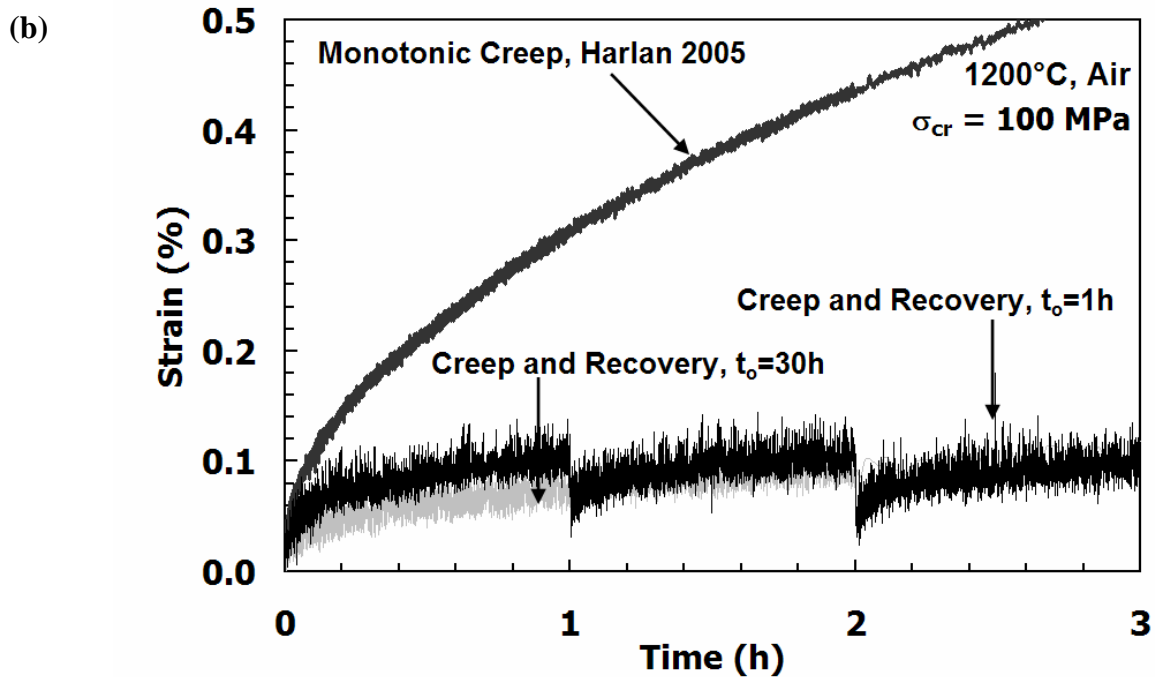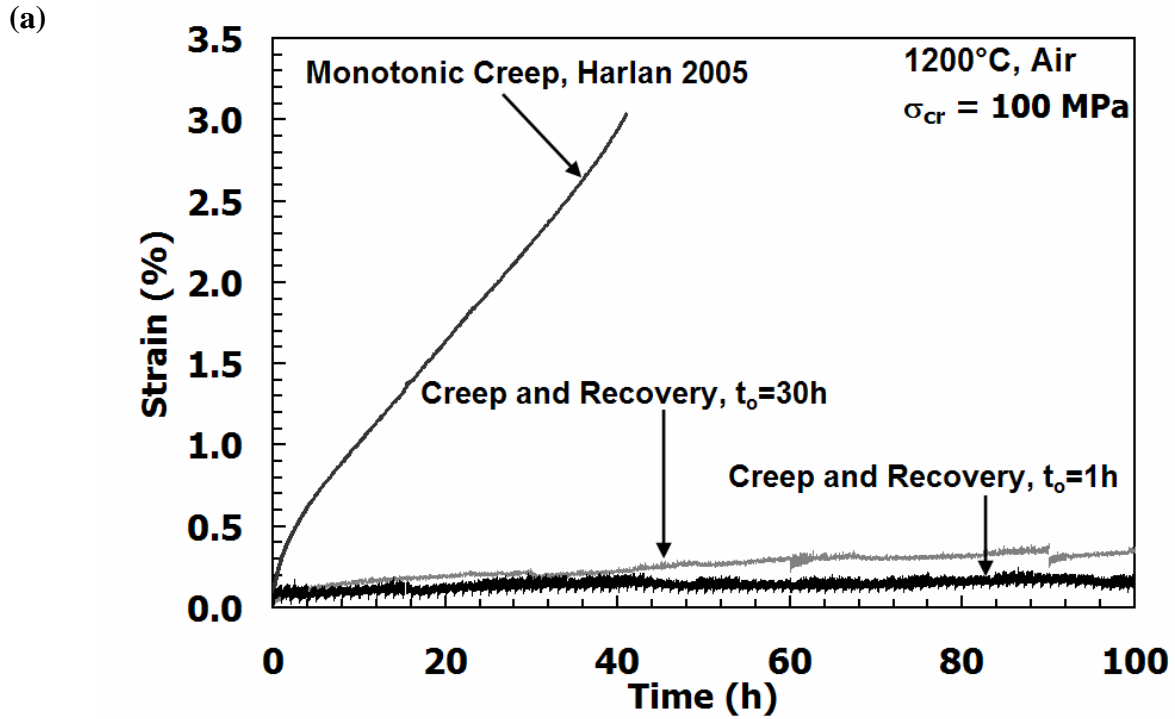
Figure 26. Creep strain vs. time curves for N720/A specimens obtained in cyclic creep tests with σ_{max} = 100 MPa and t_0 = 1 h and 30 h conducted at 1200 °C in laboratory air. Monotonic creep data at 100 MPa from Harlan [14] are also shown. (a) Time scale chosen to show up to 100 h of creep and (b) time scale reduced to clearly show creep curves produced during individual cycles.

Creep strain vs. time curve obtained in 125 MPa cyclic creep and recovery test with $t_0 = 1$ h is shown in Figure 27 together with the 125 MPa monotonic creep curve reported by Harlan [14]. As in Figure 26, the cyclic creep data in Figure 27 are compressed to permit comparison of the strain accumulated under maximum stress in cyclic creep test with that accumulated in the monotonic creep test. As expected, a higher strain of 0.8% is accumulated during the 100 h of creep in the cyclic creep and recovery test conducted with the maximums stress level of 125 MPa than in that conducted with the maximum stress level of 100 MPa. However, the creep strain accumulated during 100 h of creep in the cyclic test is nearly an order of magnitude lower than the 3.4% creep strain accumulated during 4.25 h in the monotonic creep test at 125 MPa. As in the case of the 100 MPa, introduction of the intermittent periods of unloading and recovery at near zero stress into the creep test significantly prolongs creep lifetime. While a run-out was achieved in the cyclic creep test, monotonic creep test failed after only 4.25 h.

The difference between the first hours of creep comparing the cyclic creep results to the monotonic are the same factors mentioned for the 100 MPa tests. Where within the panel the specimen originated could be a factor, if bending was involved and the uncertainty of the extensometer. It should also be noted that each test was only conducted once and for statistical purposes many more tests at the same conditions would need to be conducted to ensure repeatability. The purpose of this study was to identify trends not verify the repeatability.
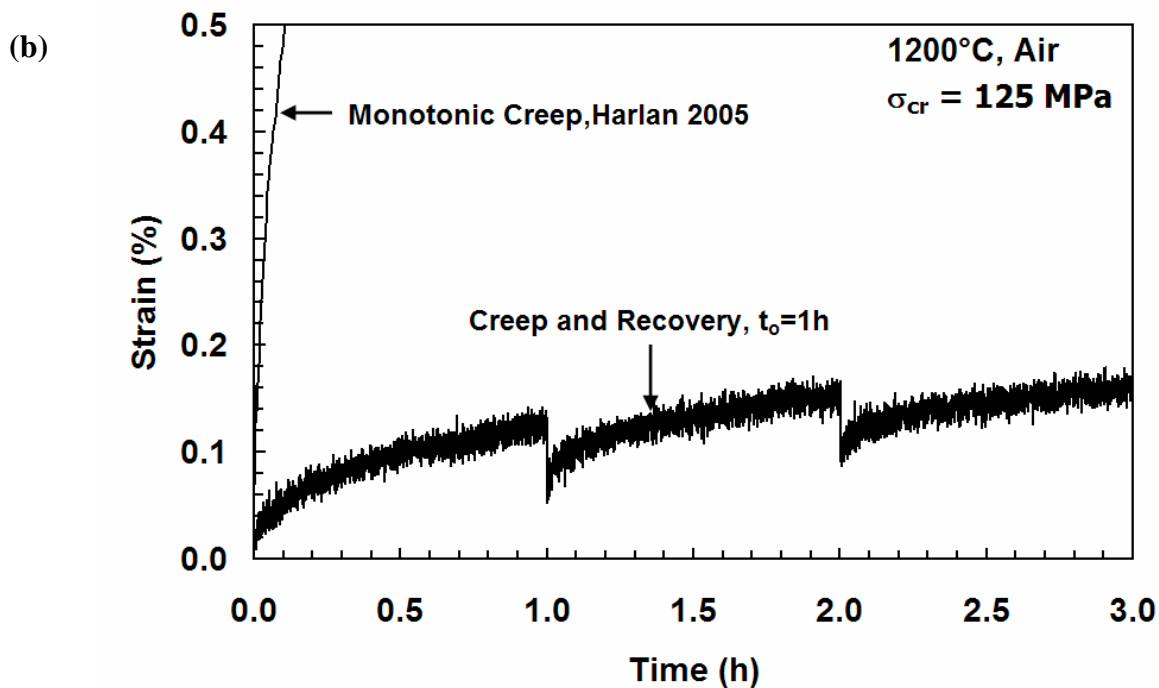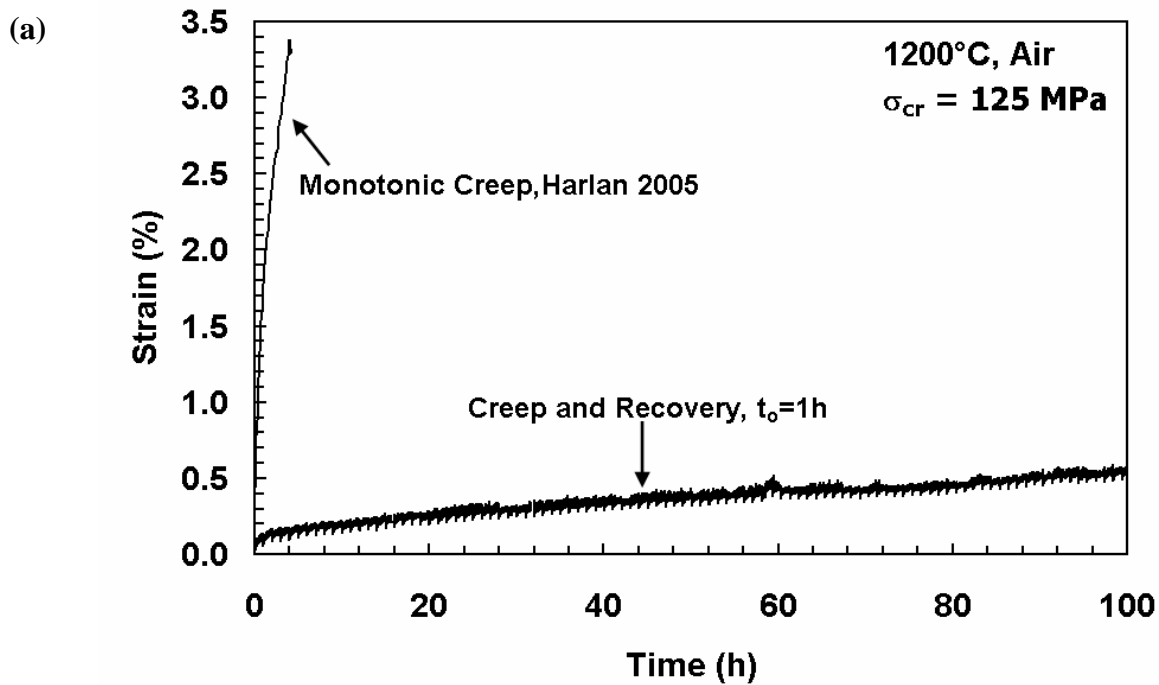
Figure 27. Creep strain vs. time curves for N720/A specimens obtained in cyclic creep tests with σ_{max} = 125 MPa and t_0 = 1 h conducted at 1200 °C in laboratory air. Monotonic creep data at 125 MPa from Harlan [14] is also shown. (a) Time scale chosen to show up to 100 h of creep and (b) time scale reduced to clearly show creep curves produced during individual cycles.

5.2.3.2   Secondary Creep Rates

Several different types of creep can be observed within one cyclic creep and recovery test. The first is the primary and secondary creep. Secondary creep is the linear portion and will also be known as the individual creep rate for a given cycle. Since each cycle has its own creep rate an average of the individual creep rate can be determined as well as a range. Finally the creep curve comprised of all the individual cycles creates its own creep curve and will be known as the overall. Its rate can be determined using a linear curve fit and will be identified as the overall equivalent creep rate.

Minimum creep rate was reached in all cyclic creep and recovery tests. The steady-state creep rate for each individual cycle was determined by applying a linear fit to the creep strain vs. time curve obtained during the last 5 h (10 min) of the cycle in the test with $t_0 = 30$ h ($t_0 = 1$ h). It is seen that for both 100 MPa cyclic creep tests, the creep strain rates produced during each cycle (see Figure 26b) are similar to the overall equivalent creep strain rate produced during the entire 100 h of creep (see Figure 26a). Furthermore, both the individual cycle creep strain rates and the overall equivalent creep strain rate are significantly lower than the creep rate produced in the monotonic creep test. In contrast, minimum creep strain rates reached during each individual cycle in the 125 MPa test are similar to that reached in the 125 MPa monotonic creep test. The primary regime of the monotonic creep has a fast creep but the secondary regime is much shallower and matches the rates found on the individual cycles of creep and recovery (see Figure 27b). A considerably lower overall equivalent creep strain rate was produced by all three tests compared to the monotonic. The lowest overall equivalent creep strain rate was during the 100 h of creep in the cyclic test (see Figure 27a).

Creep rates as a function of applied stress are presented in Figure 28, where the results of the present investigation are plotted together with the data from Harlan [14] for N720/A CMC and with the data from Wilson and Visser [37] for the Nextel 720 fibers. To facilitate comparison between the creep properties of the fiber and the composite, the Nextel 720 fiber data adjusted for $V_f = 0.22$ (volume fraction of the on-axis fibers in the N720/A composite) is also shown. Because the creep rates calculated for the cyclic creep tests varied slightly from cycle to cycle, an average creep rate and a corresponding range of creep rates are presented in Figure 28 for each cyclic test. The overall equivalent creep strain rates produced in the cyclic tests are also shown. Results in Figure 28 show that for a given creep stress level the individual creep strain rate is higher for low hold times in creep.

At 100 MPa, the highest creep rate is obtained in the monotonic creep test. The overall equivalent creep rate obtained in the cyclic creep test with $t_0 = 1$ h is nearly an order of magnitude lower than the monotonic. In the case of the cyclic creep test with $t_0 = 30$ h average creep rate further decreases by nearly another order of magnitude. The overall equivalent creep strain rate was lower than the small hold times. The small hold times individual creep rates may are an order of magnitude higher than the overall equivalent creep rates. This is due to the fact that the rates of the individual cycles for the shorter hold times are not allowed to reach the slower creep rates. Since the hold time is low the amount of creep accumulated is small, resulting in a slow overall equivalent creep rate. A similar trend is observed in the 125 MPa tests.
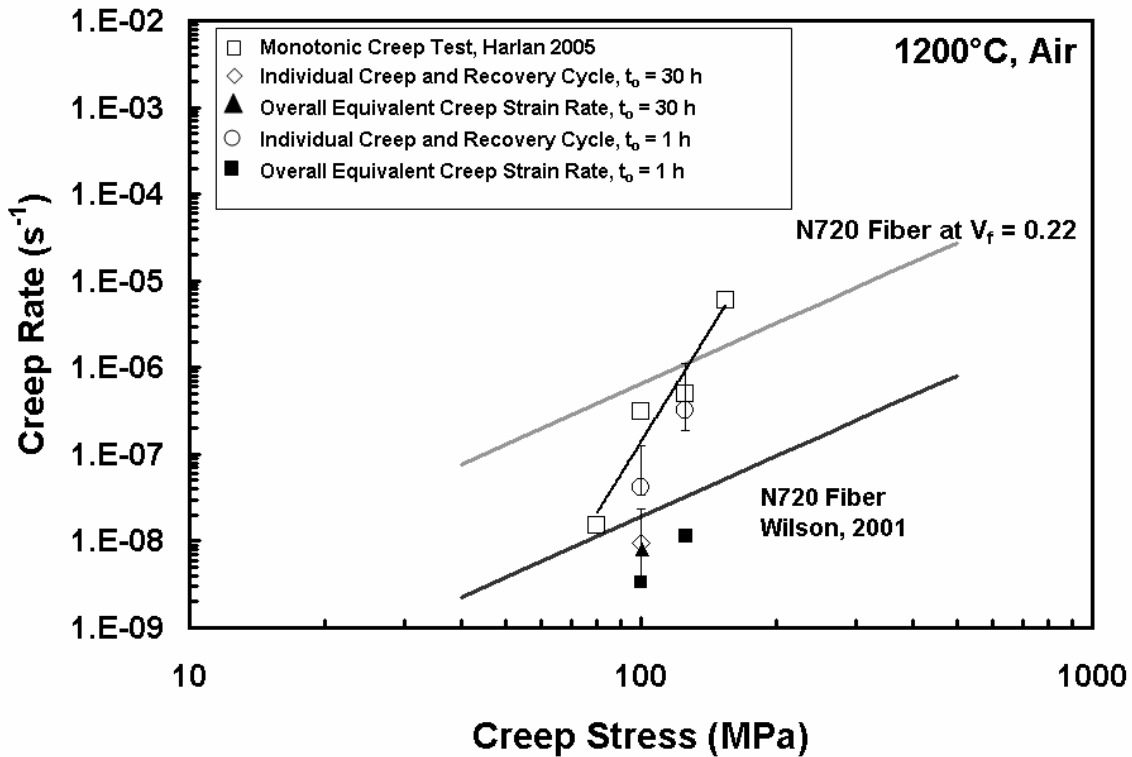
Figure 28. Secondary creep rates as a function of applied stress for N720/A ceramic matrix composite at 1200° C in laboratory air. Data for Nextel 720 fibers (Wilson [37]) and data for N720/A CMC from Harlan [14] are also shown.

5.2.3.3   Creep Lifetimes

Stress-rupture behavior in air is summarized in Figure 29, where creep stress is plotted vs. time to rupture (time under creep stress in the case of the cyclic creep tests). Stress-rupture data obtained in monotonic creep tests from Harlan [14] are included for comparison. In air introduction of intermittent periods of unloading and recovery at near zero stress has a marked influence on the creep lifetime. For a given applied stress, creep lifetimes of the specimens subjected to cyclic creep are one to two orders of magnitude longer than those of specimens subjected to monotonic creep. At 100 MPa, the specimens subjected to cyclic creep tests with $t_0 = 30$ h and $t_0 = 1$ h survived 150 h and 100 h of creep, respectively. In both cases, specimen achieved run-out, i.e. failure of specimen did

not occur when the test was terminated. Conversely, specimen subjected to monotonic creep at 100 MPa survived only 41 h. At 125 MPa, rupture time in monotonic creep test was 4.25 h, while a run-out of 100 h under creep stress was achieved in cyclic test.
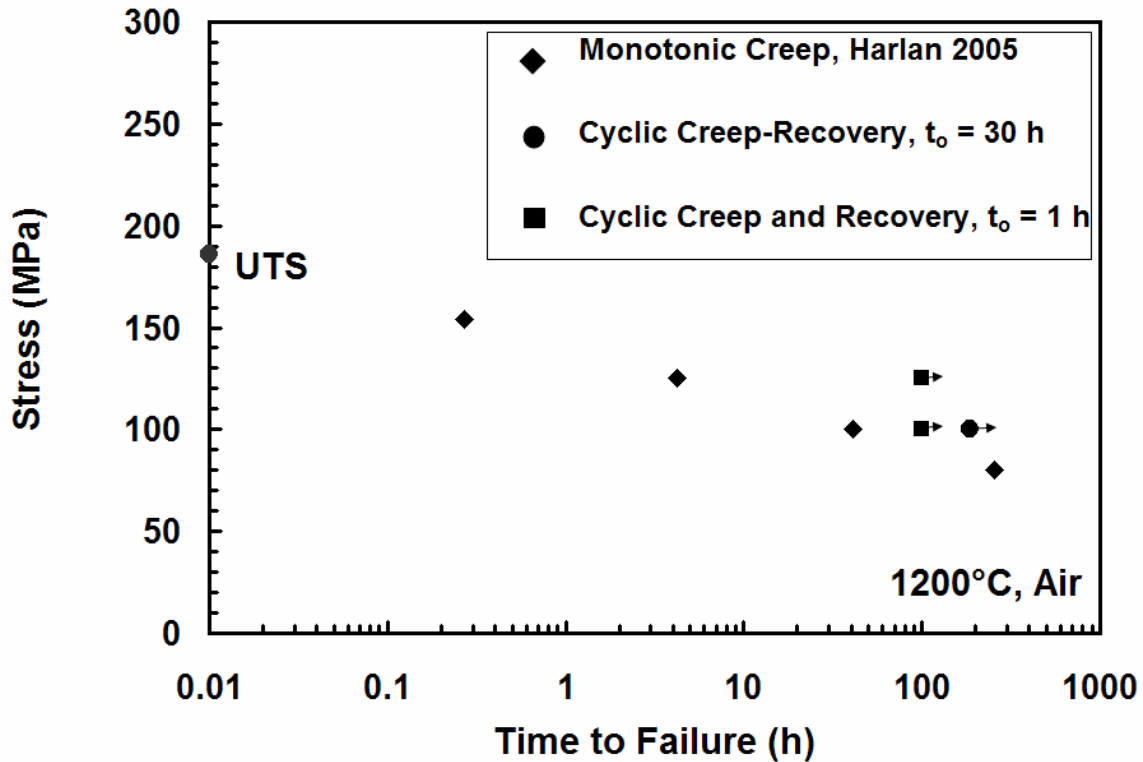
Figure 29. Creep stress vs. time to rupture for N720/A composite at 1200 °C in laboratory air. Monotonic creep data from Harlan [14]. Arrow indicates that failure of specimen did not occur when the test was terminated.

5.2.3.4   Recovery Curves and Rates

Significant strain recovery was observed in all cyclic creep and recovery tests. The qualitative strain recovery behavior is typified in Figure 30, where the strain measured during recovery period in cycle 2 of the 100 MPa cyclic creep test with $t_0 = 30$ h is plotted as the function of time. It is seen that the strain decreases rapidly

during the initial 3 h of the recovery period. After that, the strain decreases more slowly

and finally reaches a stabilized value after ~ 4 h of recovery. At that point, the strain rate

magnitude also reaches a stable value $< 10^{-8}$ s^{-1}. The recovery is now "saturated";

allowing longer recovery time at near zero stress will not lead to an additional decrease in

strain. Qualitatively similar behavior was observed in the 100 MPa cyclic creep test with

$t_0 = 1$ h. In this case the recovery saturation was reached after only 0.3 h.
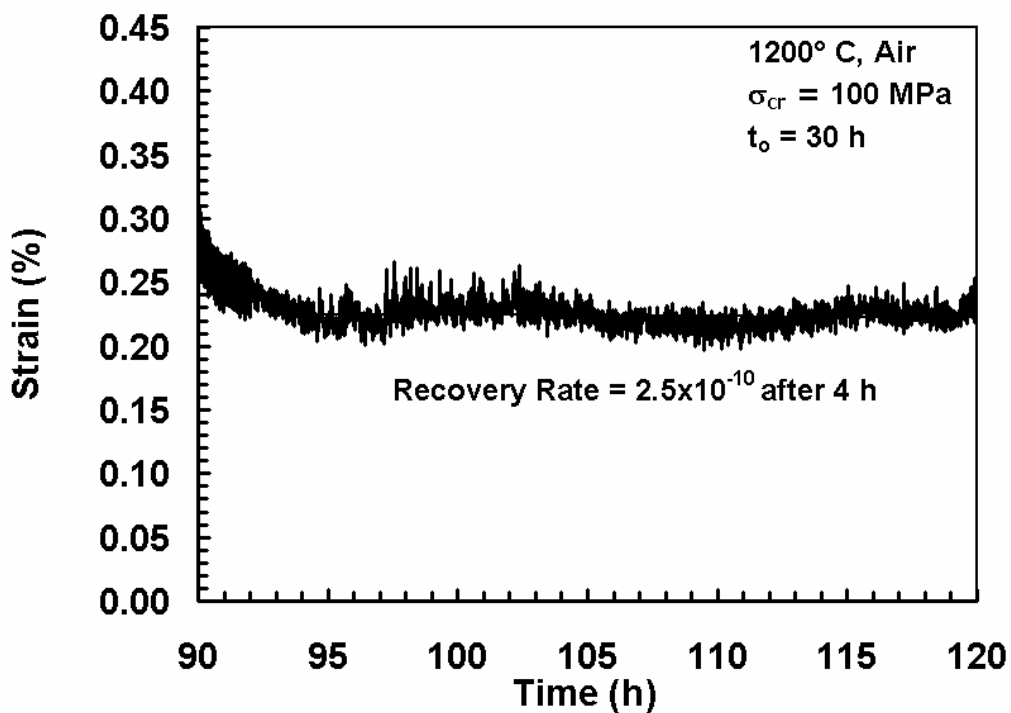
Figure 30. Strain vs. time curve for N720/A composite obtained during recovery period of cycle 2 in cyclic creep test with $\sigma_{max} = 100$ MPa and $t_0 = 30$ h conducted at 1200 °C in laboratory air. Recovery saturation after ~ 4 h at near zero stress is evident.

Presented in Figure 31 are the strain vs. time curves obtained during all five

cycles in the cyclic creep test with $t_0 = 30$ h. It is seen that the amount of strain recovered

in cycles 2 and 4 is approximately the same as that recovered in cycle 1. A somewhat

greater amount of strain is recovered in cycle 3 and 5. However, this discrepancy may be

due to noise in the extensometer used for strain measurement.
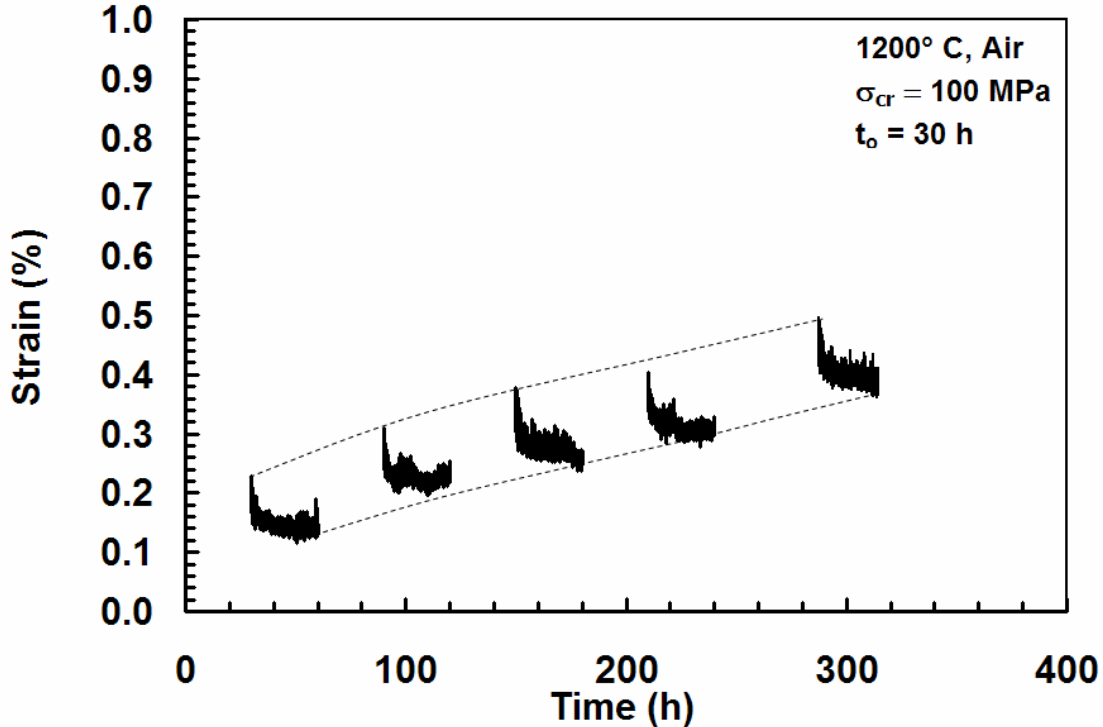
Figure 31. Strain vs. time curves for N720/A composite obtained during recovery periods of cyclic creep test with σ_{max} = 100 MPa and t_0 = 30 h conducted at 1200 °C in laboratory air. Similar amounts of strain are recovered during each cycle.

Qualitatively similar behavior was observed in the 100 MPa cyclic creep test with

t_0 = 1 h. In this case the recovery saturation was reached after only 0.3 h. Similar results

were found by the 125 MPa cyclic creep test with t_0 = 1 h which reached saturation after

0.5 h. Strain vs. time curves obtained in the 125 MPa test are shown in Figure 32 to give

an example of the behaviors of t_0 = 1 h. While Figure 32a shows all recovery periods,

the time scale in Figure 32b is reduced to clearly show a few typical recovery periods.

(a)

(b)
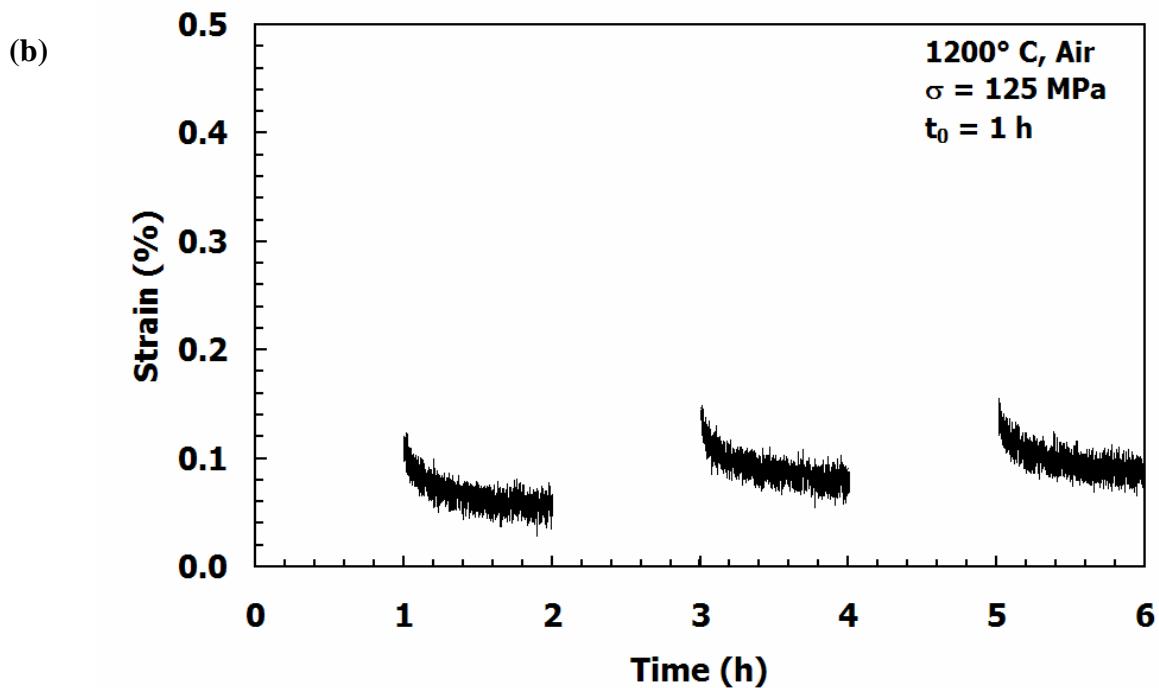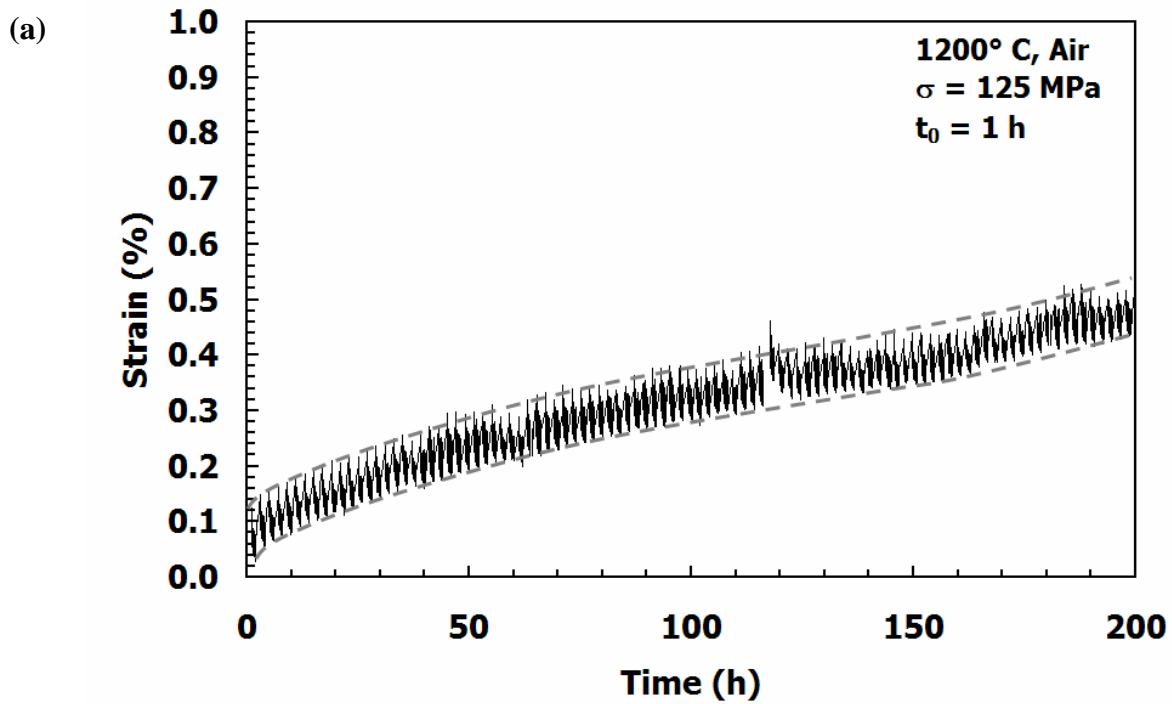
Figure 32.   Strain vs. time curves for N720/A composite obtained during recovery periods of cyclic creep test with σ_{max} = 125 MPa and t_0 = 30 h conducted at 1200 °C in laboratory air. (a) Time scale chosen to show 100 cycles and (b) time scale reduced to clearly show recovery curves produced during individual cycles.

To further assess the strain recovery occurring during each cycle as well as the cumulative strain recovery occurring during the entire cyclic test, it is useful to consider the creep-strain recovery ratio R_{cr} [17] defined as the strain change during the recovery period divided by the creep strain accumulated on that particular cycle:

$$R_{cr} = \frac{\varepsilon_{rec}}{\varepsilon_{cr}} \times 100\% \tag{2}$$

In the case of the five-cycle 100 MPa test with $t_0 = 30$ h, the creep-strain recovery ratio (R_{cr}) increased steadily from approximately 40% on cycle 1, to ~ 45% on cycle 2, to ~ 72% on cycle 3, to ~ 88% on cycle 4, to ~ 100% on cycle 5. The variation in creep-strain recovery ratio with cycles is also shown in Figure 33. In the 100 MPa test with $t_0 = 1$ h, the creep-strain recovery ratio increases with cycles until at or near 100% recovery of creep strain is achieved during cycles 10-50. At this point the amount of recovery decreases to some extent but remains above 85%. Results of the 100 MPa cyclic creep tests demonstrate that introduction of the intermittent strain recovery periods into the creep test serves to significantly reduce creep strain. This mechanism for the reduction of creep strain becomes more powerful as the creep and recovery time t_0 decreases and the frequency of the cyclic creep test increases. Results obtained in the 125 MPa cyclic creep test reveal similar trends as with the 100 MPa test with $t_0 = 1$ h, in that the amount of creep recovery increases and until it peaks at 100% around cycle 10. However, cycle 40 shows a predominate drop in creep strain recovered. The final creep strain recovery ratio for the 125 MPa with $t_0 = 1$ h is ~ 60%.
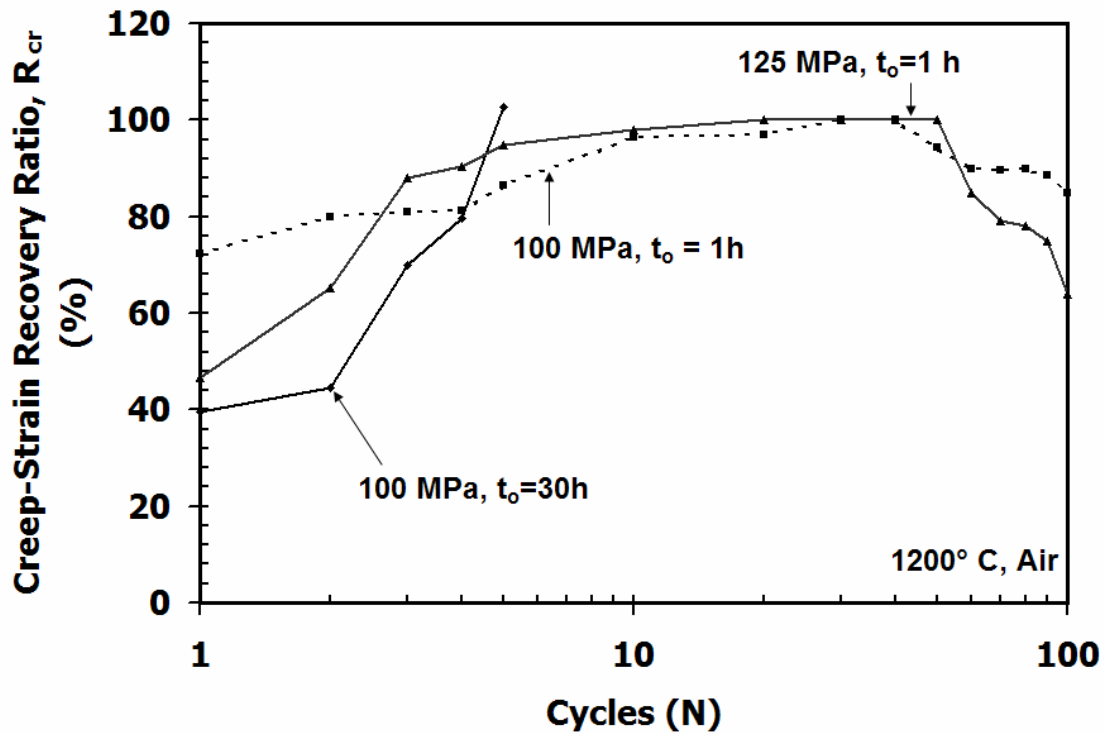
Figure 33. Variation in creep-strain recovery ratio with cycles for N720/A composite subjected to cyclic creep tests at 1200 °C in laboratory air.

5.2.3.6 *Variation in Loading Elastic Modulus*

Of importance in cyclic creep or fatigue loading is variation in elastic modulus with cycles. Decrease in elastic modulus during the cyclic creep test would reflect the damage development during the loading and creep portions of the cycle. Change in modulus with cycles is shown in Figure 34, where the normalized modulus (i. e. modulus normalized by the modulus obtained on the first cycle) is plotted vs. creep cycles. In the 100 MPa tests with $t_0 = 1$ h and 30 h, the elastic modulus remained essentially unchanged. During the final cycles of the 100 MPa with $t_0 = 1$ h, the elastic modulus shows signs of weakening. However, a decrease in normalized modulus by nearly 35%

is observed in the 125 MPa test with $t_0 = 1$ h. It is noteworthy that despite such significant reduction in modulus, indicating considerable damage developing in the specimen, a run-out was still achieved. The large decrease in the amount of creep strain recovered in the final cycles from the previous section for the 125 MPa with $t_0 = 1$ h could be caused by the large weakening of the specimen seen in Figure 34.
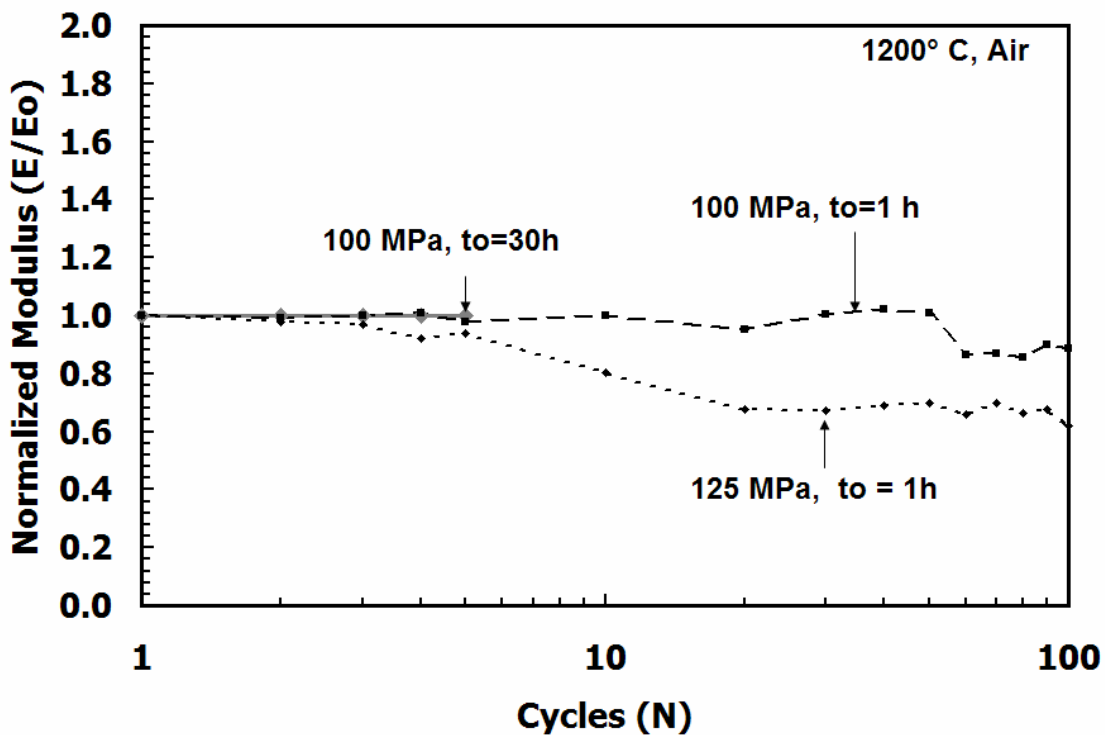
Figure 34. Normalized modulus vs. creep cycles for N720/A composite at 1200 °C in laboratory air.

5.2.4 Retained Properties

All specimens that achieved run-out in the cyclic creep tests were subjected to tensile test to failure at 1200 °C to evaluate the retained material properties. Retained strength and stiffness of the specimens, which achieved run-out are summarized in Table

10.   The initial elastic modulus of the particular specimen was used in evaluating the modulus retention for that specimen. An average UTS value from Mehrman [25] was used to evaluate strength retention for all specimens.

Table 10. Retained properties of the N720/A specimens subjected to prior cyclic creep tests at 1200 ºC in laboratory air.

Specimen #	Max Stress (MPa)	Creep and Recovery Time (h)	Retained Strength (MPa)	Strength Retention (%)	Retained Modulus (GPa)	Modulus Retention (%)	Strain at Failure (%)
P1	100	30 h	176	94.5	60.6	100	0.33
P2	100	1 h	174	93.5	60.7	99.8	0.35
P3	125	1 h	175	94.1	44.6	67.1	0.36

The specimens subjected to the 100 MPa cyclic creep tests retained nearly 100% of their modulus, while the specimen subjected to the 125 MPa cyclic creep test retained only 67% of its elastic modulus. All specimens subjected to cyclic creep tests in air retained over 93% of their tensile strength. Prior creep and recovery history had minimal effect on the failure strain. Failure strains for the specimens subjected to prior cyclic creep tests were similar to those for the as-processed material. Tensile stress-strain curves obtained for the N720/A specimens subjected to prior cyclic creep tests are presented in Figure 35 together with the tensile stress-strain curve for the as-processed material. It is seen that that prior cyclic creep and recovery history had little qualitative effect on tensile stress-strain behavior.
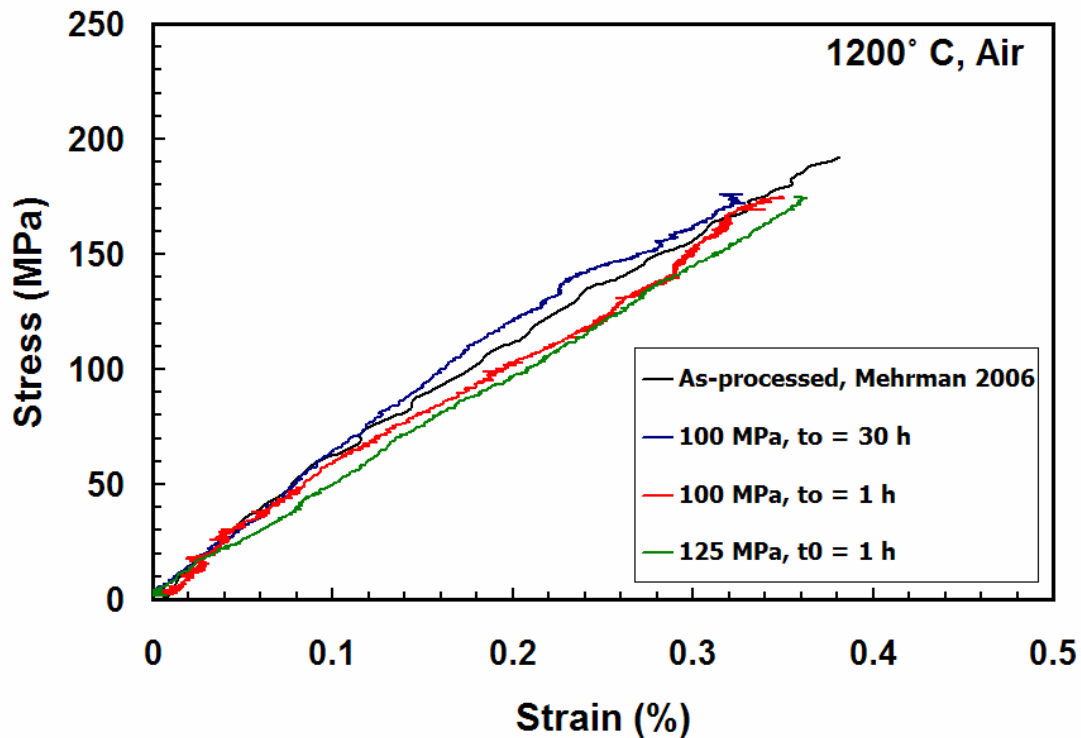
Figure 35. Effects of prior cyclic creep and recovery at 1200 °C in laboratory air on tensile stress-strain behavior of the N720/A composite.

5.2.5 Cyclic Creep and Recovery in Steam

Several tests were conducted in steam, however only two experienced a recovery period with traditional behaviors in the loading phase. The first test of 100 MPa with $t_0 =$ 1 h had the longest life time, but the stress-strain curves showed signs of kinking. Table 11 summarizes all tests in steam along with data collected by Harlan [14]. Note that P5, P6, P7 and P11 all failed before recovery could be experienced. P4 and P10 did have recovery, but both showed signs of kinking. Only P8 and P9 will be used from here on.

Table 11. Nextel 720/A test results for steam 1200 ° C.

Specimen	Max stress (MPa)	Creep and Recovery Time, t_o (h)	Creep strain (%)	Time to rupture (h)
P4	100	1	1.48	4.5
P6[b]	100	1	▪	<1
P7[b]	100	1	▪	<1
P8	100	1	1. 24	3.5
P5	125	0.167	0.77	0.147
P9	125	0.05	0.45	0.075
P10[b]	125	0.083	▪	0.108
P11	125	0.083	0.4	0.033
H1[a]	100	N/A	1.41	2.49
H2[a]	125	N/A	0.9	0.23

[a]Harlan [14]
[b]No strain data collected

5.2.5.1   Creep Curves

Results obtained in cyclic creep and recovery tests in the steam environment with the creep stress of 100 MPa are presented in Figure 36, where results obtained in the 100 MPa monotonic creep test by Harlan [14] are included for comparison. The cyclic creep data in Figure 36 as with the air tests have been compressed by removing the loading, unloading and recovery periods and plotting only strain accumulated during creep periods of each cycle. The results in Figure 36 reveal that the introduction of the unloading and recovery at near zero stress into the creep cycle increase the life slightly, but still achieves the same amount of accumulated creep strain. Both the monotonic creep test and the creep and recovery test achieved a creep strain around 1.3%, whereas in air the strain accumulated remained an order of magnitude lower after 100 h.

Creep strain vs. time curve obtained in 100 MPa cyclic creep and recovery tests (Figure 36) exhibit primary, secondary and in the final cycle a tertiary creep regimes. The same regimes were experienced by the 100 MPa monotonic creep test. Contrast to the

100 MPa creep and recovery tests in air that only had the primary and secondary creep regimes.   Finally, while the 100 MPa cyclic creep and recovery tests achieved 3.50 h, the 100 MPa monotonic creep test survived only 2.49 h.
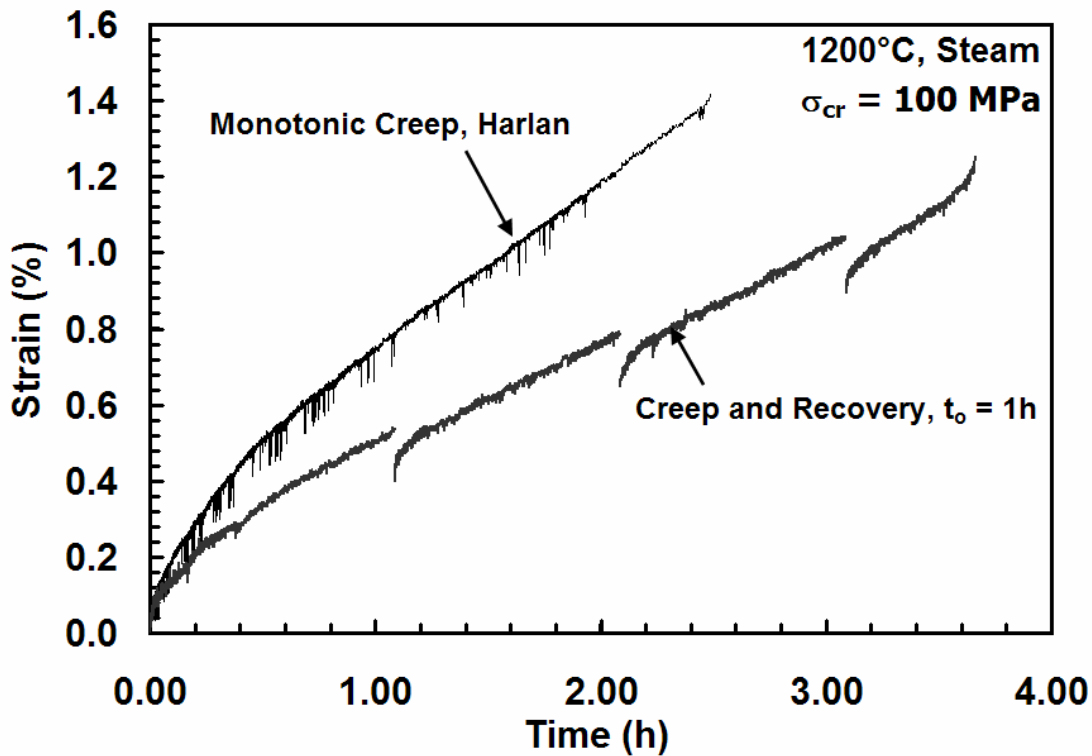
Figure 36. Creep strain vs. time curves for N720/A specimens obtained in cyclic creep tests with σ_{max} = 100 MPa and t_0 = 1 h conducted at 1200 °C in steam. Monotonic creep data at 100 MPa from Harlan [14] are also shown.

Creep strain vs. time curve obtained in 125 MPa cyclic creep and recovery test with t_0 = 0.05 h (3 min) is shown in Figure 37 together with the 125 MPa monotonic creep curve reported by Harlan [14]. As in Figure 36, the cyclic creep data in Figure 37 are compressed to permit comparison of the strain accumulated under maximum stress in cyclic creep test with that accumulated in the monotonic creep test. The specimen failed

on the second cycle at 0.075 h (4.5 min).   The final strain was less than that achieved on

the first cycle, 0.45%.   This is most likely due to a weakened specimen.   For the

monotonic creep, a creep strain of 0.9% was reached after 0.23 h (14.4 min). Clearly, the

addition of steam has significant effects on the strain and lifetime of a specimen than in

air that after 100 h of creep only achieved 0.8% of creep strain.
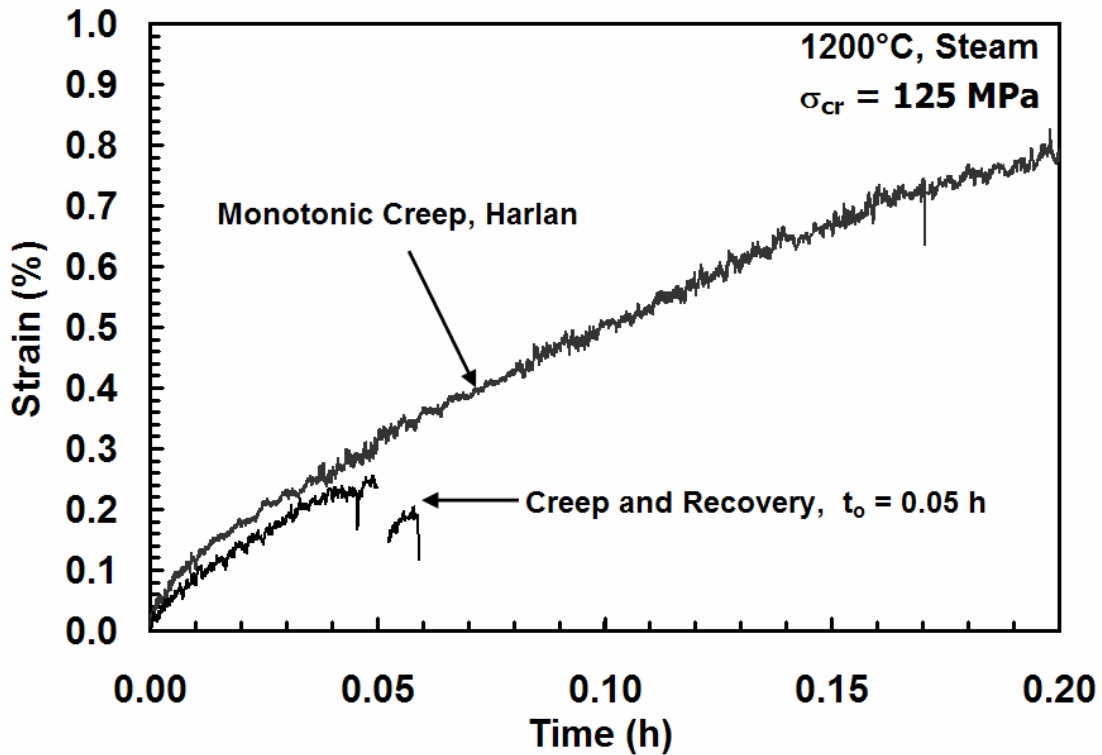
Figure 37. Creep strain vs. time curves for N720/A specimens obtained in cyclic creep tests with σ_{max} = 125 MPa and t_0 = 0.05 (3 min) conducted at 1200 °C in steam. Monotonic creep data at 100 MPa from Harlan [14] are also shown.

5.2.5.2   *Secondary Creep Rates*

Minimum creep rate, also known as secondary creep rate, was reached in both

cyclic creep and recovery tests. The steady-state creep rate for each individual cycle was

determined by applying a linear fit to the creep strain vs. time curve obtained during the

last 0.167 h (10 min) of the cycle in the test with t_0 = 1 h and 0.0083 h (0.5 min) of the

cycle in the test with t_0 = 0.05 h (3 min). It is seen in Figure 38 that for both cyclic creep tests, the creep strain rates produced during each cycle are similar to the creep rate found from the monotonic creep tests by Harlan [14]. An overall equivalent could not be found for the 125 MPa with t_0 = 0.05 h (3 min) since not enough cycles were completed. The overall equivalent creep strain rate for the 100 MPa with t_0 = 1 h is below both the average creep strain rate for the individual cycles and the monotonic creep rate. Air on the other hand not only had significant decreases in individual creep rates but the equivalent creep rates were an order of magnitude lower still compared to the monotonic creep rates.   Creep rates as a function of applied stress are presented in Figure 38, where the results of the present investigation are plotted together with the data from Harlan [14] for N720/A CMC and Nextel 720 fibers rates.
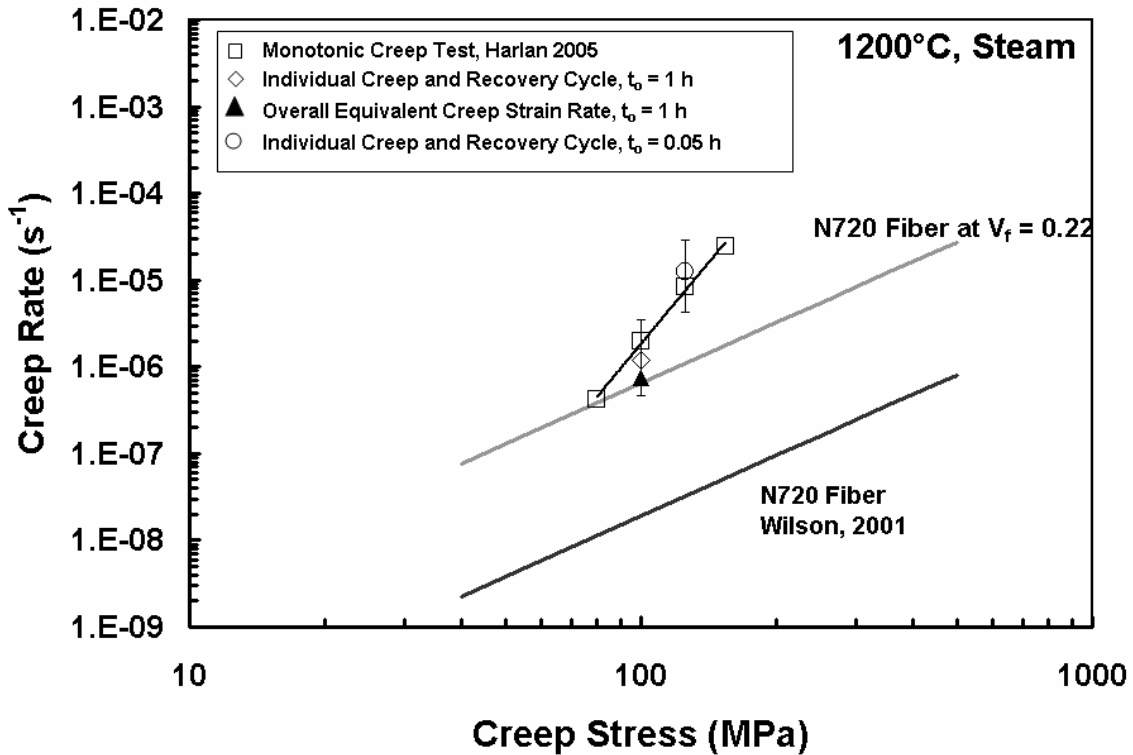
Figure 38. Secondary creep rates as a function of applied stress for N720/A ceramic matrix composite at 1200° C in steam. Data for Nextel 720 fibers (Wilson [135]) and data for N720/A from Harlan [14] are also shown.

5.2.5.3   Creep Lifetimes

Stress-rupture behavior in air is summarized in Figure 39, where creep stress is plotted vs. time to rupture (time under creep stress in the case of the cyclic creep tests). Stress-rupture data obtained in monotonic creep tests from Harlan [14] are included for comparison. The effect of introducing steam to the unloading and recovery at near zero stress effects are minimal, at best, on extending the creep life. At 100 MPa, the specimens subjected to cyclic creep tests with $t_0 = 1$ h survived 3.5 h of creep, whereas a specimen subjected to monotonic creep at 100 MPa survived 2.5 h. At 125 MPa, rupture time in monotonic creep test was 0.23 h (14.4 min), while a 0.075 h (4.5 min) time to rupture was

found in the cyclic test.   In air the life times were increased by an order of magnitude whereas in steam life was barely increased if any.
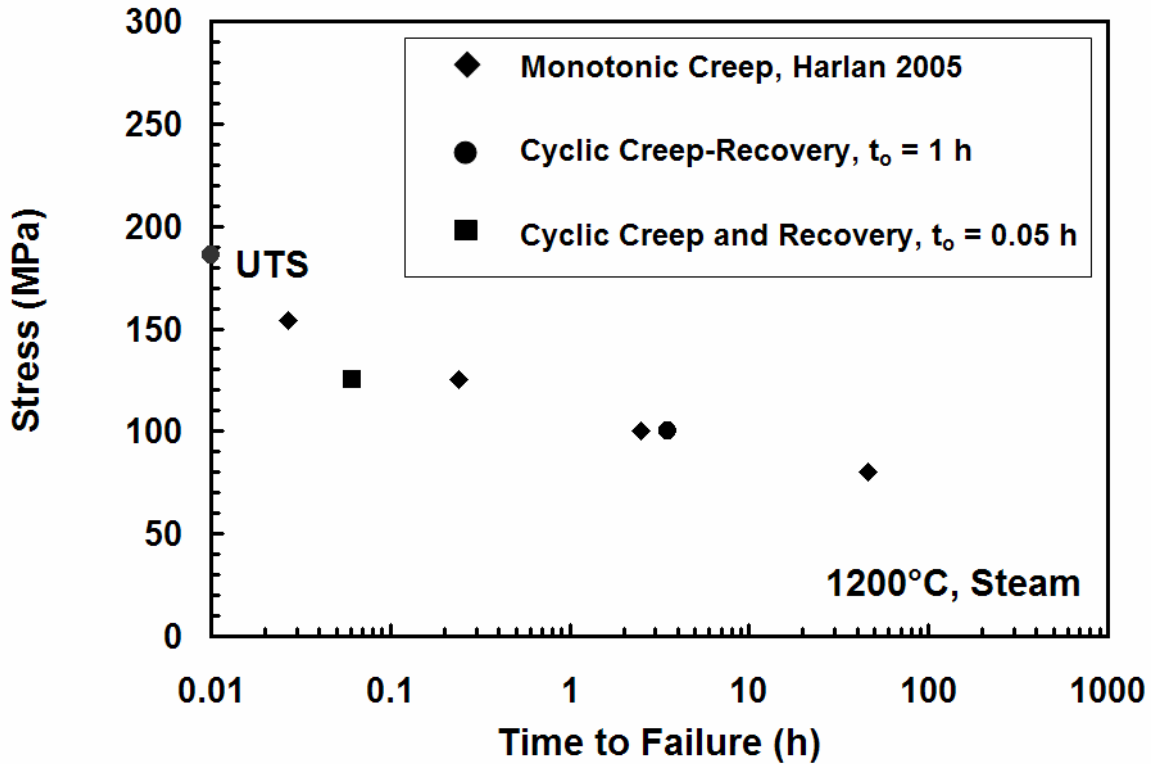
Figure 39. Creep stress vs. time to rupture for N720/A composite at 1200 °C in laboratory air. Monotonic creep data from Harlan [14].

5.2.5.4   *Recovery Curves*

Presented in Figure 40 are the strain vs. time curves obtained during all three recovery cycles in the cyclic creep test with $t_0 = 1$ h. It is seen that the amount of strain recovered is fairly constant for all cycles. Also saturation can be seen in Figure 40. After 0.3 hours, the rate of recovery is $<10^{-8}$ s^{-1}.
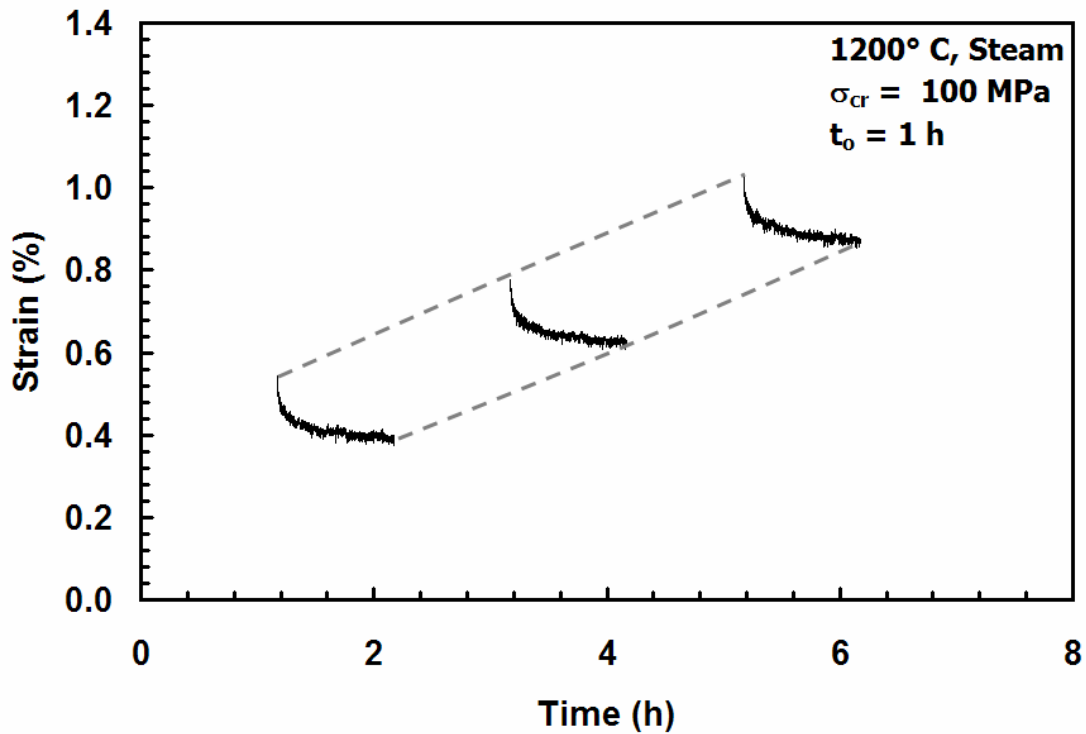
Figure 40. Strain vs. time curves for N720/A composite obtained during recovery periods of cyclic creep test with σ_{max} = 100 MPa and t_0 = 1 h conducted at 1200 °C in steam.

Only one recovery period was achieved during the 125 MPa cyclic creep test with t_0 = 0.05 h (3 min) as seen in Figure 41. A comparison cannot be made to other cycles, but a quantitative analysis on the required time to reach saturation can still be made. After 0.025 h (1.5 min), saturation was achieved. Recovery in steam after 125 MPa creep stress levels is possible, but did not increase the life.
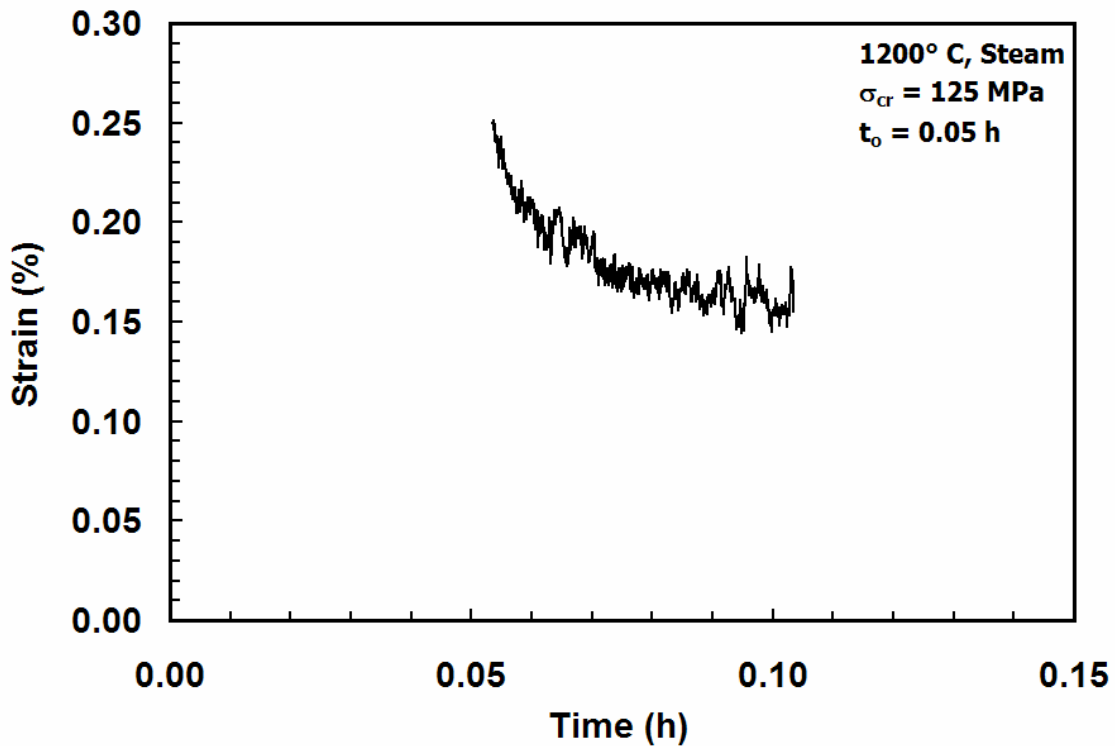
Figure 41. Strain vs. time curves for N720/A composite obtained during recovery periods of cyclic creep test with σ_{max} = 125 MPa and t_0 = 0.05 (3 min) conducted at 1200 °C in steam.

5.2.5.5   *Recovery Ratios*

In the case of the three-cycle 100 MPa test with t_0 = 1 h, the creep-strain recovery ratio (R_{cr}) increased from approximately 27% on cycle 1, to ~ 36% on cycle 2 and finally to ~ 40% on cycle 3. These results match air in that the initial cycles all increased in the amount of creep strain recovered.   However, the initial value in steam is lower than the air, >40%. The amount of recovery in the 125 MPa with t_0 = 0.05 h (3 min) is fairly large value, ~35%. Overall, recovery is possible in steam, but at lower creep stress levels the life can be increased.

57

A decrease in elastic modulus during the cyclic creep test reflects the damage development during the loading and creep portions of the cycles for both tests. The decrease for the 100 MPa with $t_0 = 1$ h reaches ~70% of the initial elastic modulus by the 3rd cycle.   In air for the 100 MPa the elastic modulus did not decrease until the 40th cycle. In comparison, after the first cycle in the 125 MPa with $t_0 = 0.05$ h (3 min) the elastic modulus was ~65 % of the initial.   This supports the early failure of the specimen.   In air the elastic modulus decreased throughout the first few cycles but leveled off at ~67% of the initial.

5.2.6   Composite Microstructure

Both optical and scanning electron microscopes were utilized to observe the fracture surfaces in order to develop a better understanding of the damage and failure mechanisms. The specimen fracture surfaces produced in this investigation exhibited several common trends. Three common types of failure and damage were observed: (1) brushy failure indicative of fiber pullout, (2) nearly planar coordinated failure of fibers and matrix, and (3) matrix densification. Brushy fracture surface represents random fiber failures and indicates that the cracks are being deflected around the fibers, i.e. the matrix porosity is maintained at a level sufficient to provide for damage tolerance. Coordinated fiber failure occurs in the regions where matrix densification took place decreasing the matrix porosity and inhibiting crack deflection. In this case the matrix cracks are not deflected around the fibers, but propagate through the matrix and the fibers.

5.2.7 Optical Microscopy

5.2.7.1 Air

Optical micrographs of fracture surfaces obtained in cyclic creep and recovery tests conducted at 1200 °C in air with maximum stresses of 100 and 125 MPa are shown in Figure 42 and 43, respectively. Optical micrographs of the fracture surfaces obtained in the monotonic creep tests at 100 and 125 MPa, at 1200 °C in air from prior work [14] are included in Figure 42 and 43 for comparison. Side views of the fracture surfaces obtained in cyclic creep and recovery tests conducted in air are presented in Figure 44.
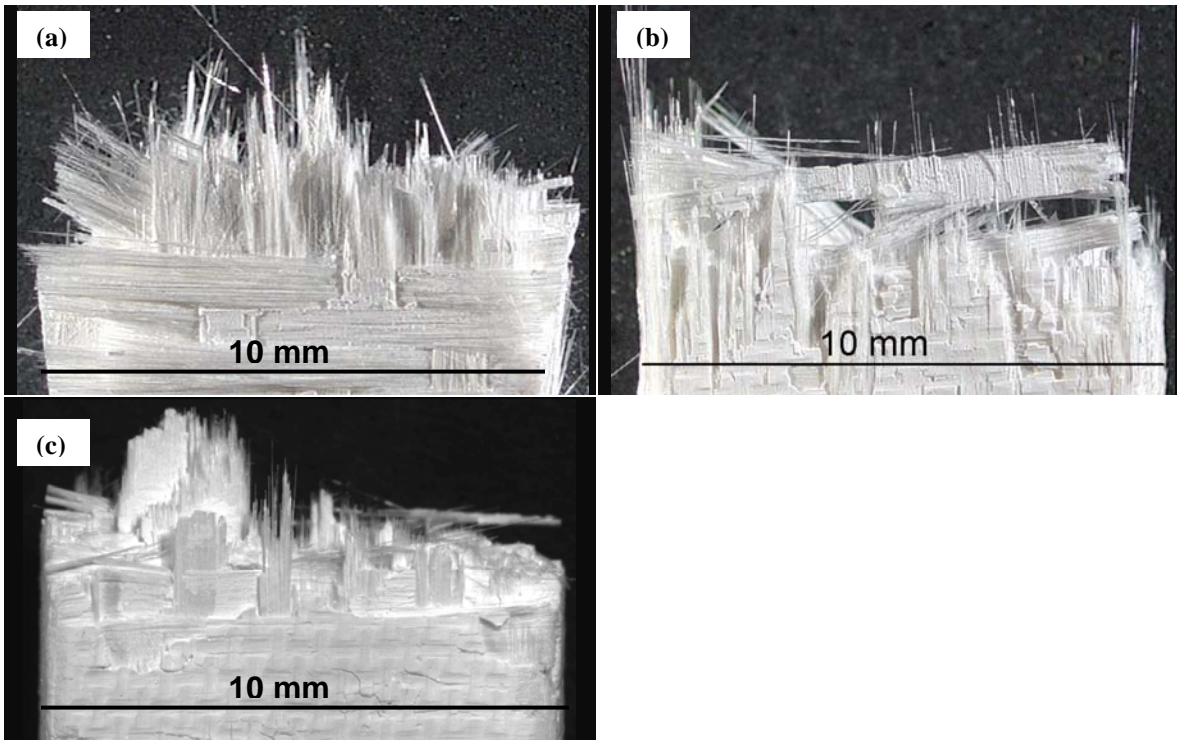
Figure 42. Fracture surfaces of the N720/A specimens subjected to tests with $\sigma_{max} =$ 100 MPa at 1200 °C in laboratory air: (a) cyclic creep and recovery test with $t_0 = 1$ h, (b) cyclic creep and recovery test with $t_0 = 30$ h, (c) monotonic creep test, data from Harlan [14].
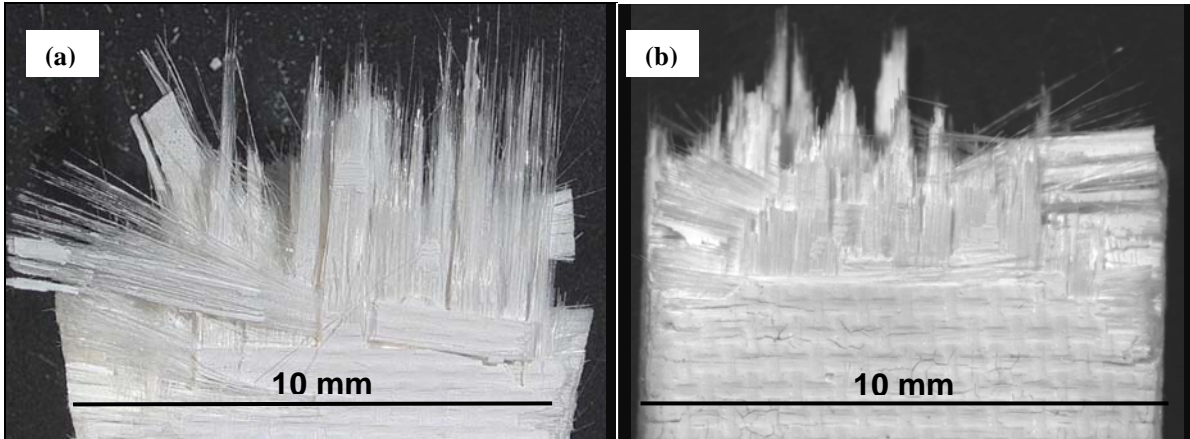
Figure 43. Fracture surfaces of the N720/A specimens subjected to tests with σ_{max} = 125 MPa at 1200 °C in laboratory air: (a) cyclic creep and recovery test with t_0 = 1 h, (b) monotonic creep test, data from Harlan [14].
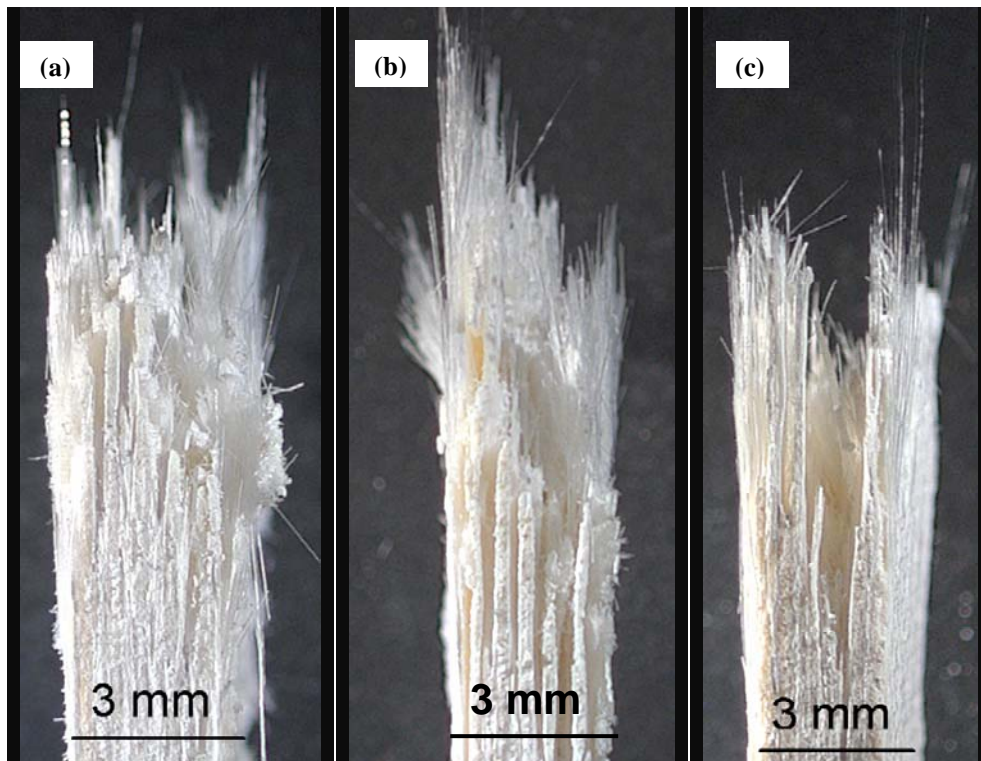
Figure 44. Fracture surfaces (side views) of the N720/A specimens subjected to cyclic creep and recovery tests at 1200 °C in laboratory air: (a) σ_{max} = 100 MPa and t_0 = 1 h, (b) σ_{max} = 100 MPa and t_0 = 30 h, (c) σ_{max} = 125 MPa and t_0 = 1 h.

Note that all specimens tested in cyclic creep and recovery in air achieved a run-out and failed in the subsequent tensile test. The fracture planes of all specimens tested in

cyclic creep and recovery in air are not well defined. The 0° fiber tows break over a wide range of axial locations, in general spanning the entire width of the specimen. The fibers in the 0° tows in each cloth layer exhibit random failure, producing brushy fracture surfaces. It is seen that the specimens tested in cyclic creep and recovery exhibit longer damage zones than the specimens tested in monotonic creep, which also produced considerably shorter lifetimes. It has been observed in prior work [26] that N720/A specimens which exhibit longer lifetimes invariably produce longer damage zones. This observation can be extended to the results of the present investigation.

Optical micrographs of fracture surfaces obtained in cyclic creep and recovery tests conducted at 1200 °C in steam are shown in Figure 45, where optical micrographs of the fracture surfaces obtained in the monotonic creep tests at 100 and 125 MPa at 1200 °C in steam from prior work [14] are included for comparison. Side views of the fracture surfaces obtained in cyclic creep and recovery tests conducted in steam are presented in Figure 46. It is seen that the damage zones produced in cyclic creep and recovery tests conducted in steam are considerably shorter than those produced in cyclic creep in air. The lifetimes produced in cyclic creep tests in steam are much reduced compared to those obtained in like tests in air. Still, the damage zones obtained in cyclic creep tests conducted in steam are somewhat longer than those obtained in the monotonic creep tests in steam for a given creep stress level. Once again, longer damage zones correspond to longer lifetimes.

The time to rupture for the 100 MPa with $t_0 = 1$ h was 3.5 h, while the monotonic creep test resulted in 2.49 h until failure. The damage areas reflect these lifetimes. The 125 MPa with $t_0 = 0.05$ h (3 min) test only lasted 0.075 h (4.5 min), less than the

monotonic creep of 0.23 h (14.4 min). The 90° two fibers are pulled out on both specimens, but the creep and recovery test specimen shows the fibers glued together, whereas the monotonic creep fibers are more separated.
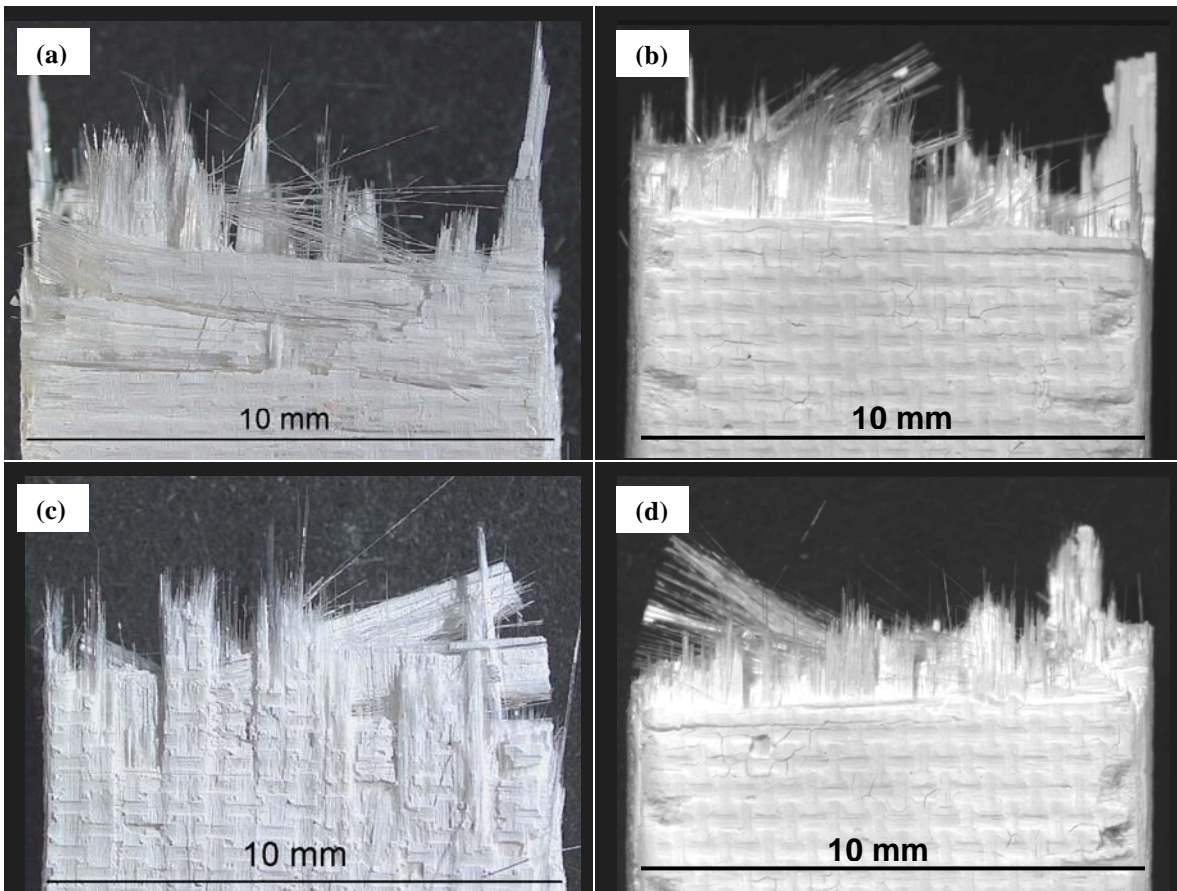
Figure 45. Fracture surfaces of the N720/A specimens tested at 1200 °C in steam: (a) cyclic creep and recovery test with σ_{max} = 100 MPa t_0 = 1 h, (b) monotonic creep test with σ_{max} = 100 MPa, from Harlan [14], (c) cyclic creep and recovery test with σ_{max} = 125 MPa t_0 = 0.05 h (3 min), (d) monotonic creep test with σ_{max} = 125 MPa, from Harlan [14].
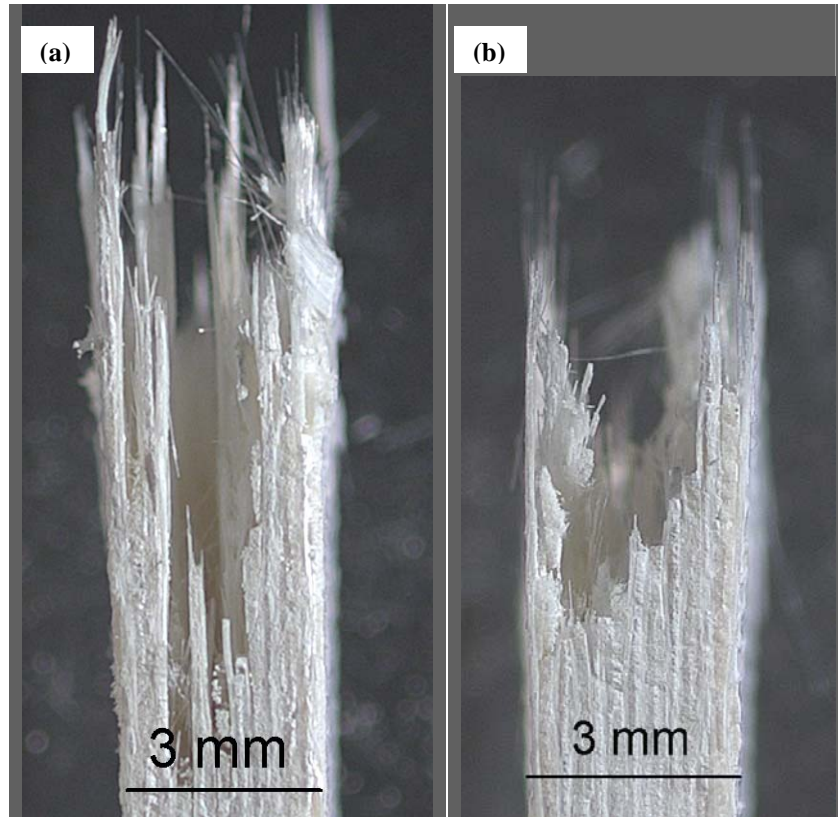
Figure 46. Fracture surfaces (side views) of the N720/A specimens subjected to cyclic creep and recovery tests at 1200 °C in steam: (a) σ_{max} = 100 MPa and t_0 = 1 h, (b) σ_{max} = 125 MPa and t_0 = 0.05 (3 min).

5.2.8   Scanning Electron Microscopy

The typical failure phenomena's will be overviewed first. In Figure 47 (a) is an example of matrix densification in a Nextel 720/A specimen. When the matrix becomes denser the interface between the fibers and the matrix degrades, allowing the matrix to attach to the fibers as in Figure 47 (b). Fiber pullout is a commonality in all specimens and is seen in Figure 47 (c). The final phenomenon looked for is planar fractures Figure 47 (d).
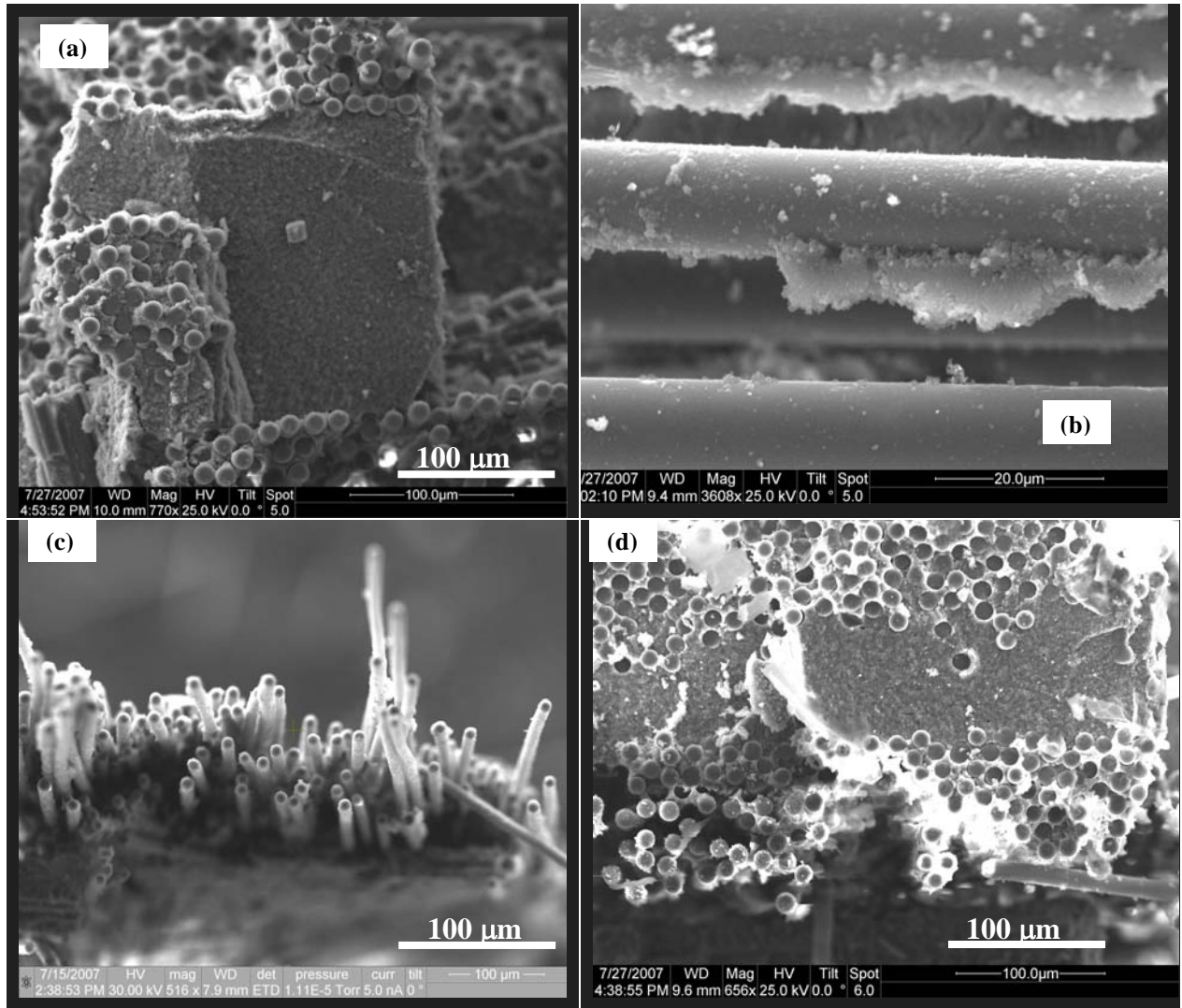
Figure 47. Fracture surfaces of the N720/A specimen tested for creep recovery in steam (a,c and d) and air (c) at 1200 °C showing: (a) σ_{max} = 125 MPa with t_o =0.05 h, (b) σ_{max} = 125 MPa with t_o =0.05 h, (c) σ_{max} = 125 MPa with t_o = 1 h (d) σ_{max} = 125 MPa with t_o = 0.05 h.

The porous nature of alumina allows for crack deflection. In Figure 48 (a) a crack can be seen down the center and around the 0 ° fibers. Also demonstrated is a trough where a 90 ° fiber was pulled out. The grains of the alumina matrix are about ~0.5 μm. In Figure 48 (b) a micrograph of those grains can be seen as well as how porous the matrix is.

64
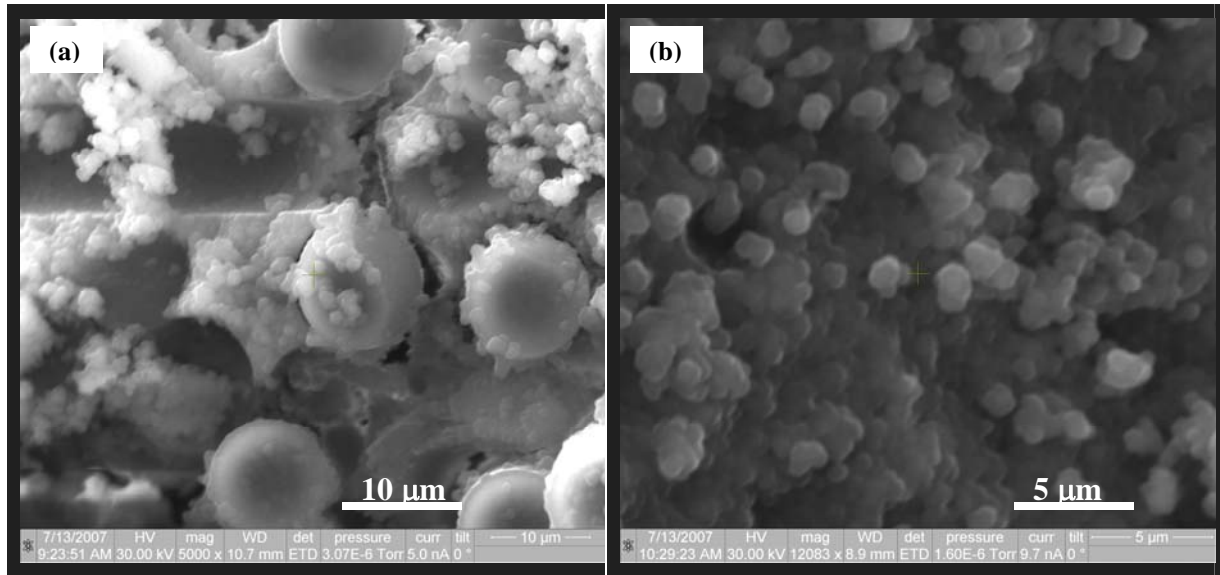
Figure 48. Fracture surfaces of the N720/A specimen tested for creep recovery in air at 1200 °C 100 MPa with 30 hour hold times showing: (a) crack deflection and (b) alumina matrix.

All fracture surfaces obtained in this effort were observed with the SEM. Fracture surfaces of the specimens subjected to cyclic creep and recovery tests in air are presented in Figure 49 followed by micrographs provided by Harlan [14] in Figure 50.
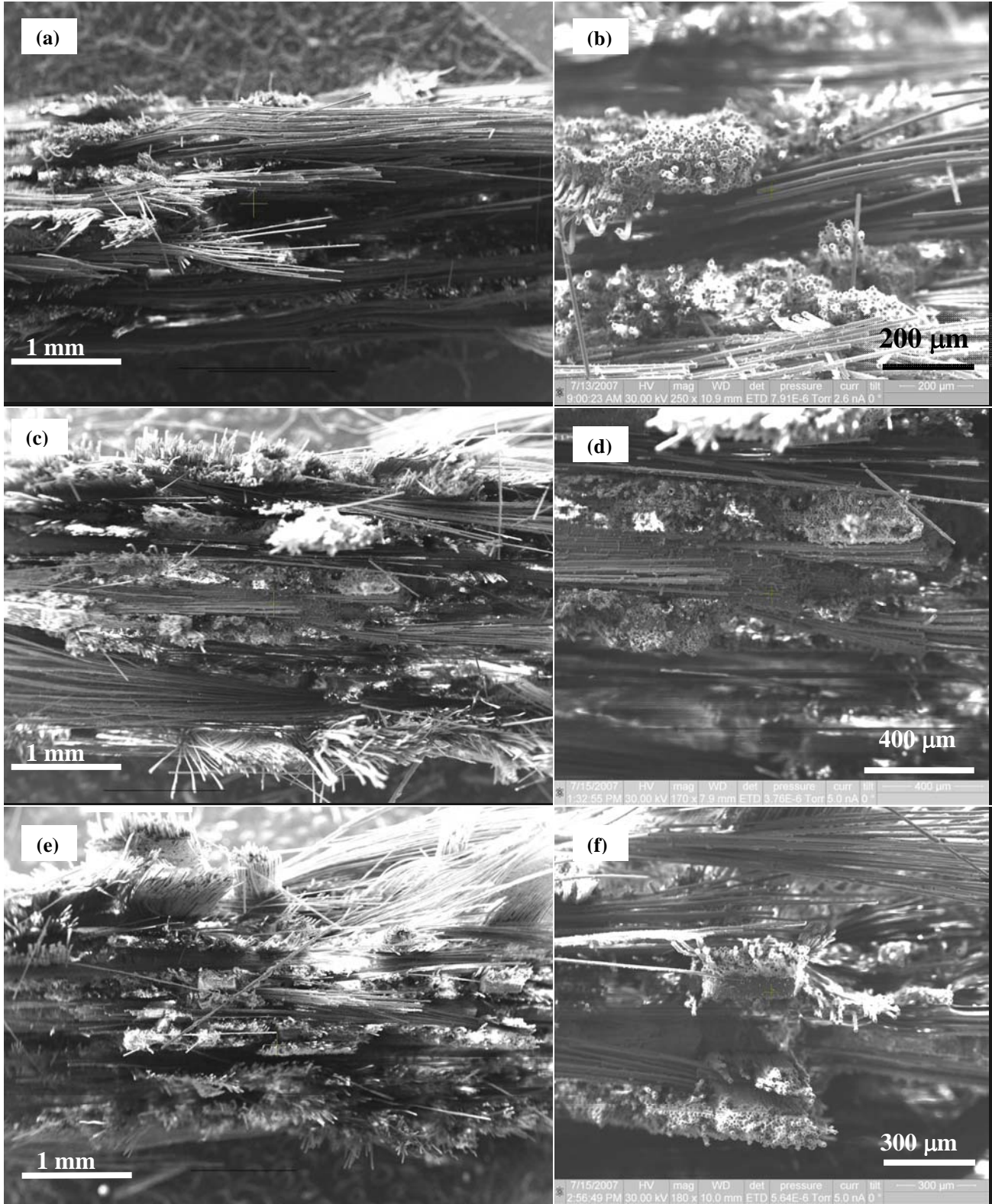
Figure 49. Fracture surfaces of the N720/A specimens subjected to cyclic creep and recovery tests at 1200 °C in laboratory air: (a)-(b) σ_{max} = 100 MPa and t_0 = 1 h, (c)-(d) σ_{max} = 100 MPa and t_0 = 30 h, (e)-(f) σ_{max} = 125 MPa and t_0 = 1 h.
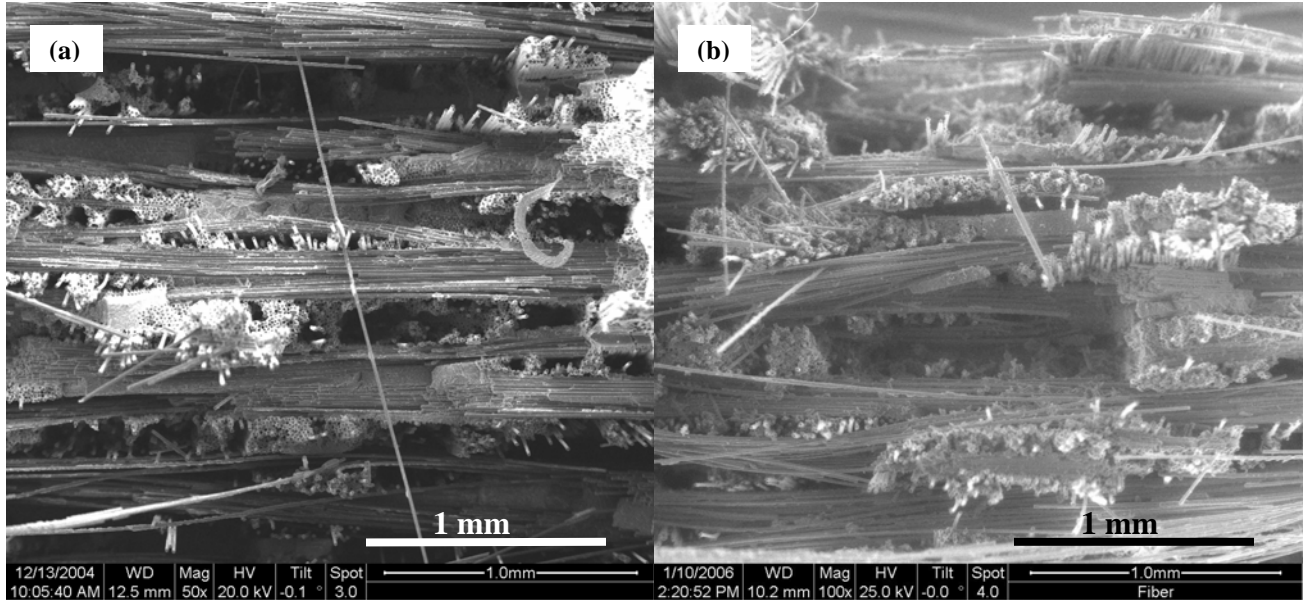
Figure 50. Fracture surfaces of the N720/A specimens subjected to monotonic creep at 1200 °C in laboratory air from Harlan [14]: (a) σ_{max} = 100 MPa and (b) σ_{max} = 125 MPa.

It is seen that all fracture surfaces in Figure 49 contain brushy regions of fibrous fracture as well as regions of flatter, more coordinated fracture topography. The balance of these two fracture topographies within a given fracture surface is influenced by the test parameters, i. e. creep stress level and the uninterrupted time under creep stress. It is seen that the amount of fiber pullout decreases with increasing hold time and with increasing applied stress. Note that similar observations were reported in prior investigations of N720/A CMC [14; 25]. Even though the fracture surfaces of the specimens subjected to cyclic creep tests in air are dominated by the areas of fibrous fracture with noticeable fiber pullout, the fibers are not "cleanly" pulled and pieces of matrix material remain bonded to the pulled out fibers (see Figure 51).
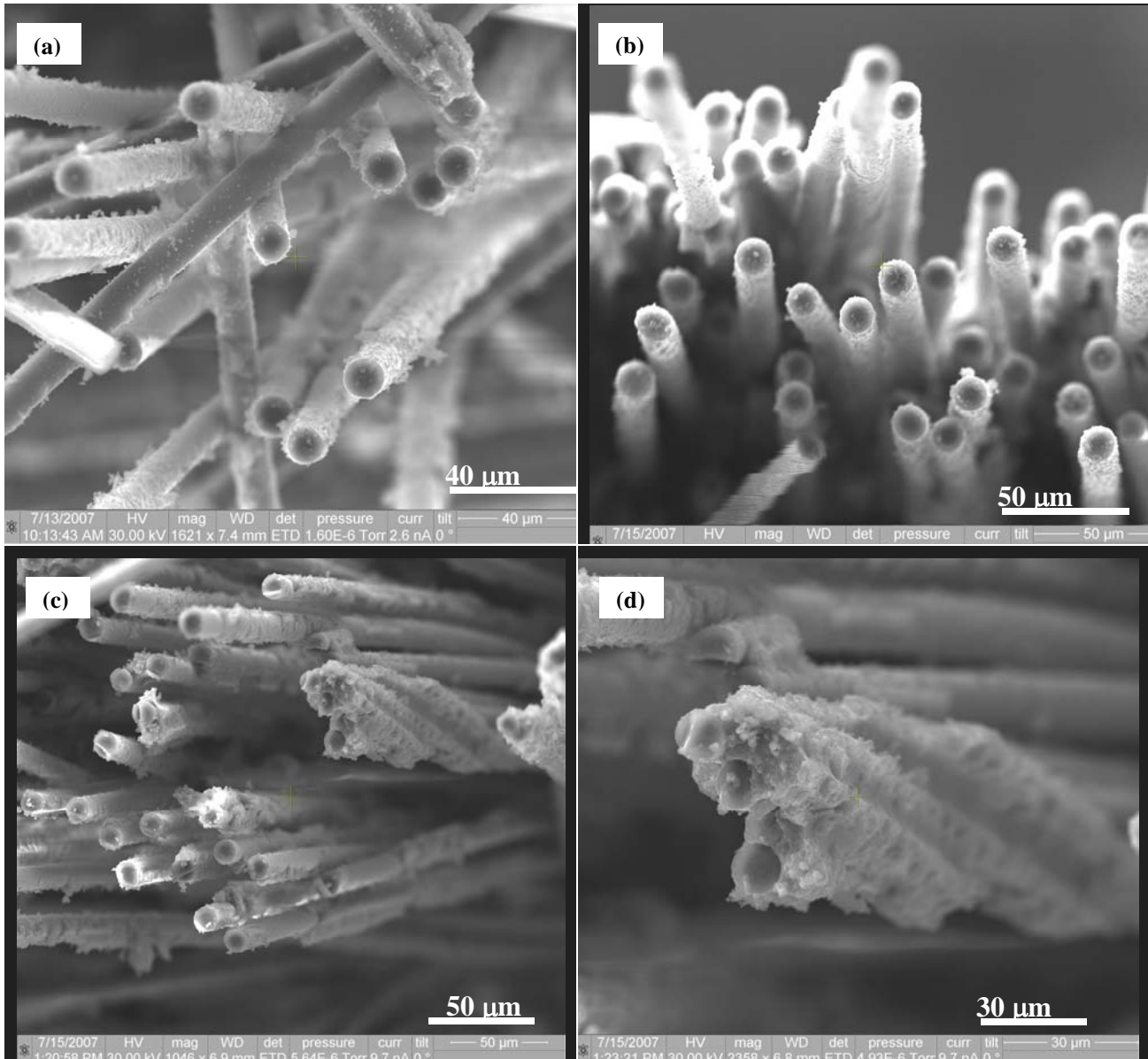
Figure 51. Fracture surfaces of the N720/A specimens subjected to cyclic creep and recovery tests at 1200 °C in laboratory air: (a) σ_{max} = 100 MPa and t_0 = 1 h, (b) σ_{max} = 100 MPa and t_0 = 30 h, and (c-d) σ_{max} = 125 MPa and t_0 = 1 h. All micrographs show matrix particles bonded to the pulled out fibers.

Fracture surfaces of the specimens subjected to cyclic creep and recovery tests in steam are shown in Fig. 30 along with the fracture surfaces obtained in monotonic creep tests conducted at 100 and 125 MPa in steam from prior work by Harlan [14] for comparison. It is seen that the fracture surfaces produced in steam also exhibit both the regions of fibrous fracture and the areas of coordinated fiber failure. However, in this

case coordinated fiber fracture is the prevailing failure mechanism. Consistent with the previously described observations, the fracture surfaces dominated by the coordinated fiber fracture go together with the shorter lifetimes (3.5 h in the 100 MPa cyclic creep test, 2.49 h in the 100 MPa monotonic creep test, 0.075 h in the 125 cyclic creep test, and 0.23 h in the 125 MPa monotonic creep test). Note that the shortest lifetimes as well as the most planar fracture surfaces were produced in monotonic creep tests.

All optical micrographs and SEM micrographs not pictured in this section can be seen in Appendix A and B, respectively.
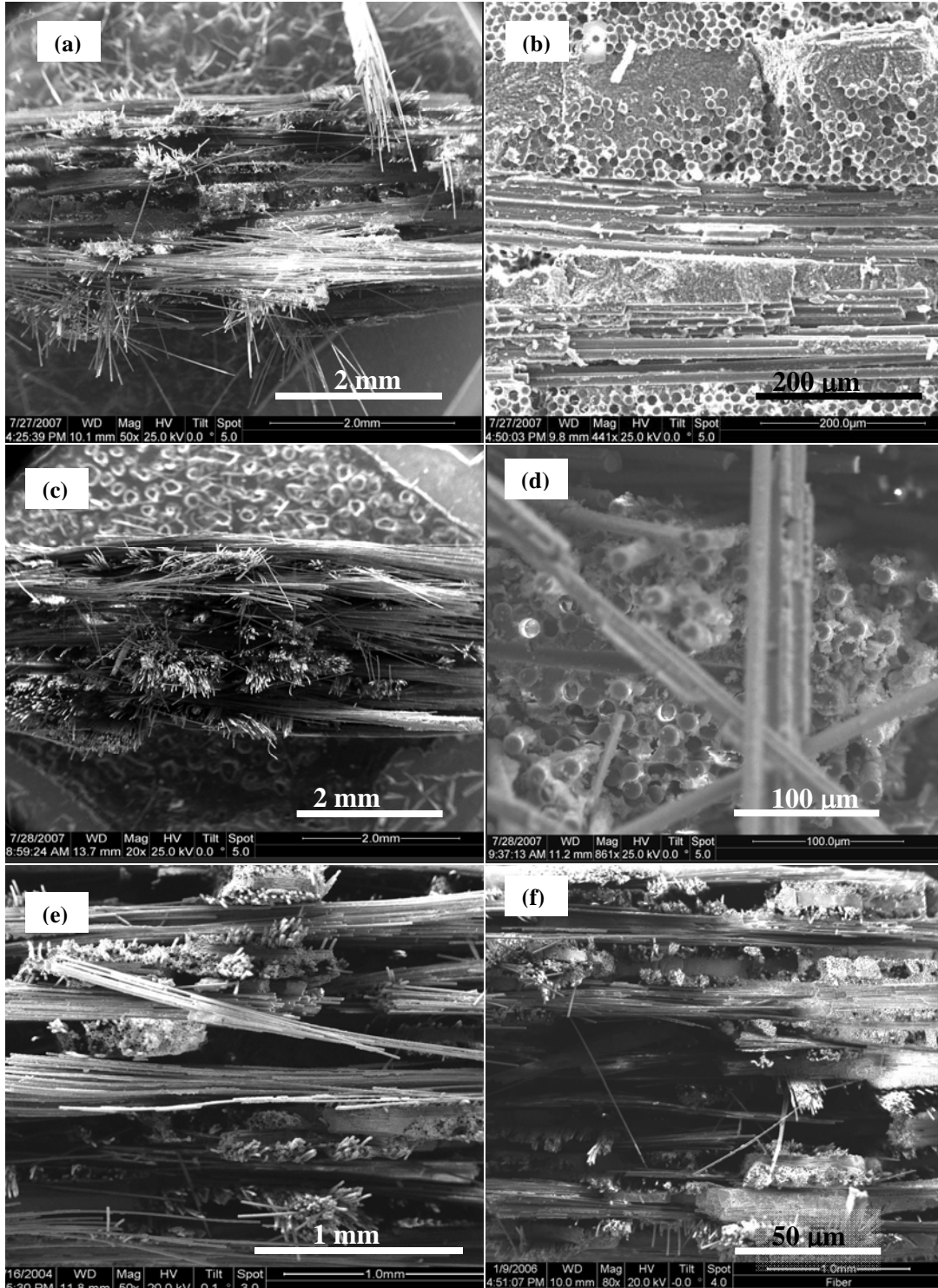
Figure 52. Fracture surfaces of the N720/A specimens tested at 1200 °C in steam: (a)-(b) cyclic creep and recovery test with σ_{max} = 100 MPa and t_0 = 1 h (c)-(d) cyclic creep and recovery test with σ_{max} = 125 MPa and t_0 = 0.05 h (3 min) , (e) monotonic creep test with σ_{cr} = 100 MPa, and (f) monotonic creep test with σ_{max} = 125 MPa.

70

VI. Observations and Conclusions

6.1 Concluding Remarks on the Compressive Behavior of the N610/A Composite with Z-Pin Reinforcement

Initial compressive testing of the N610/A specimens with the Z-pin reinforcement produced compressive strength values on the order of 14 MPa, which were considerably below the expected compressive strength values in excess of 190 MPa. Optical micrographs of the as-processed material revealed extensive interlaminar matrix cracking, suggesting that the composite was not properly fabricated and that further testing would not be useful.

Process control is critical to the fabrication of CMCs. Although the N610/A panels without the Z-pin reinforcement were supposedly processed in the same manner as the composite used in prior work [12], the microstructural investigation revealed that the processing of the N610/A panels supplied for this research was different. The as-processed N610/A panels with and without the Z-pin reinforcement contained multiple large interlaminar cracks, which caused early failures in compression. The details of the CMC processing could not be obtained. Therefore, it is difficult to comment on what aspects of the CMC fabrication process may have caused the extensive interlaminar cracking.

6.2 Cyclic Creep and Recovery of the N720/A Ceramic Composite at 1200 °C in Air

In laboratory air, introduction of the intermittent periods of unloading and recovery at near zero stress into the creep test had a profound effect on the creep lifetime. While creep lifetimes in all cyclic creep tests conducted in air exceeded 100 h, creep

lifetimes obtained in the monotonic creep tests were 41 h (at 100 MPa) and mere 4.25 h (at 125 MPa). Strain recovery provides a powerful mechanism for the reduction of creep strain and extension of creep lifetime of the N720/A ceramic composite at 1200 °C in air. Recognizing that in the case of this porous-matrix ceramic composite creep loading is considerably more damaging than cyclic fatigue, it is likely that the strain recovery can significantly increase the life of cyclically loaded N720/A structural components.

Minimum creep rates were reached in all tests. In air, overall equivalent creep strain rates produced in cyclic creep tests were one to two orders of magnitude lower than those obtained in the monotonic creep tests for a given creep stress level.

The N720/A ceramic composite subjected to over 100 h of creep in the course of the cyclic creep and recovery tests at 100 MPa in air retained over 94% of its tensile strength and near 100 % of its elastic modulus. Specimens subjected to prior cyclic creep and recovery tests at 125 MPa in air retained over 94 % of their tensile strength, but only ~ 67% of their tensile modulus. The decrease in modulus may be due to progressive matrix microcracking.

Considerable recovery of creep strain was observed in all tests conducted in laboratory air. In creep and recovery tests conducted in air, 80 to 98 % of creep strain was recovered during each cycle. Specimens tested with a shorter 1-h creep and recovery time were able to recover a larger percentage of the creep strain accumulated during each individual cycle. Less creep strain is accumulated during the shorter creep time. The lower creep strain is then more readily recovered. Recovery saturation, defined as reaching recovery strain rate magnitude of ~ 10^{-8} s^{-1} was achieved in all cycles of each

72

test. Time required to achieve recovery saturation increases with increasing prior creep time.

6.3 Cyclic Creep and Recovery of the N720/A Ceramic Composite at 1200° C in Steam

The presence of steam significantly degraded material performance and reduced creep lifetimes in the cyclic creep and recovery tests at 100 and 125 MPa. Furthermore, in the presence of steam, introduction of the intermittent periods of unloading and recovery at near zero stress had no effect on the overall creep lifetimes. At 100 MPa, overall creep lifetime in the cyclic creep test (3.5 h) was only slighter higher than that obtained in the monotonic creep test (2.5 h) in prior work [14]. At 125 MPa, the creep lifetimes were ~ 0.23 h (14 min) in monotonic creep test and ~ 0.075 h (4.5 min) in cyclic creep test. The equivalent overall creep rates obtained in cyclic creep and recovery tests were also similar to those obtained in monotonic creep test at a given creep stress level.

It is noteworthy that despite negligible effects of recovery on creep lifetimes in steam, recovery of creep strain was still observed. In creep and recovery tests conducted in steam, percentage of creep strain recovered during each individual cycle ranged from 35 - 40%. As with air saturation was achieved even in steam. Tests at 100 MPa required 0.3 h to reach saturation, while steam needed 0.0083 (1.5 min).

6.4 Composite Microstructure

Observations pertaining to composite microstructure and damage and failure mechanisms were similar to those reported earlier [5; 14; 25]. All fracture surfaces

obtained in this study contain regions of uncoordinated brushy failure with extensive fiber pullout as well as areas of nearly planar fracture. Balance of the two types of fracture topography within a fracture surface is influenced by applied stress level, duration of the creep period, and test environment. Extensive uncorrelated fracture is prevalent in fracture surfaces produced in laboratory air, while coordinated fiber failure dominates those obtained in steam. The appearance of the fracture surface can be correlated with time to failure. Predominantly planar fracture surface accompanies a short lifetime, while brushy fibrous fracture corresponds to a longer life.

Prior research into the mechanical behavior of the N720/A ceramic composite at 1200 °C and in steam [32; 26] revealed that slow crack growth in the fiber due to stress corrosion is the governing failure mechanism in steam. In the presence of steam, crack growth in the fiber is caused by a chemical interaction of water molecules with mechanically strained Si-O bonds at the crack tip with the rate of chemical reaction increasing exponentially with applied stress. Results of the present investigation are consistent with these observations.

6.5 Recommendations

Future efforts can be focused on understanding the microstructural mechanisms occurring during recovery at near zero stress. It is possible that both fibers and matrix undergo beneficial transformations during the recovery periods. Strain recovery should be further studied and analyzed to determine the extent of its effects on life extension of cyclically loaded porous-matrix CMC structural components. Different temperatures should be investigated in both air and in steam to identify regimes where strain recovery

can be used to reduce creep strains and extend lifetimes under cyclic creep or fatigue loading.
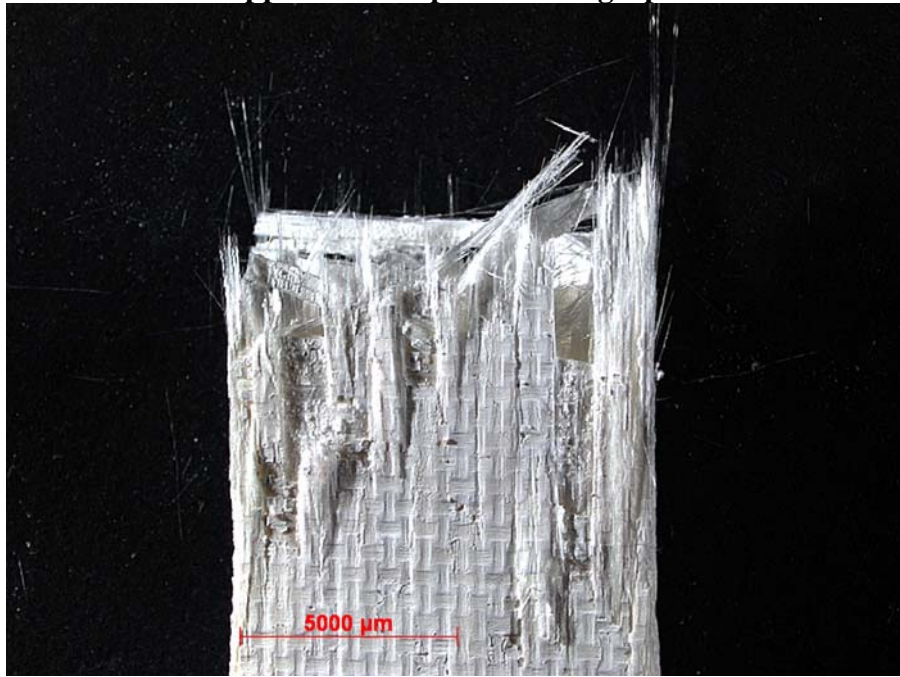
Figure 53. Fracture surface of N720/A specimen tested with cyclic creep-recovery with 30 hour hold times at 100 MPa in air at 1200 °C.

Figure 54. Fracture surface of N720/A specimen tested with cyclic creep-recovery with 30 hour hold times at 100 MPa in air at 1200 °C.
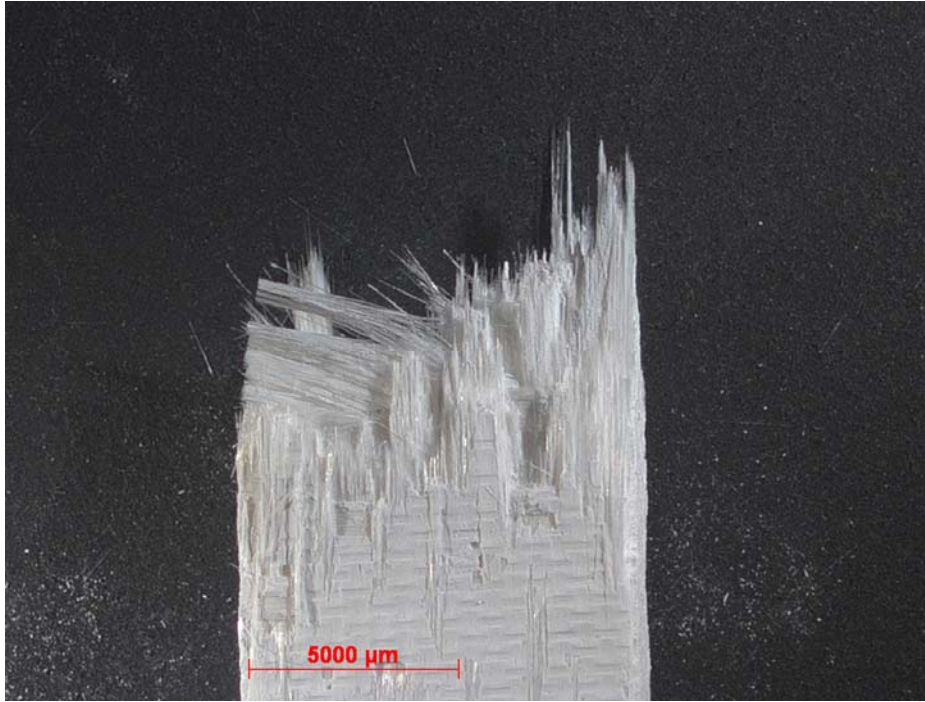
Figure 55. Fracture surface of N720/A specimen tested with cyclic creep-recovery with 30 hour hold times at 100 MPa in air at 1200 °C.
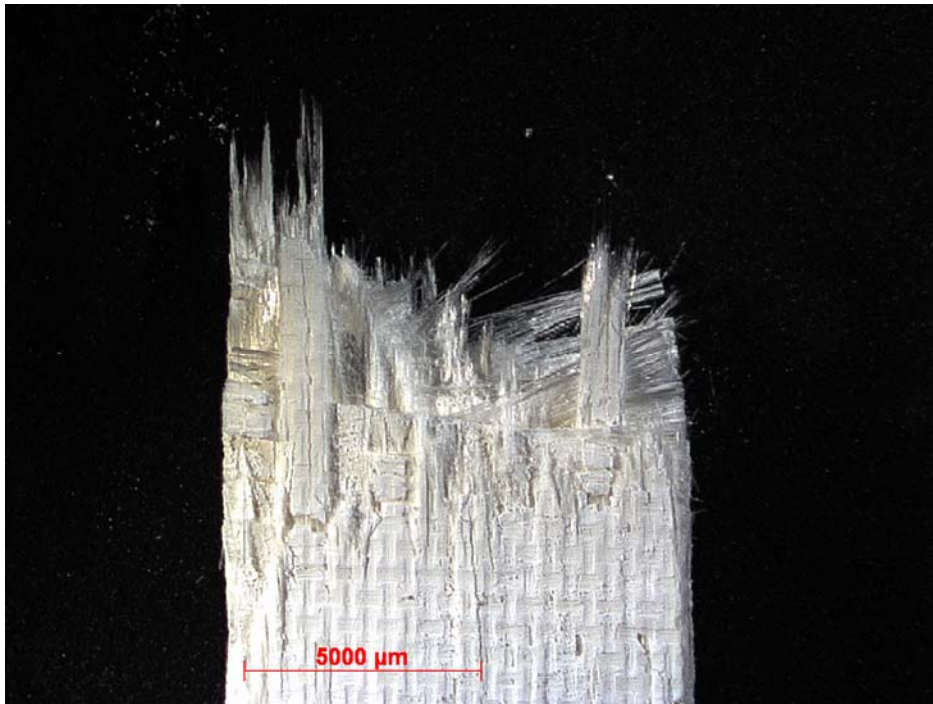

Figure 56. Fracture surface of N720/A specimen tested with cyclic creep-recovery with 30 hour hold times at 100 MPa in air at 1200 °C.
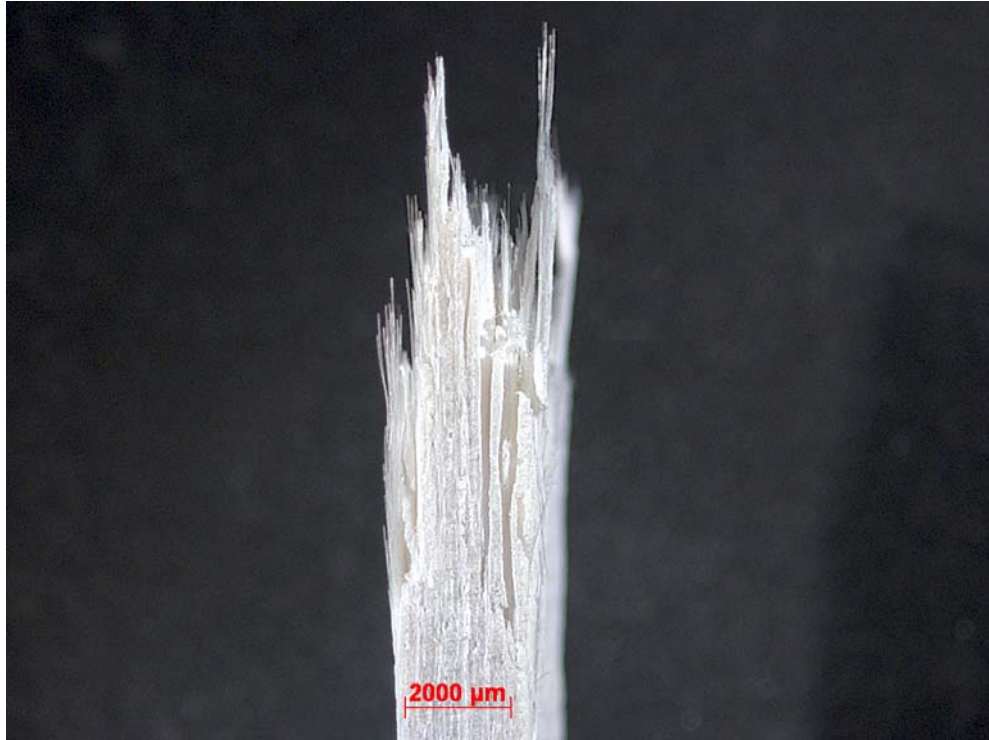
Figure 57. Fracture surface of N720/A specimen tested with cyclic creep-recovery with 30 hour hold times at 100 MPa in air at 1200 °C.
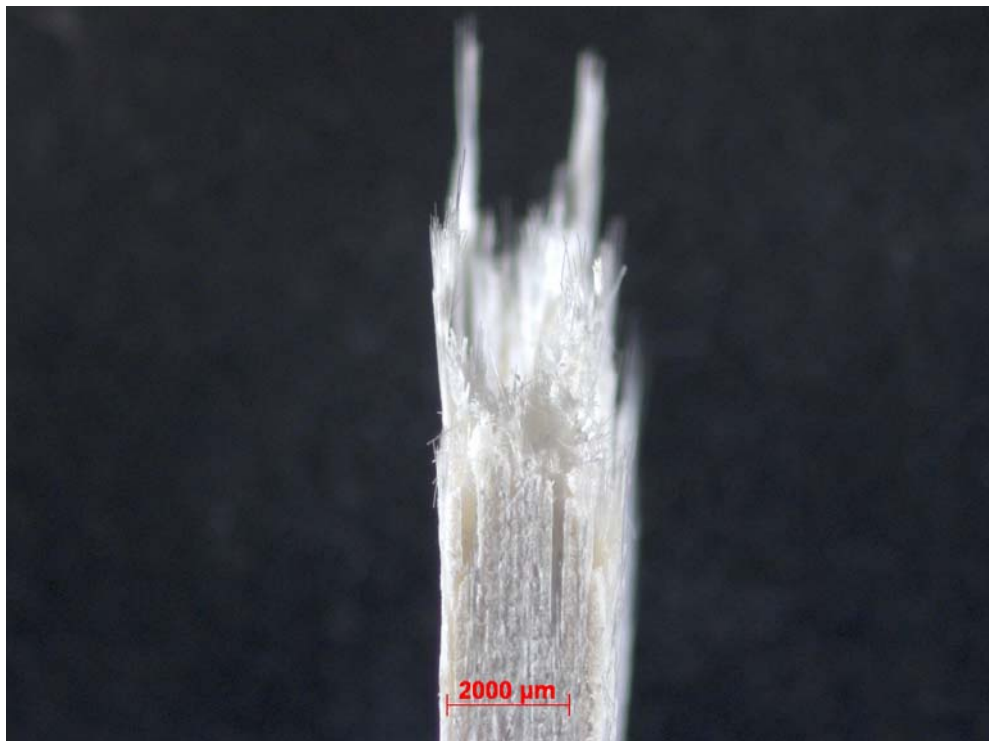
Figure 58. Fracture surface of N720/A specimen tested with cyclic creep-recovery with 30 hour hold times at 100 MPa in air at 1200 °C.
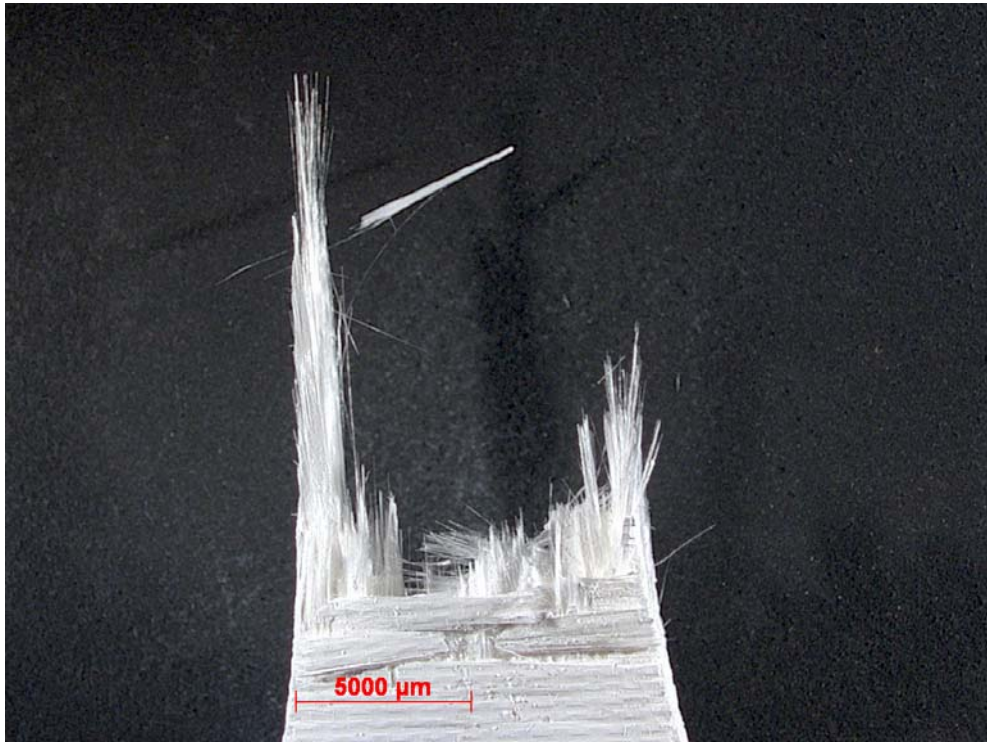
Figure 59. Fracture surface of N720/A specimen tested with cyclic creep-recovery with 1 hour hold times at 100 MPa in air at 1200 °C.
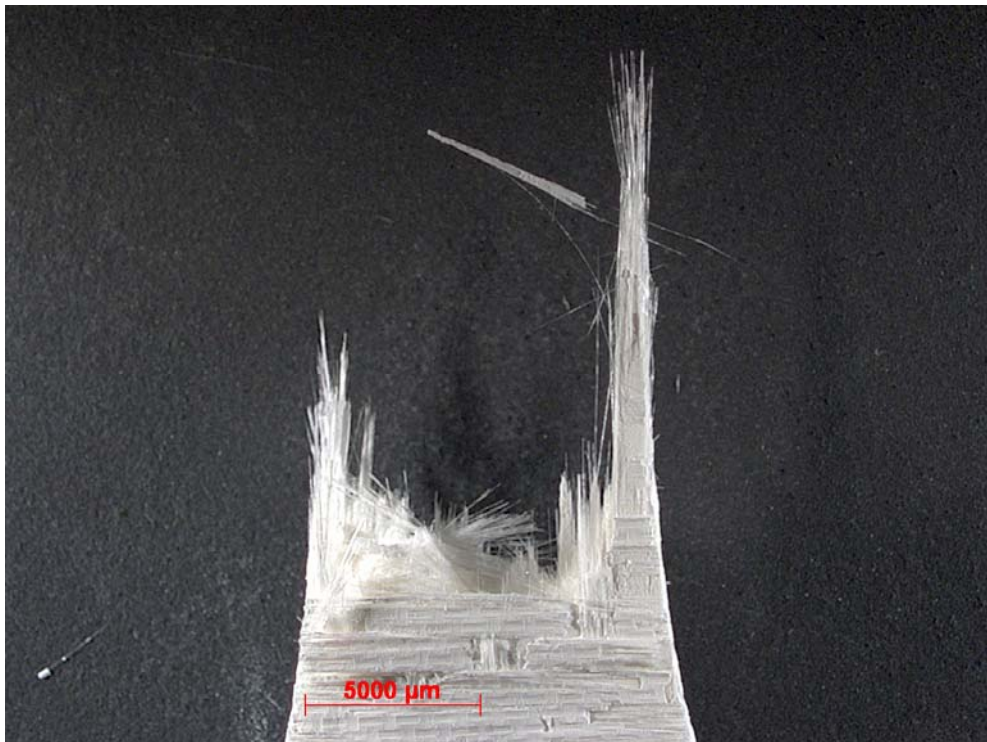
Figure 60. Fracture surface of N720/A specimen tested with cyclic creep-recovery with 1 hour hold times at 100 MPa in air at 1200 °C.

Figure 61. Fracture surface of N720/A specimen tested with cyclic creep-recovery with 1 hour hold times at 100 MPa in air at 1200 °C.


Figure 62. Fracture surface of N720/A specimen tested with cyclic creep-recovery with 1 hour hold times at 100 MPa in air at 1200 °C.

Figure 63. Fracture surface of N720/A specimen tested with cyclic creep-recovery with 1 hour hold times at 100 MPa in air at 1200 °C.

Figure 64. Fracture surface of N720/A specimen tested with cyclic creep-recovery with 1 hour hold times at 100 MPa in air at 1200 °C.
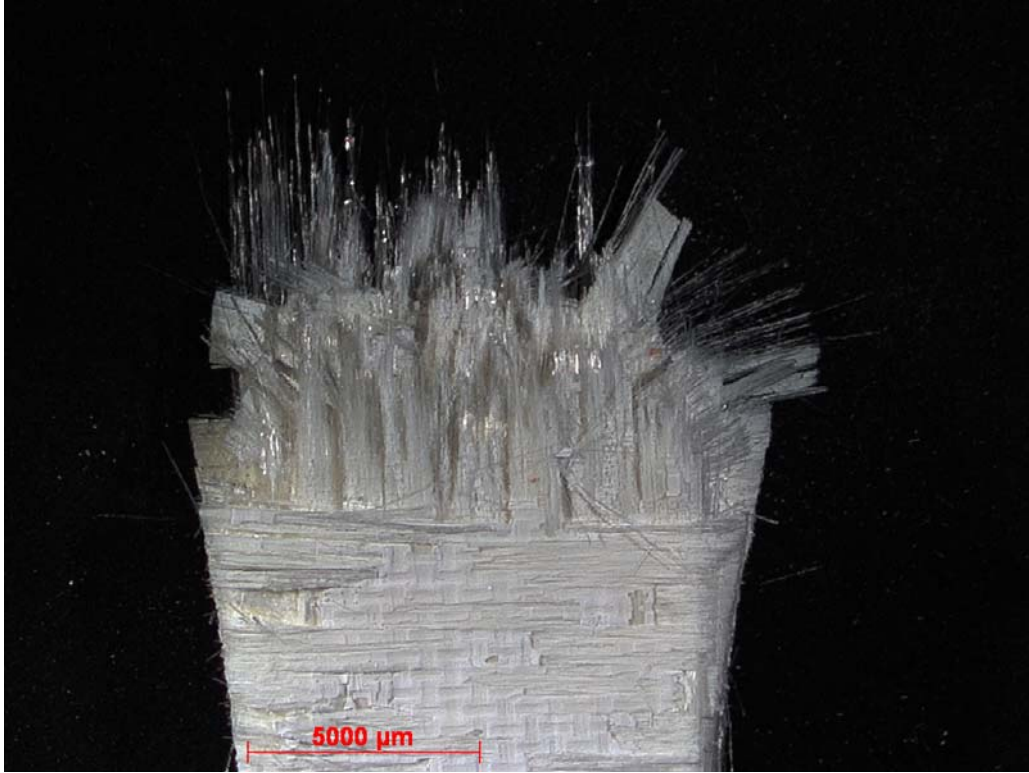
Figure 65. Fracture surface of N720/A specimen tested with cyclic creep-recovery with 1 hour hold times at 125 MPa in air at 1200 °C.


Figure 66. Fracture surface of N720/A specimen tested with cyclic creep-recovery with 1 hour hold times at 125 MPa in air at 1200 °C.

Figure 67. Fracture surface of N720/A specimen tested with cyclic creep-recovery with 1 hour hold times at 125 MPa in air at 1200 °C.

Figure 68. Fracture surface of N720/A specimen tested with cyclic creep-recovery with 1 hour hold times at 125 MPa in air at 1200 °C.

Figure 69. Fracture surface of N720/A specimen tested with cyclic creep-recovery with 1 hour hold times at 125 MPa in air at 1200 °C.
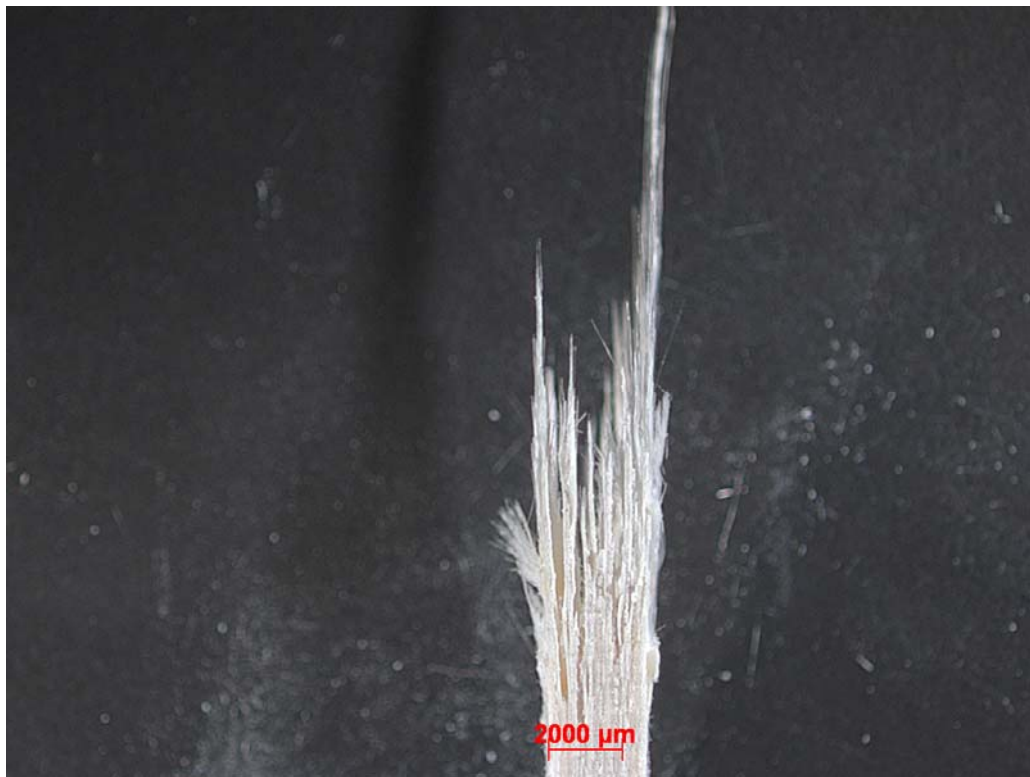

Figure 70. Fracture surface of N720/A specimen tested with cyclic creep-recovery with 1 hour hold times at 125 MPa in air at 1200 °C.
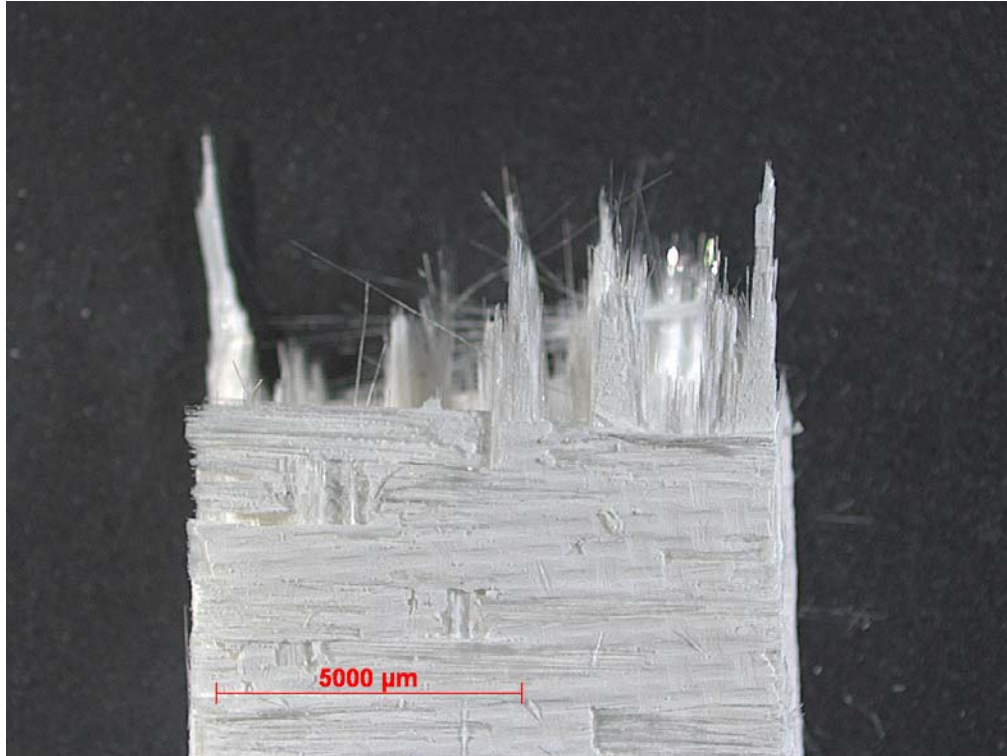
Figure 71. Fracture surface of N720/A specimen tested with cyclic creep-recovery with 1 hour hold times at 100 MPa in steam at 1200 °C.

Figure 72. Fracture surface of N720/A specimen tested with cyclic creep-recovery with 1 hour hold times at 100 MPa in steam at 1200 °C.
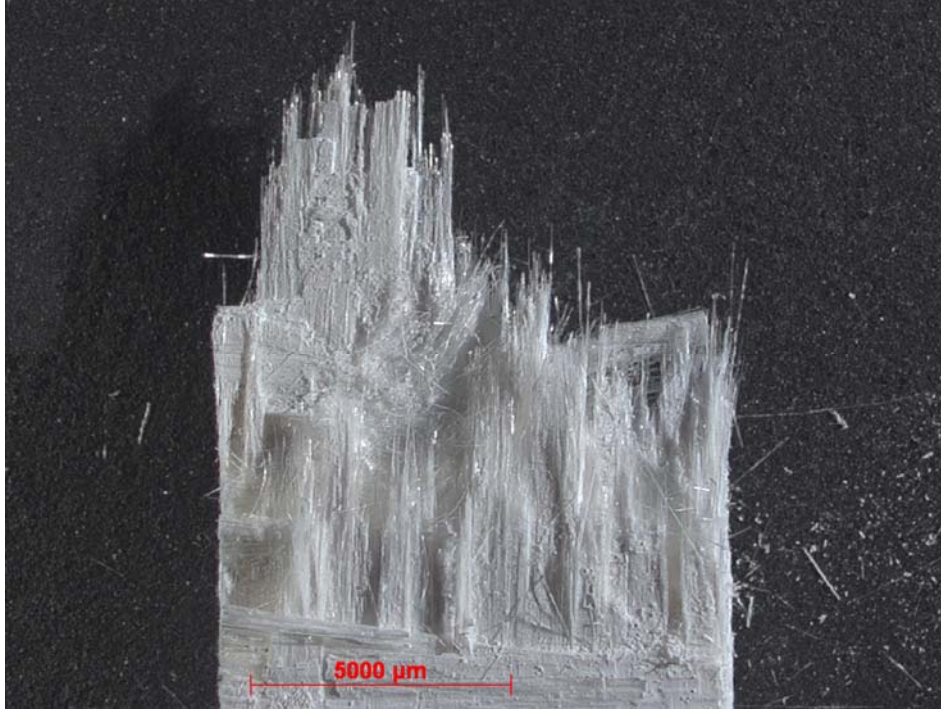
Figure 73. Fracture surface of N720/A specimen tested with cyclic creep-recovery with 1 hour hold times at 100 MPa in steam at 1200 °C.
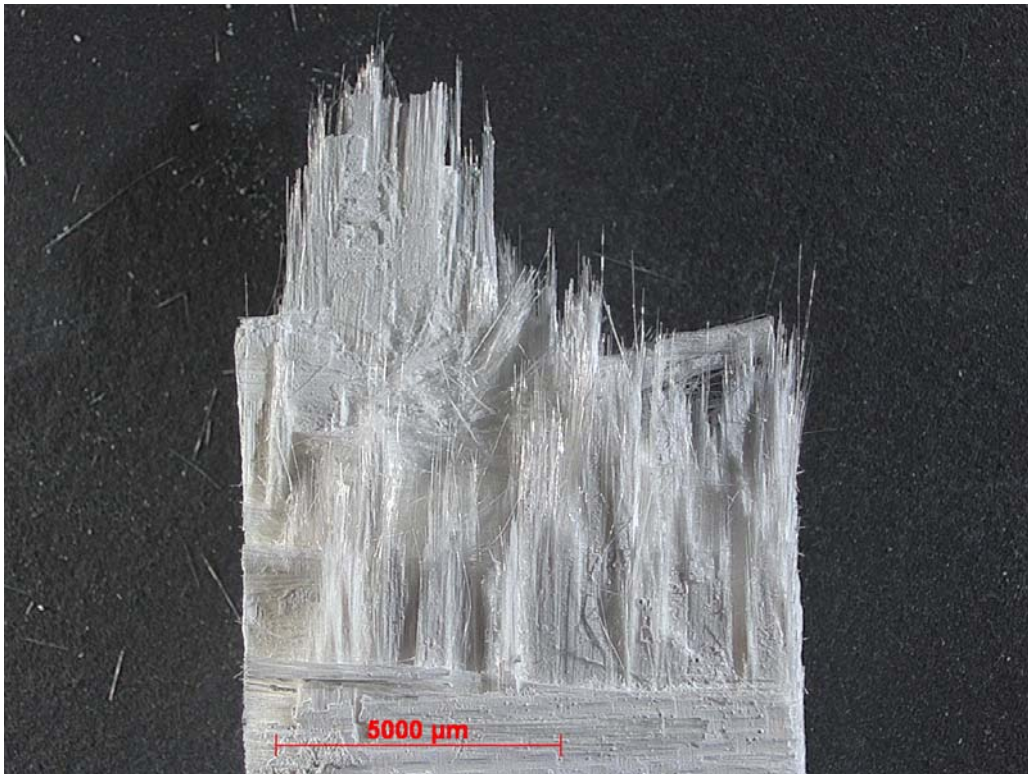
Figure 74. Fracture surface of N720/A specimen tested with cyclic creep-recovery with 1 hour hold times at 100 MPa in steam at 1200 °C.

Figure 75. Fracture surface of N720/A specimen tested with cyclic creep-recovery with 1 hour hold times at 100 MPa in steam at 1200 °C.

Figure 76. Fracture surface of N720/A specimen tested with cyclic creep-recovery with 1 hour hold times at 100 MPa in steam at 1200 °C.
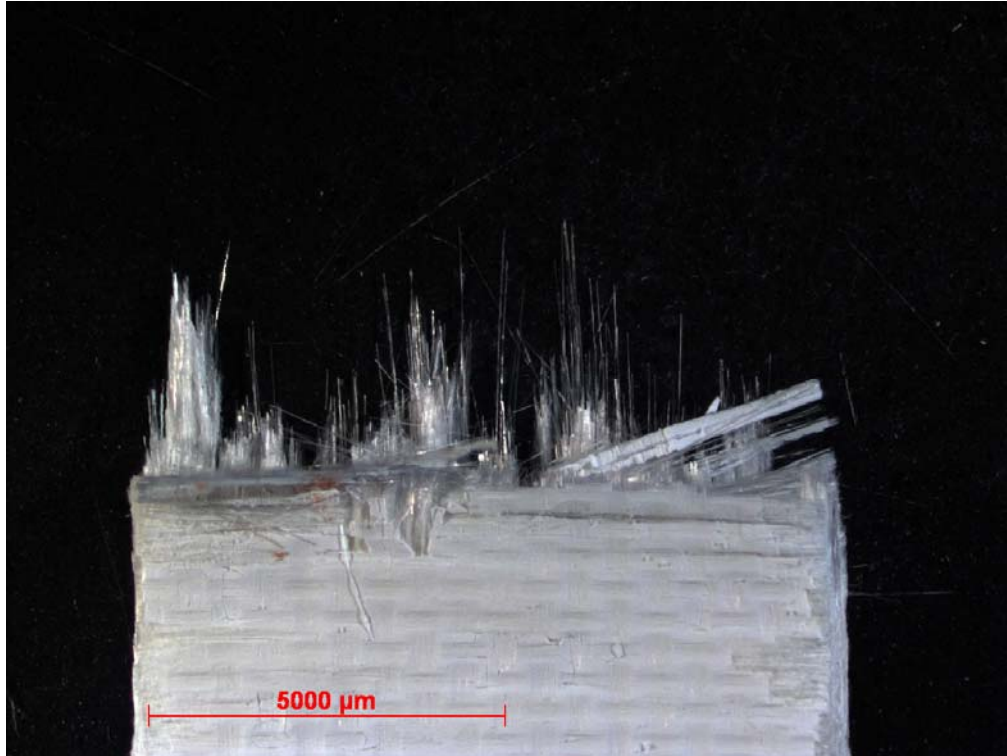
Figure 77. Fracture surface of N720/A specimen tested with cyclic creep-recovery with 1 hour hold times at 100 MPa in steam at 1200 °C, possible kinking.


Figure 78. Fracture surface of N720/A specimen tested with cyclic creep-recovery with 1 hour hold times at 100 MPa in steam at 1200 °C, possible kinking.

Figure 79. Fracture surface of N720/A specimen tested with cyclic creep-recovery with 1 hour hold times at 100 MPa in steam at 1200 °C, possible kinking.
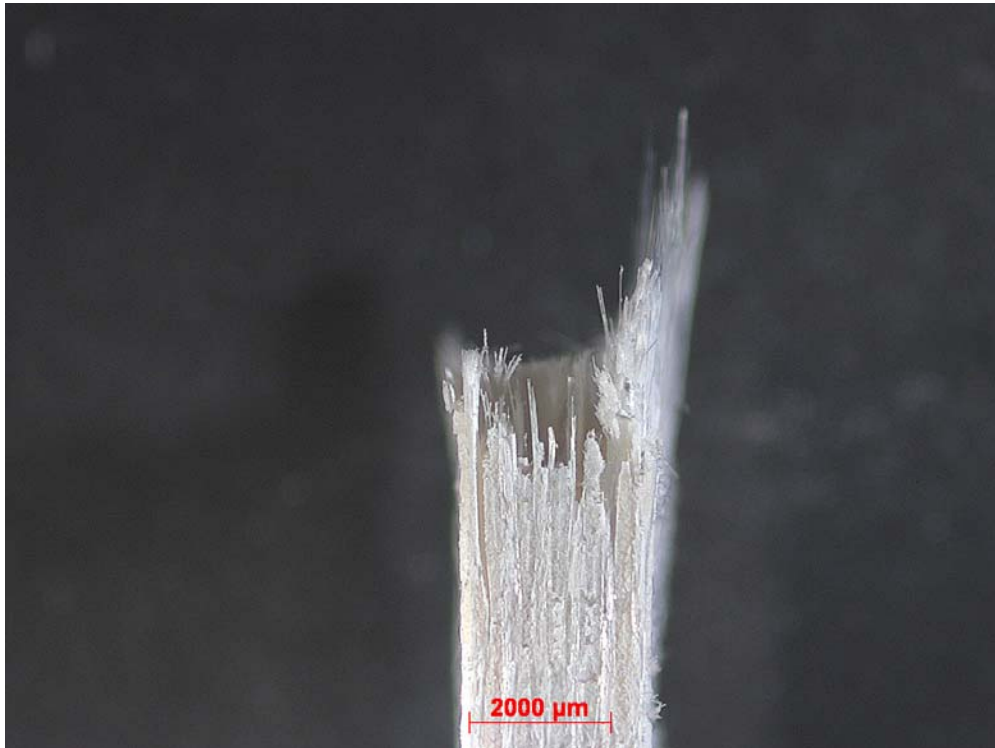
Figure 80. Fracture surface of N720/A specimen tested with cyclic creep-recovery with 1 hour hold times at 100 MPa in steam at 1200 °C, possible kinking.

Figure 81. Fracture surface of N720/A specimen tested with cyclic creep-recovery with 1 hour hold times at 100 MPa in steam at 1200 °C, possible kinking.
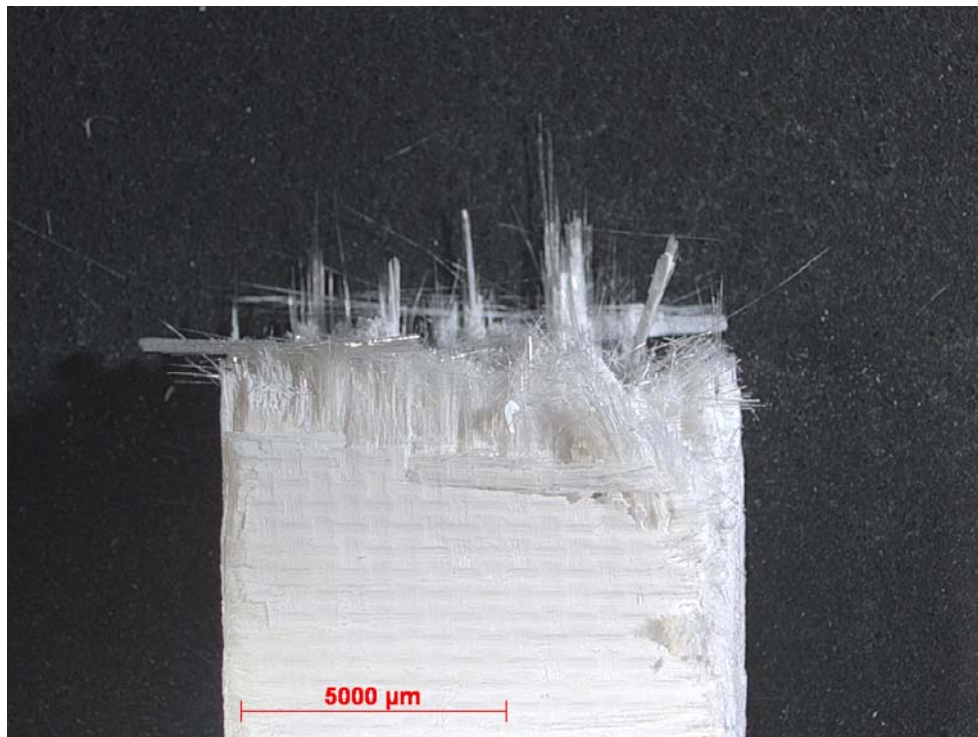
Figure 82. Fracture surface of N720/A specimen tested with cyclic creep-recovery with 1 hour hold times at 100 MPa in steam at 1200 °C, possible kinking.

Figure 83. Fracture surface of N720/A specimen tested with cyclic creep-recovery with 1 hour hold times at 100 MPa in steam at 1200 °C, possible kinking.


Figure 84. Fracture surface of N720/A specimen tested with cyclic creep-recovery with 1 hour hold times at 100 MPa in steam at 1200 °C, possible kinking.
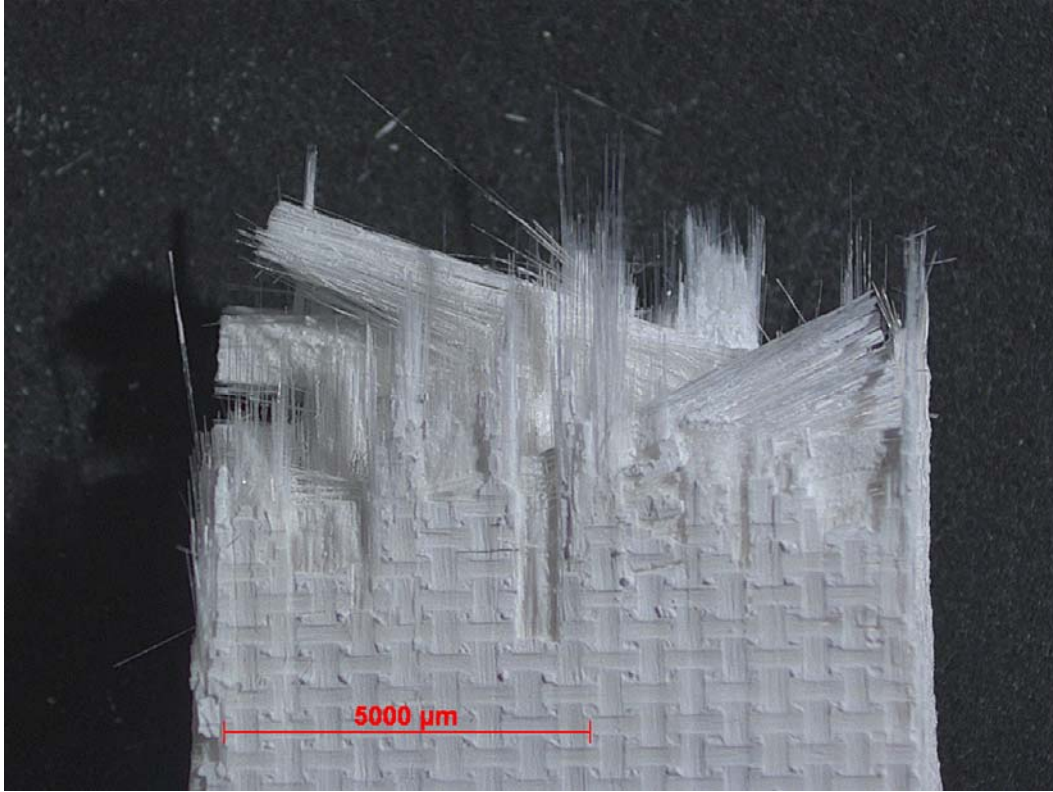
**Figure 85. Fracture surface of N720/A specimen tested with cyclic creep-recovery
with 0.05 hour hold times at 125 MPa in steam at 1200 °C.**
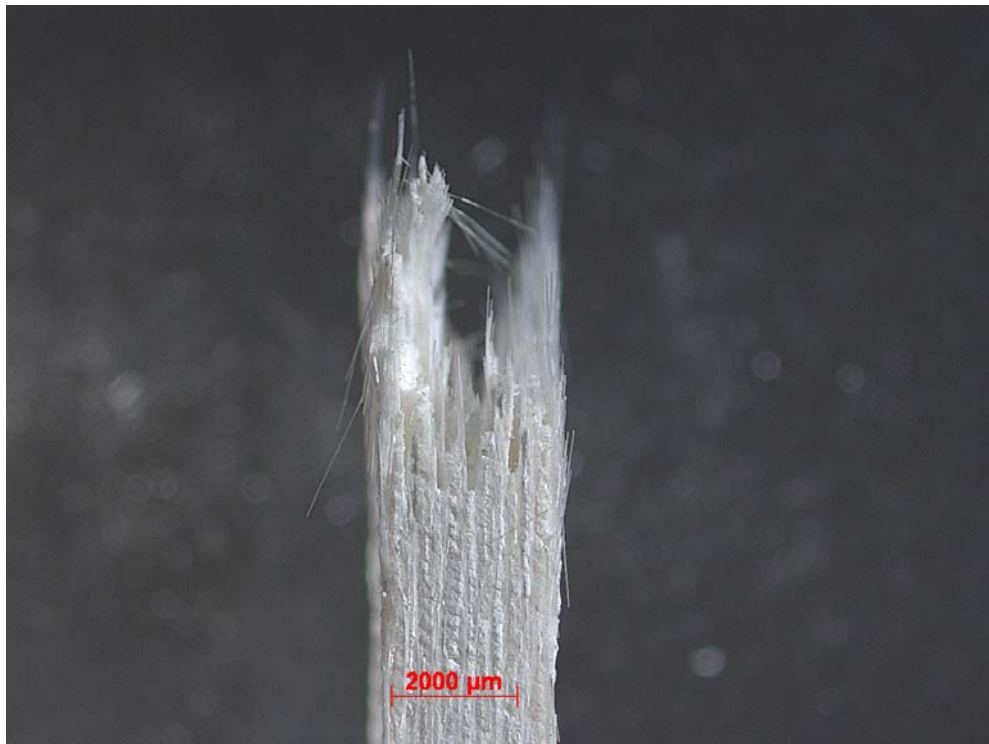
**Figure 86. Fracture surface of N720/A specimen tested with cyclic creep-recovery
with 0.05 hour hold times at 125 MPa in steam at 1200 °C.**

Figure 87. Fracture surface of N720/A specimen tested with cyclic creep-recovery with 0.05 hour hold times at 125 MPa in steam at 1200 °C.
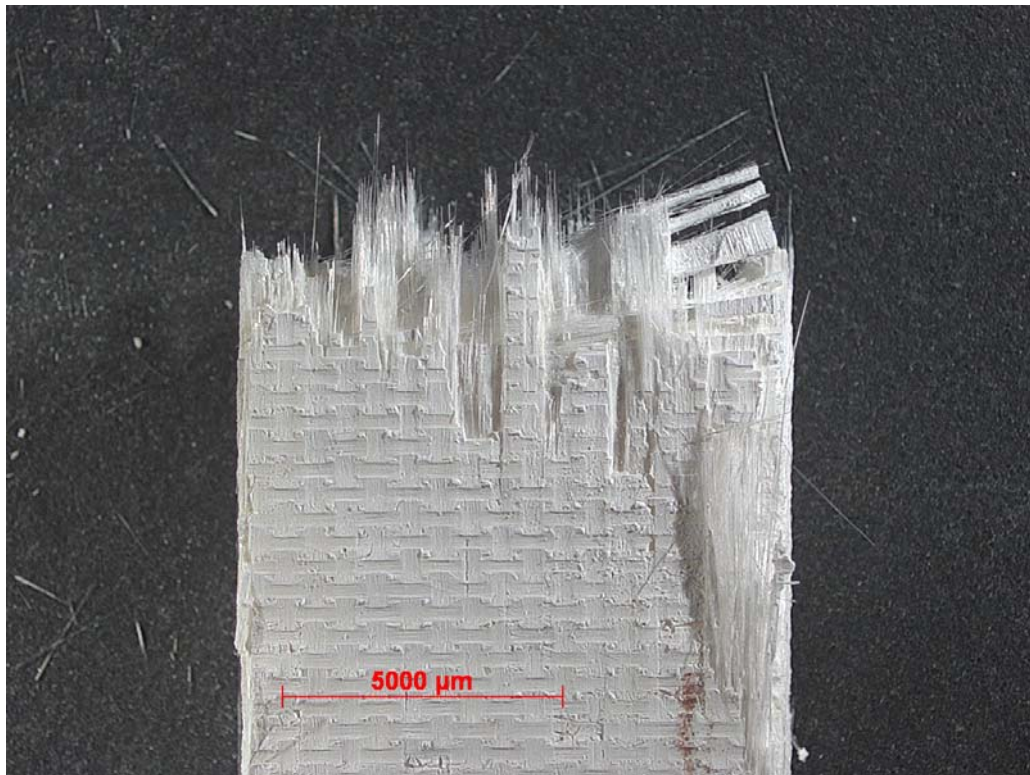

Figure 88. Fracture surface of N720/A specimen tested with cyclic creep-recovery with 0.05 hour hold times at 125 MPa in steam at 1200 °C.

Figure 89. Fracture surface of N720/A specimen tested with cyclic creep-recovery with 0.05 hour hold times at 125 MPa in steam at 1200 °C.
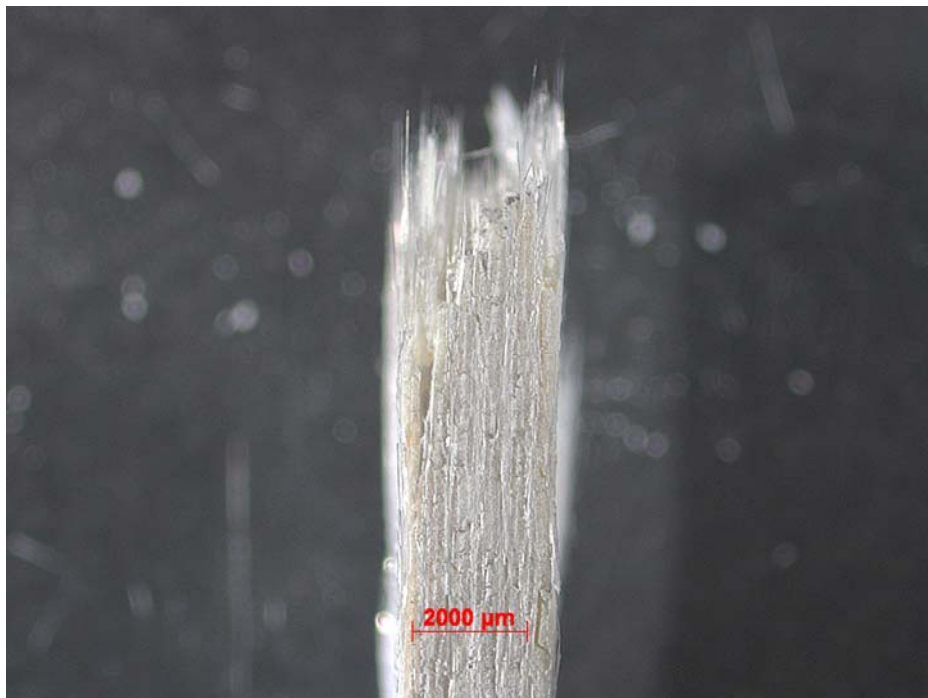
Figure 90. Fracture surface of N720/A specimen tested with cyclic creep-recovery with 0.05 hour hold times at 125 MPa in steam at 1200 °C.
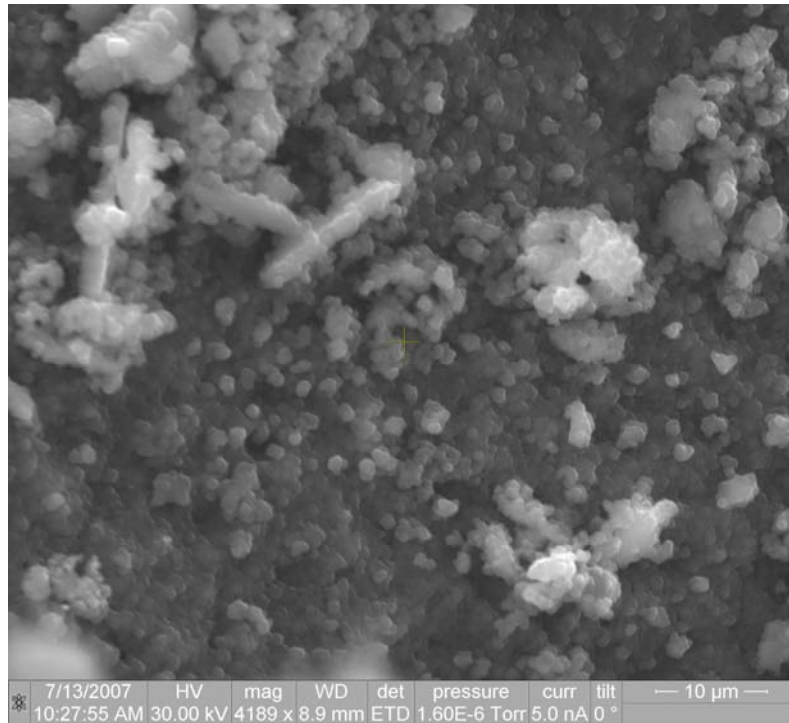
Figure 91. Fracture surface of N720/A specimen tested with cyclic creep-recovery with 30 hour hold times at 100 MPa in air at 1200 °C.
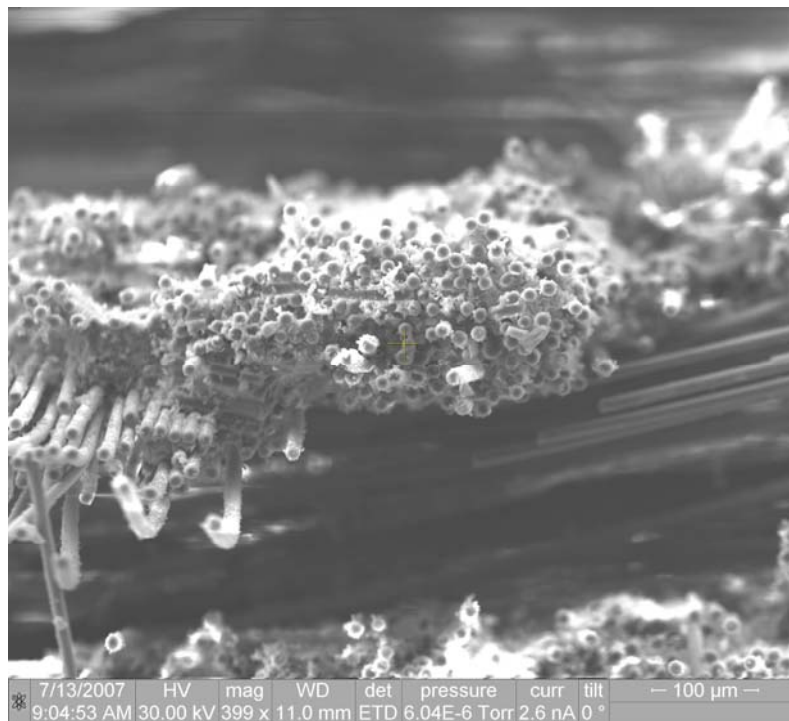
Figure 92. Fracture surface of N720/A specimen tested with cyclic creep-recovery with 30 hour hold times at 100 MPa in air at 1200 °C.
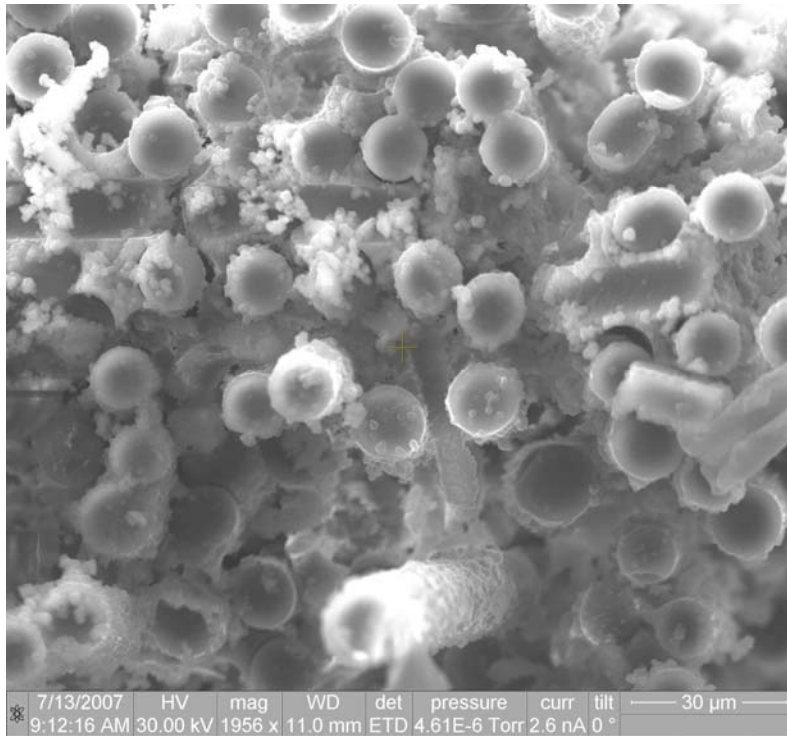
Figure 93. Fracture surface of N720/A specimen tested with cyclic creep-recovery with 30 hour hold times at 100 MPa in air at 1200 °C.
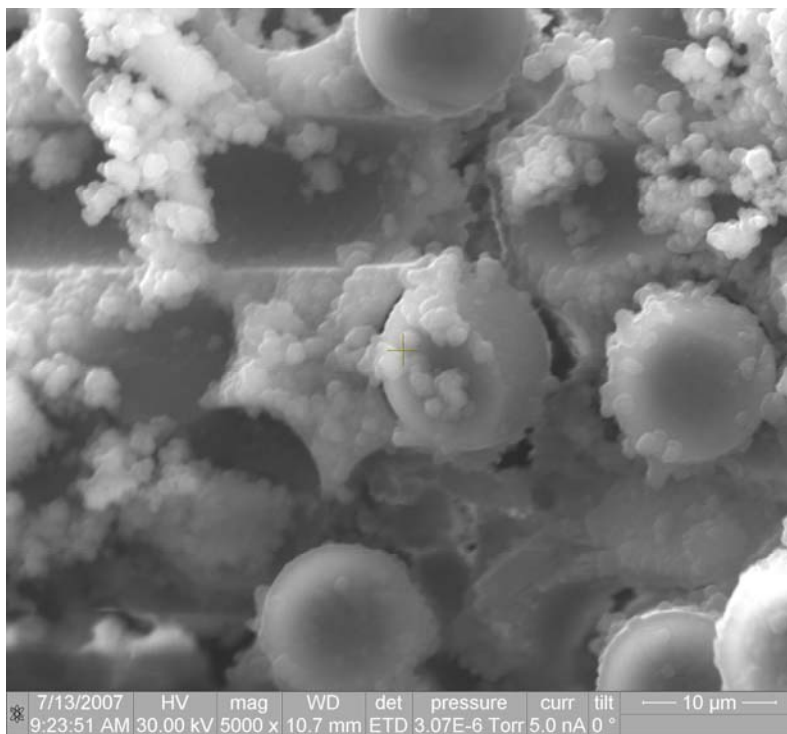
Figure 94. Fracture surface of N720/A specimen tested with cyclic creep-recovery with 30 hour hold times at 100 MPa in air at 1200 °C.

Figure 95. Fracture surface of N720/A specimen tested with cyclic creep-recovery with 30 hour hold times at 100 MPa in air at 1200 °C.
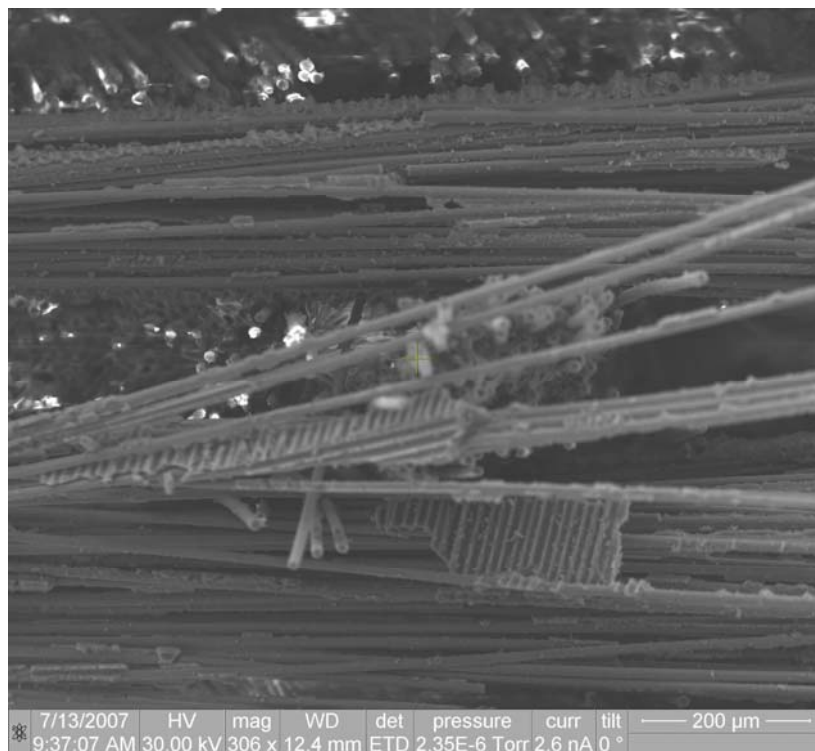

Figure 96. Fracture surface of N720/A specimen tested with cyclic creep-recovery with 30 hour hold times at 100 MPa in air at 1200 °C.
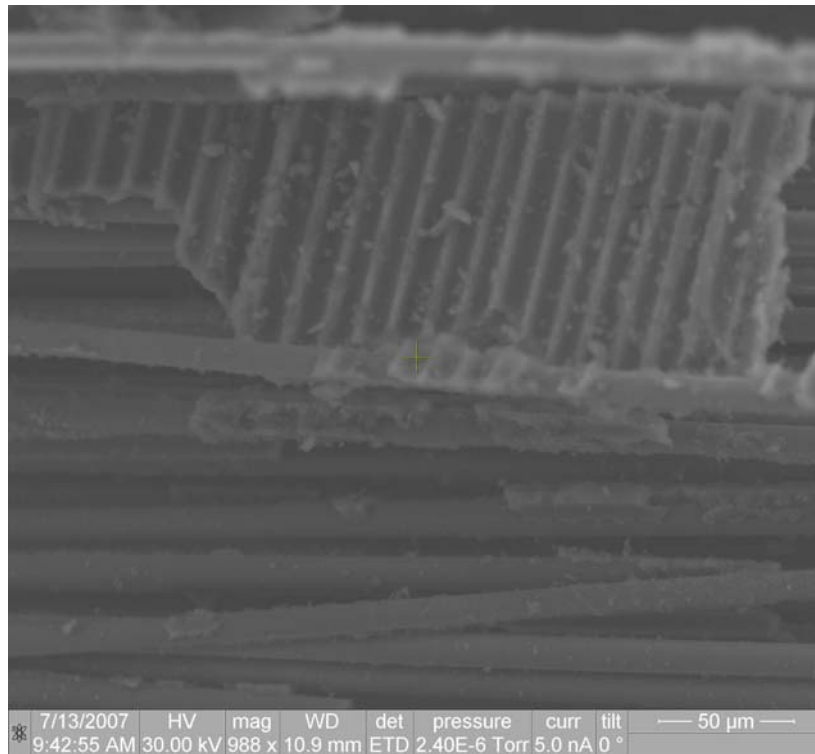
Figure 97. Fracture surface of N720/A specimen tested with cyclic creep-recovery with 30 hour hold times at 100 MPa in air at 1200 °C.
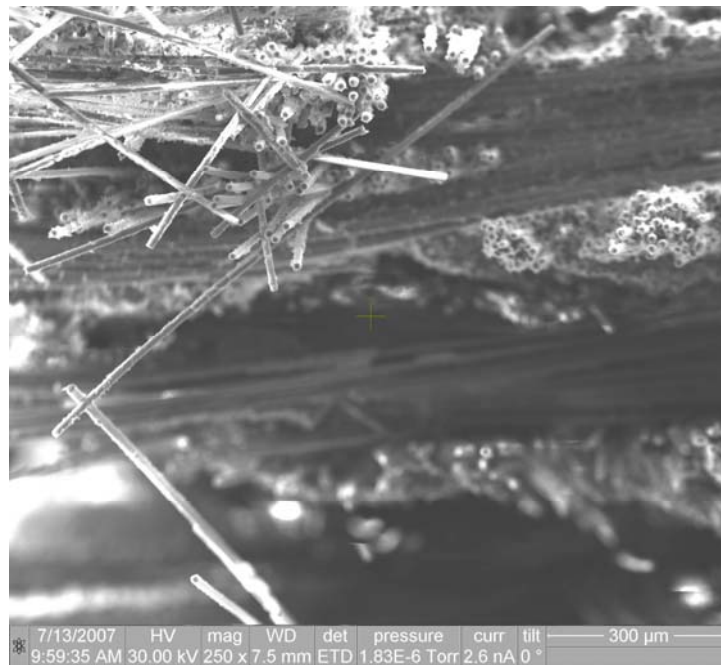
Figure 98. Fracture surface of N720/A specimen tested with cyclic creep-recovery with 30 hour hold times at 100 MPa in air at 1200 °C.
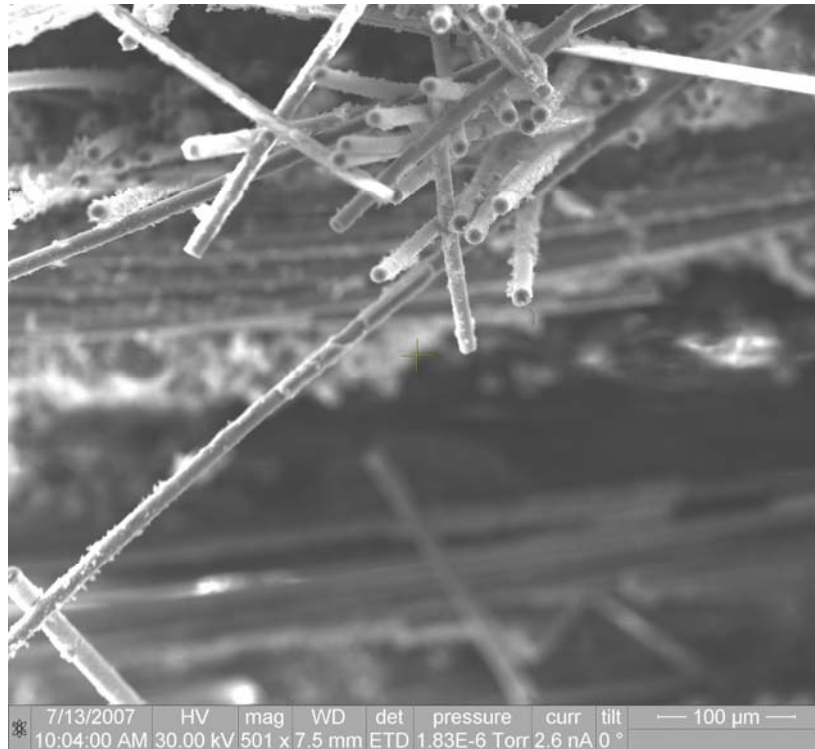
Figure 99. Fracture surface of N720/A specimen tested with cyclic creep-recovery with 30 hour hold times at 100 MPa in air at 1200 °C.


Figure 100. Fracture surface of N720/A specimen tested with cyclic creep-recovery with 30 hour hold times at 100 MPa in air at 1200 °C.
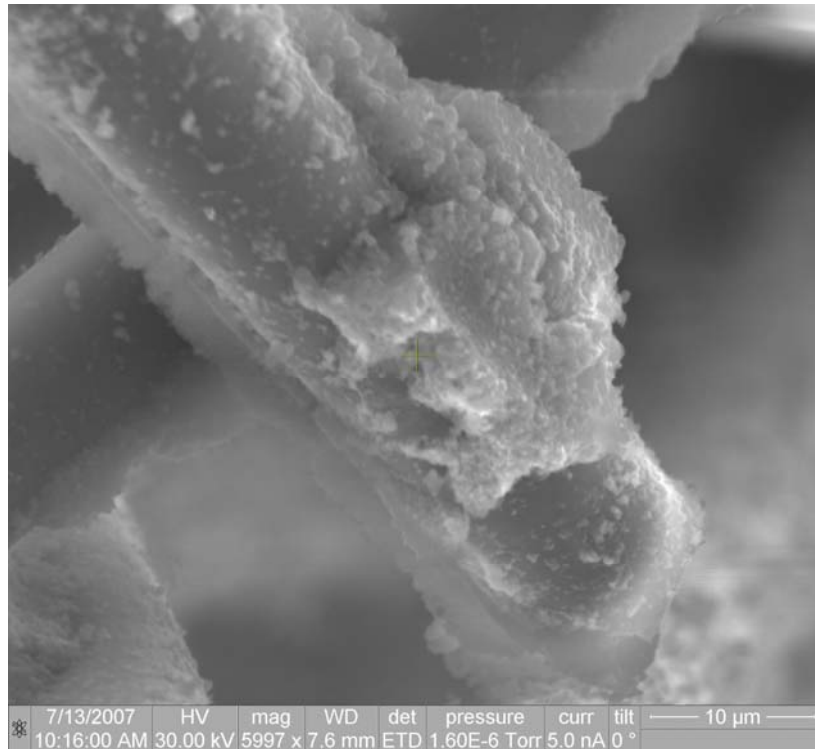
Figure 101. Fracture surface of N720/A specimen tested with cyclic creep-recovery with 30 hour hold times at 100 MPa in air at 1200 °C.
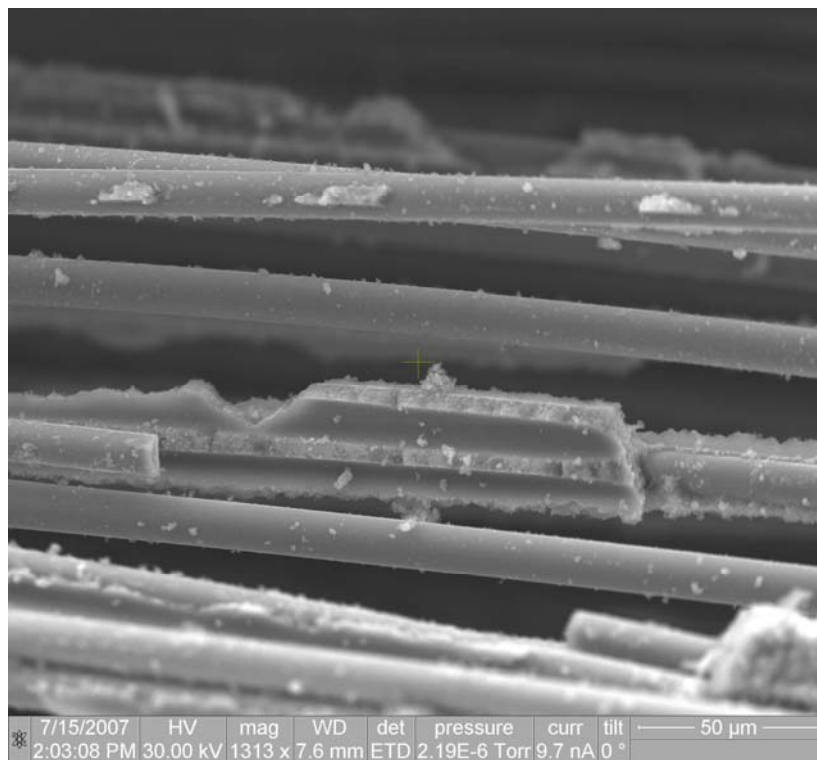


Figure 102. Fracture surface of N720/A specimen tested with cyclic creep-recovery with 1 hour hold times at 100 MPa in air at 1200 °C.
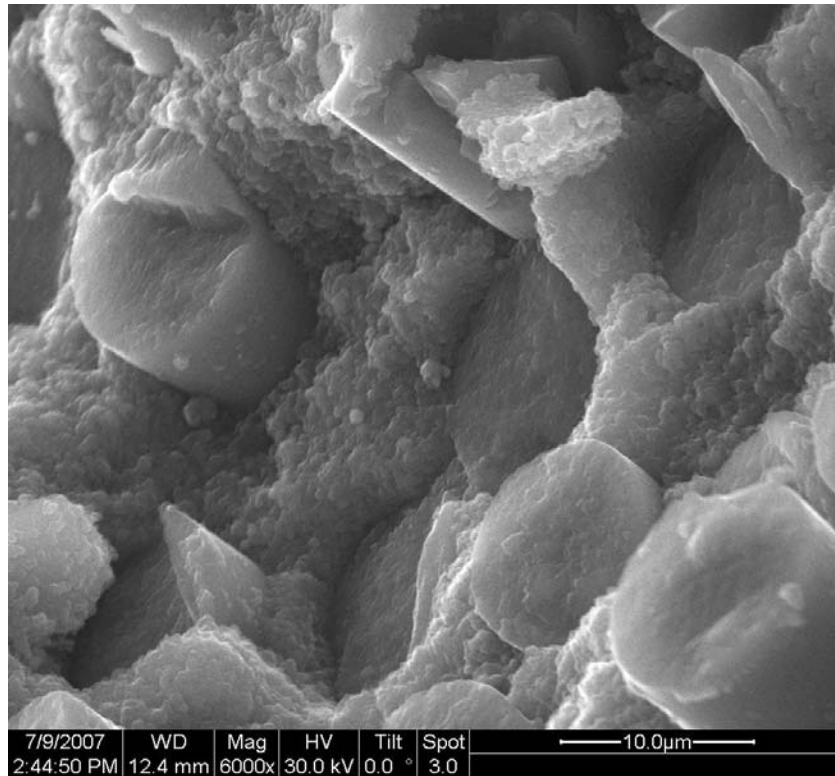
Figure 103. Fracture surface of N720/A specimen tested with cyclic creep-recovery with 1 hour hold times at 100 MPa in air at 1200 °C.
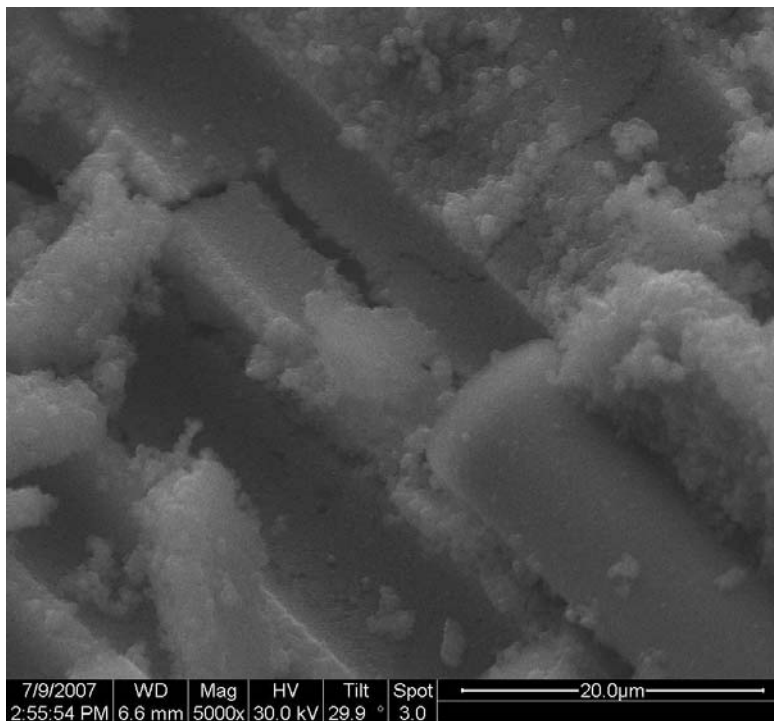

Figure 104. Fracture surface of N720/A specimen tested with cyclic creep-recovery with 1 hour hold times at 100 MPa in air at 1200 °C.

Figure 105. Fracture surface of N720/A specimen tested with cyclic creep-recovery with 1 hour hold times at 100 MPa in air at 1200 °C.

Figure 106. Fracture surface of N720/A specimen tested with cyclic creep-recovery with 1 hour hold times at 100 MPa in air at 1200 °C.
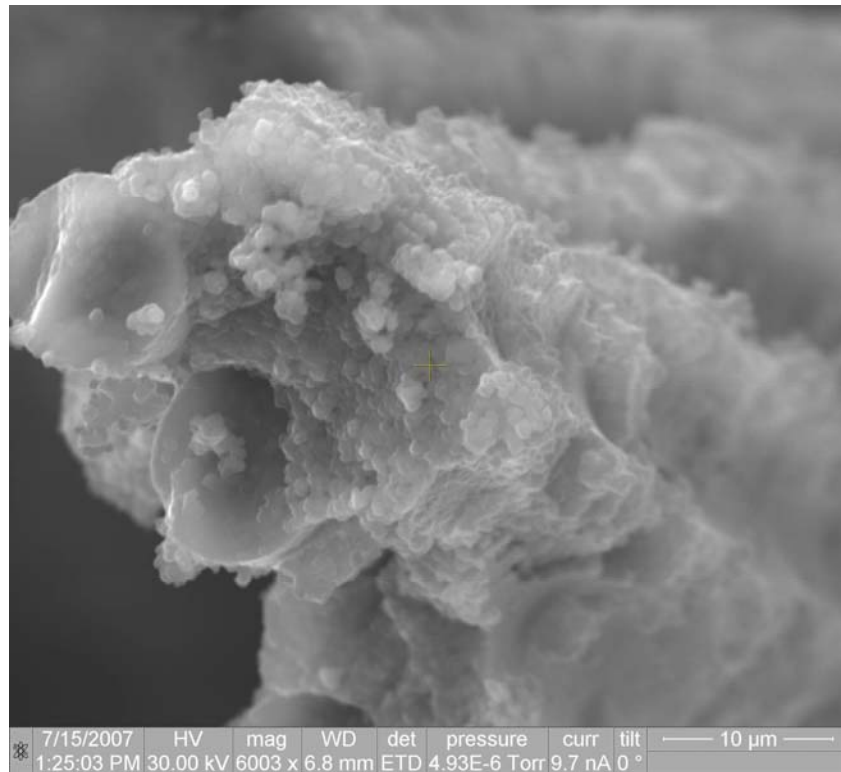
Figure 107. Fracture surface of N720/A specimen tested with cyclic creep-recovery with 1 hour hold times at 100 MPa in air at 1200 °C.
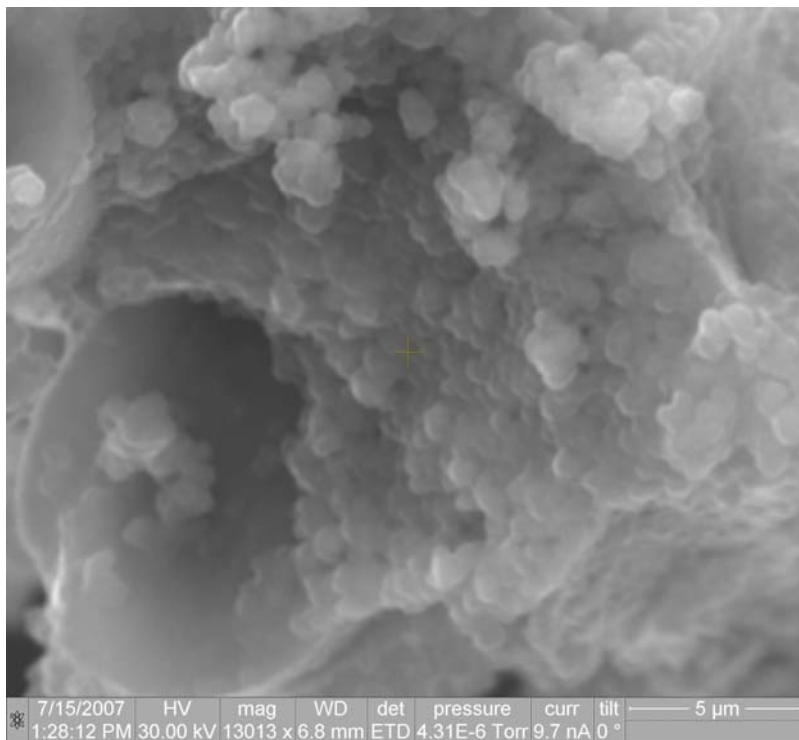
Figure 108. Fracture surface of N720/A specimen tested with cyclic creep-recovery with 1 hour hold times at 100 MPa in air at 1200 °C.
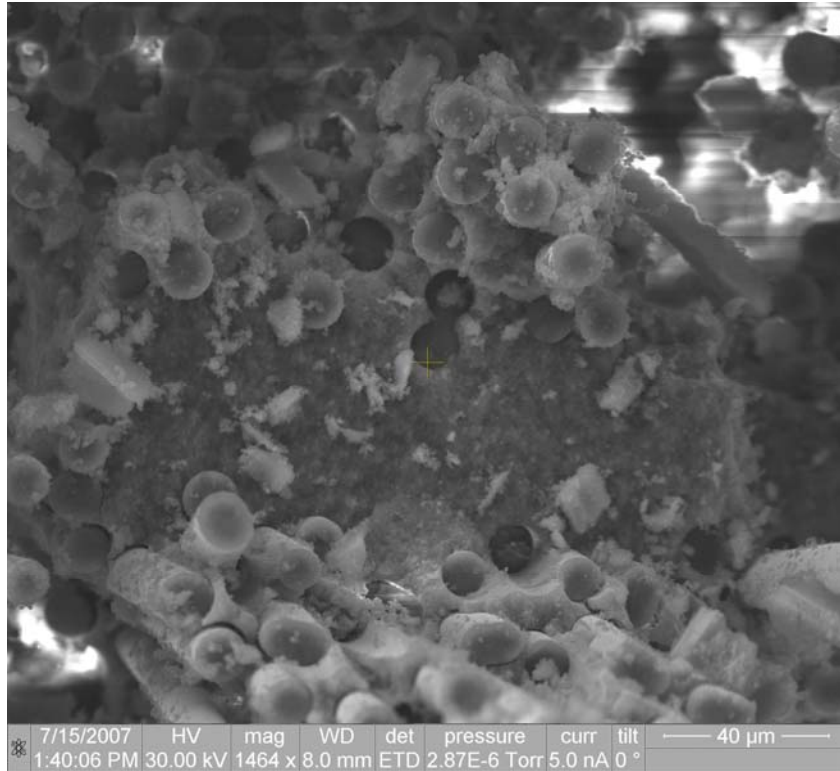
Figure 109. Fracture surface of N720/A specimen tested with cyclic creep-recovery with 1 hour hold times at 100 MPa in air at 1200 °C.
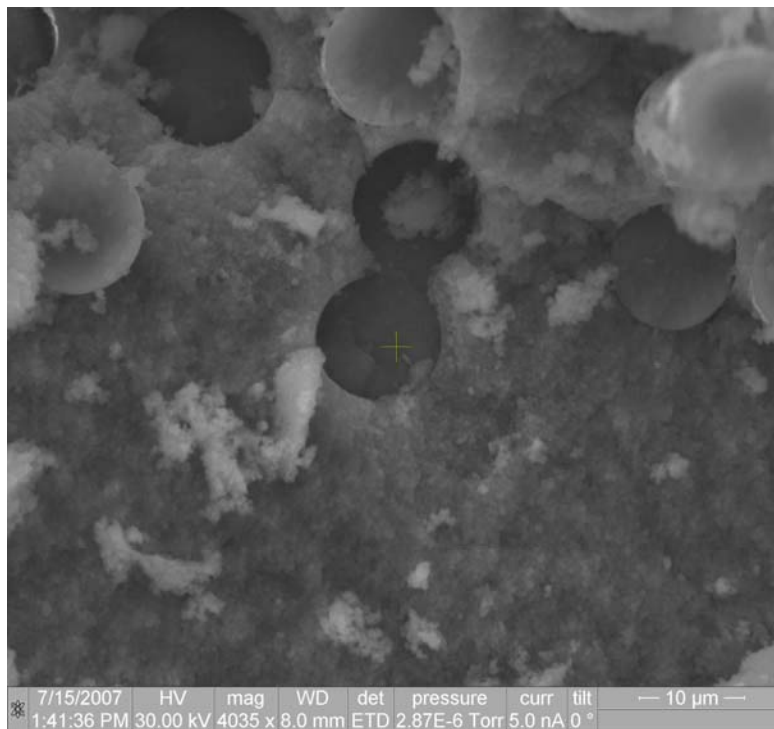


Figure 110. Fracture surface of N720/A specimen tested with cyclic creep-recovery with 1 hour hold times at 100 MPa in air at 1200 °C.
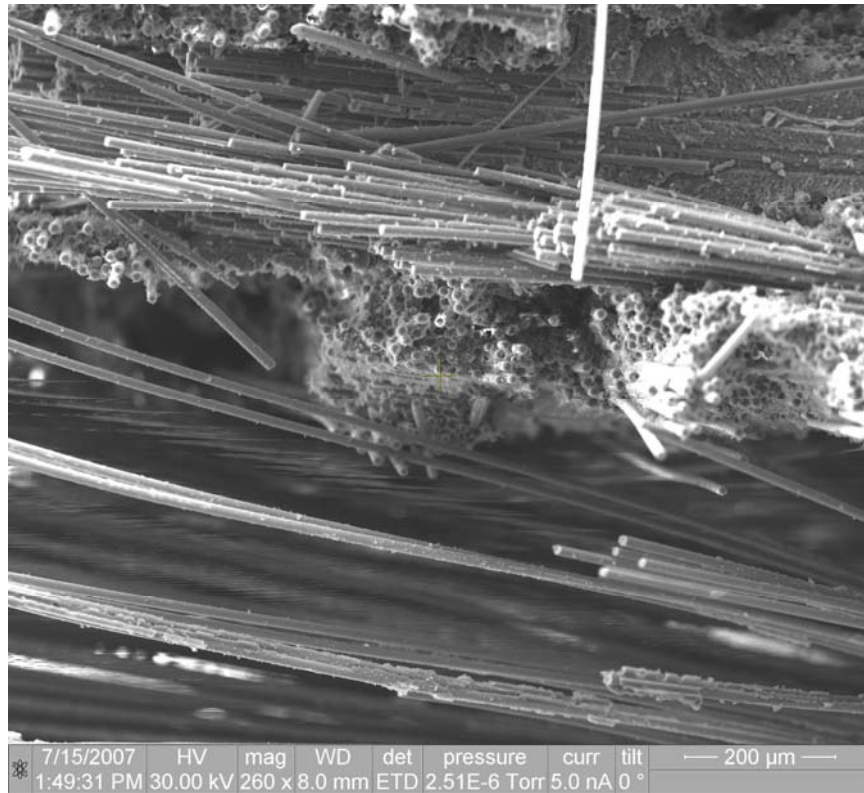
Figure 111. Fracture surface of N720/A specimen tested with cyclic creep-recovery with 1 hour hold times at 100 MPa in air at 1200 °C.
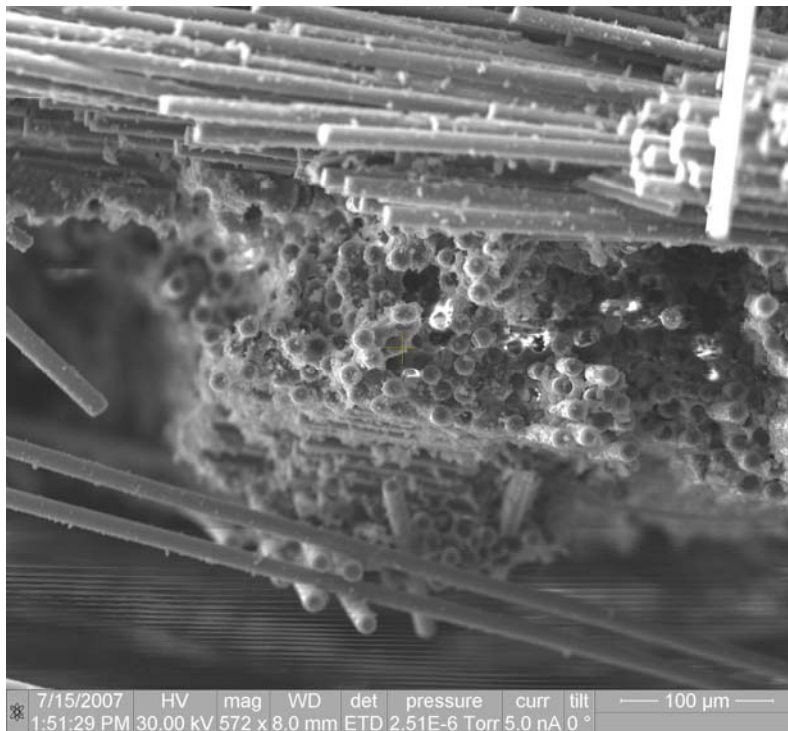

Figure 112. Fracture surface of N720/A specimen tested with cyclic creep-recovery with 1 hour hold times at 100 MPa in air at 1200 °C.
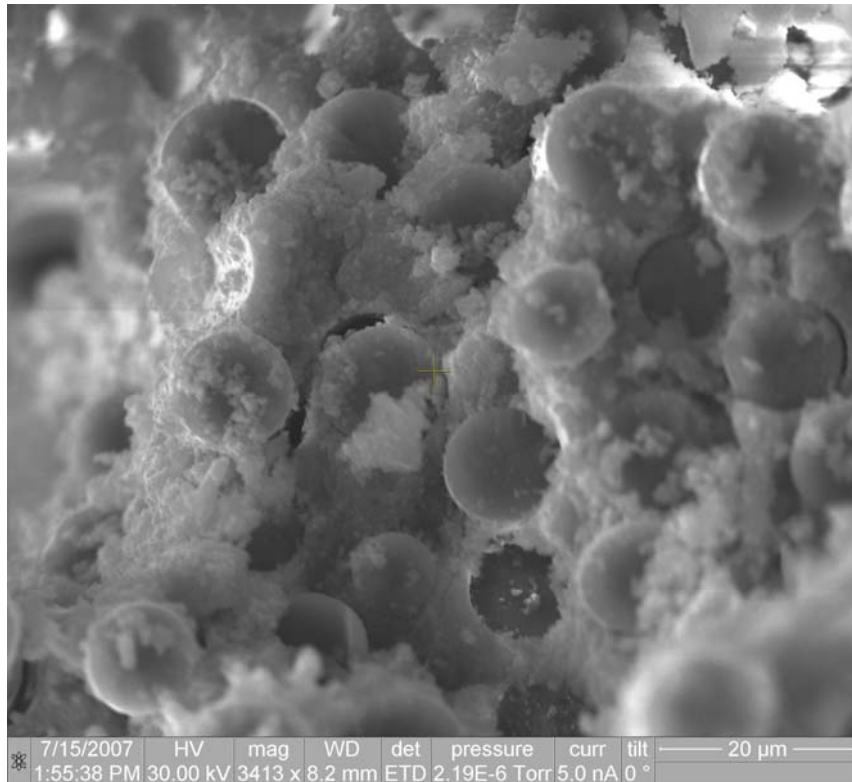
Figure 113. Fracture surface of N720/A specimen tested with cyclic creep-recovery with 1 hour hold times at 100 MPa in air at 1200 °C.
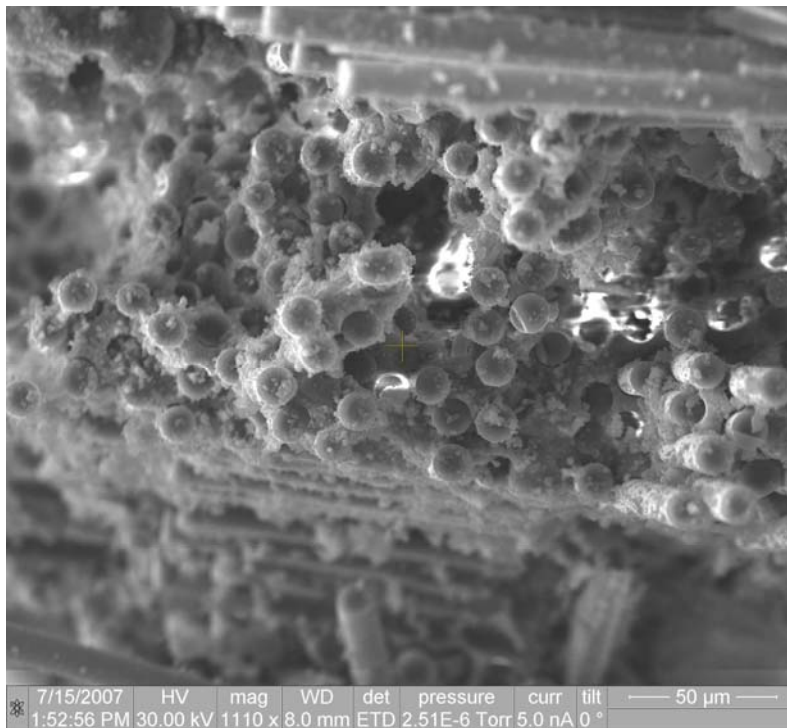
Figure 114. Fracture surface of N720/A specimen tested with cyclic creep-recovery with 1 hour hold times at 100 MPa in air at 1200 °C.

Figure 115. Fracture surface of N720/A specimen tested with cyclic creep-recovery with 1 hour hold times at 100 MPa in air at 1200 °C.
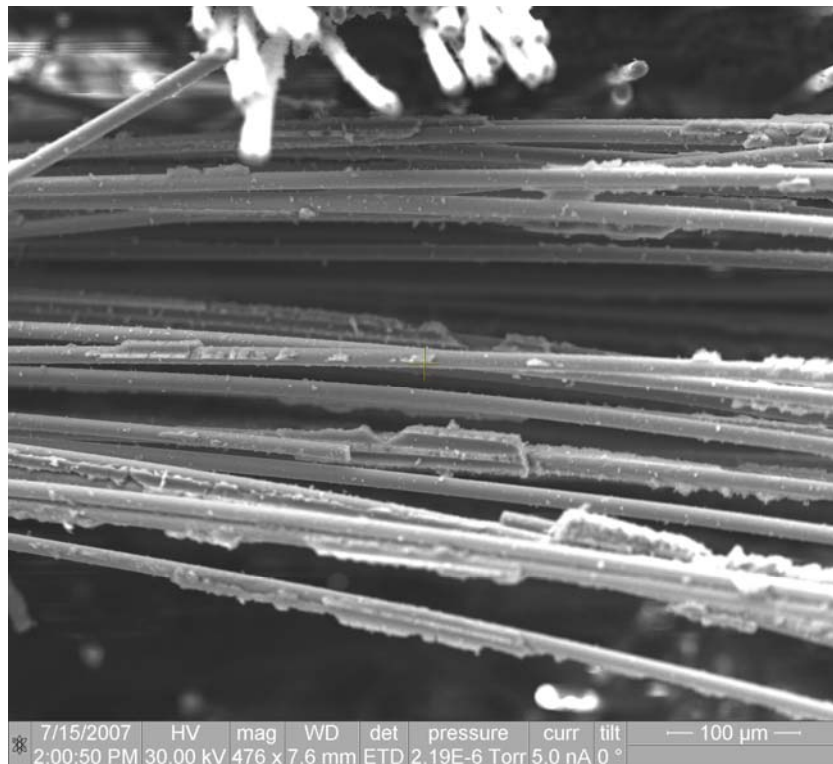
Figure 116. Fracture surface of N720/A specimen tested with cyclic creep-recovery with 1 hour hold times at 100 MPa in air at 1200 °C.
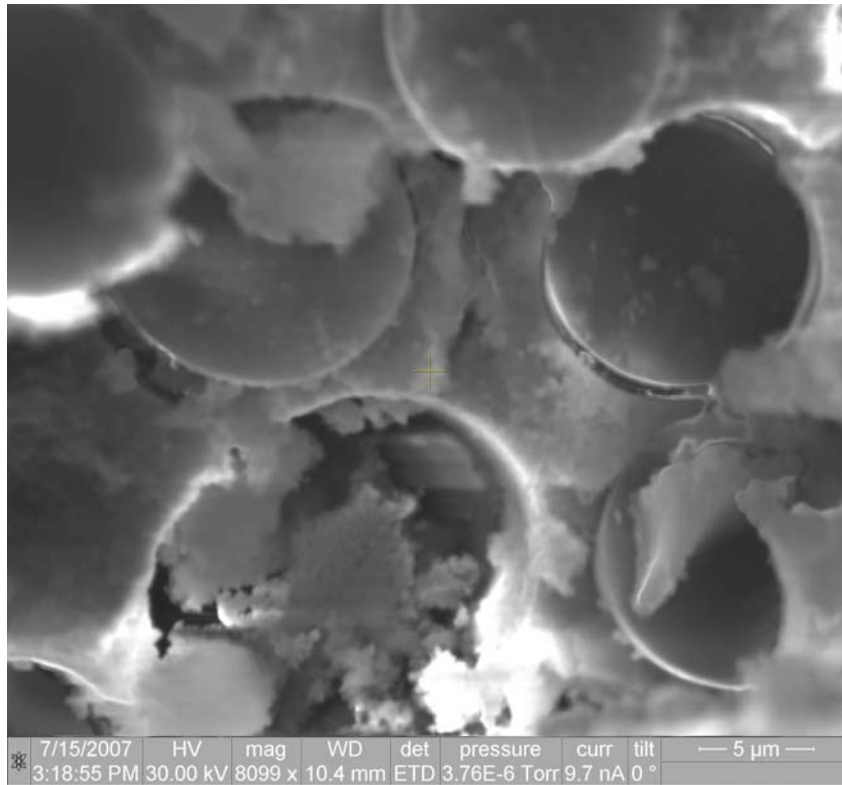
Figure 117. Fracture surface of N720/A specimen tested with cyclic creep-recovery with 1 hour hold times at 125 MPa in air at 1200 °C.
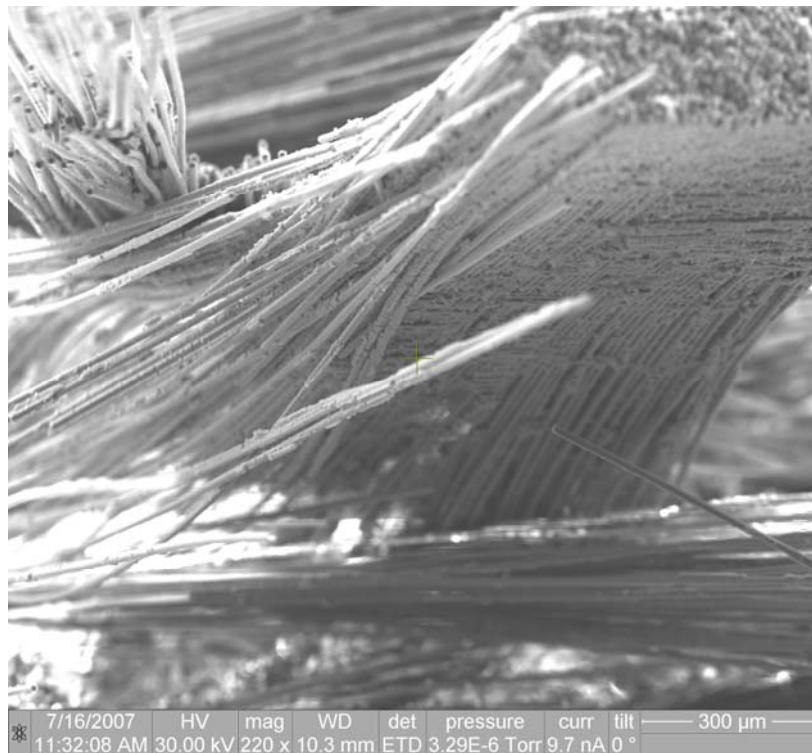
Figure 118. Fracture surface of N720/A specimen tested with cyclic creep-recovery with 1 hour hold times at 125 MPa in air at 1200 °C.
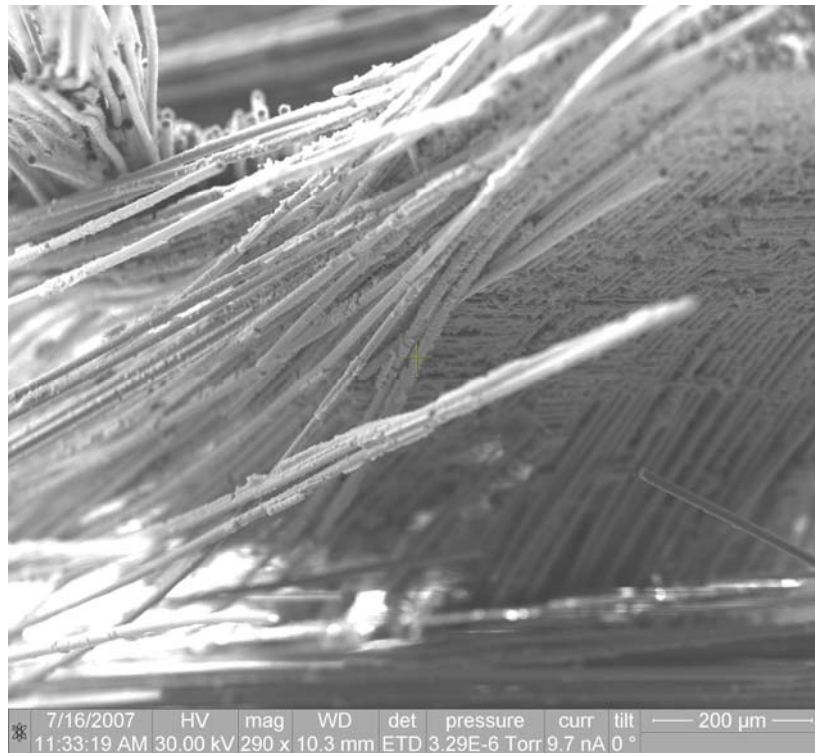
Figure 119. Fracture surface of N720/A specimen tested with cyclic creep-recovery with 1 hour hold times at 125 MPa in air at 1200 °C.
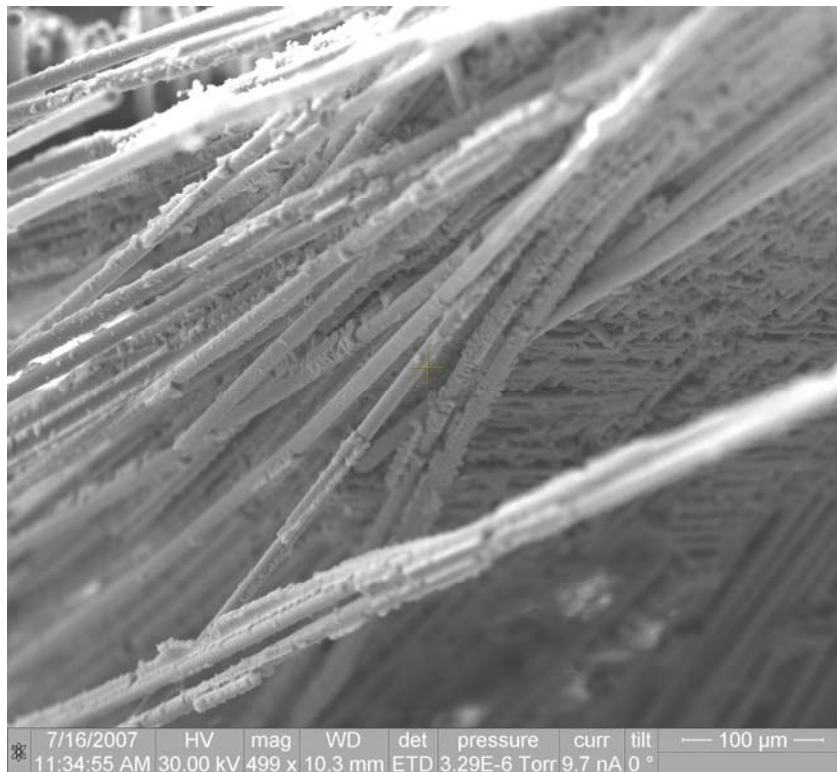

Figure 120. Fracture surface of N720/A specimen tested with cyclic creep-recovery with 1 hour hold times at 125 MPa in air at 1200 °C.
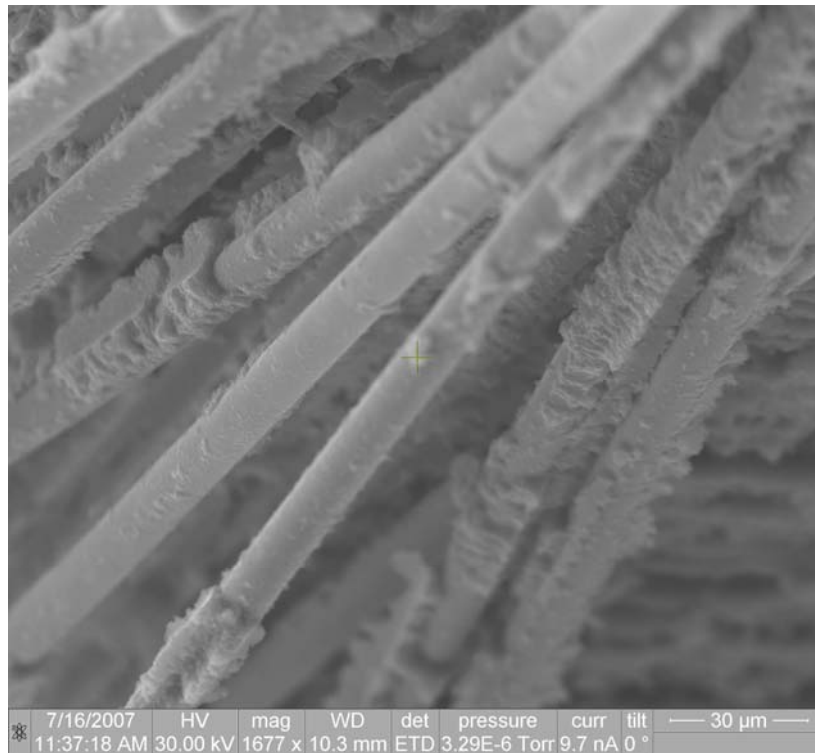
Figure 121. Fracture surface of N720/A specimen tested with cyclic creep-recovery with 1 hour hold times at 125 MPa in air at 1200 °C.
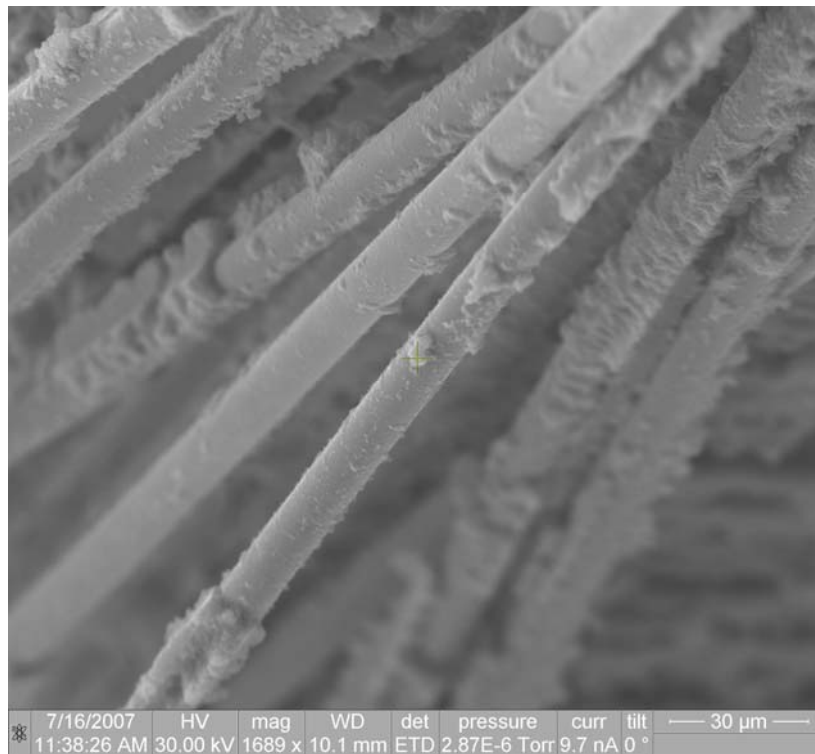

Figure 122. Fracture surface of N720/A specimen tested with cyclic creep-recovery with 1 hour hold times at 125 MPa in air at 1200 °C.
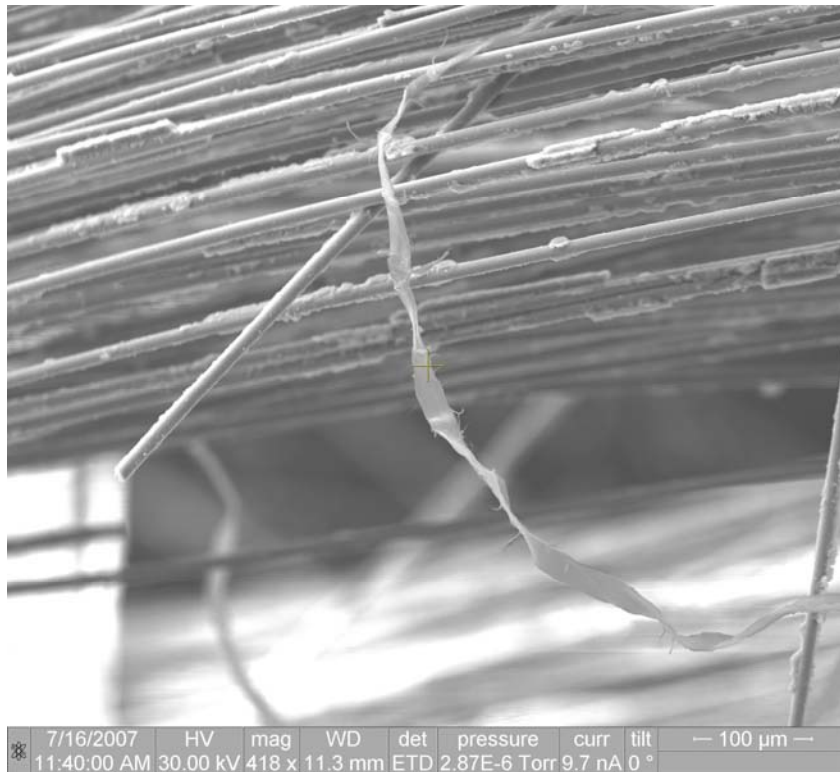
Figure 123. Fracture surface of N720/A specimen tested with cyclic creep-recovery with 1 hour hold times at 125 MPa in air at 1200 °C.
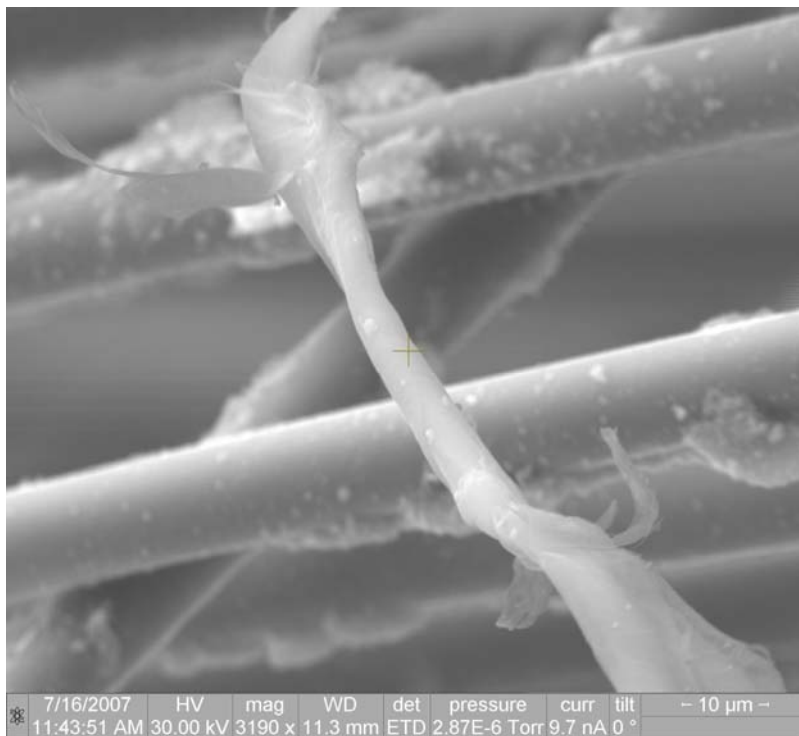

Figure 124. Fracture surface of N720/A specimen tested with cyclic creep-recovery with 1 hour hold times at 125 MPa in air at 1200 °C.
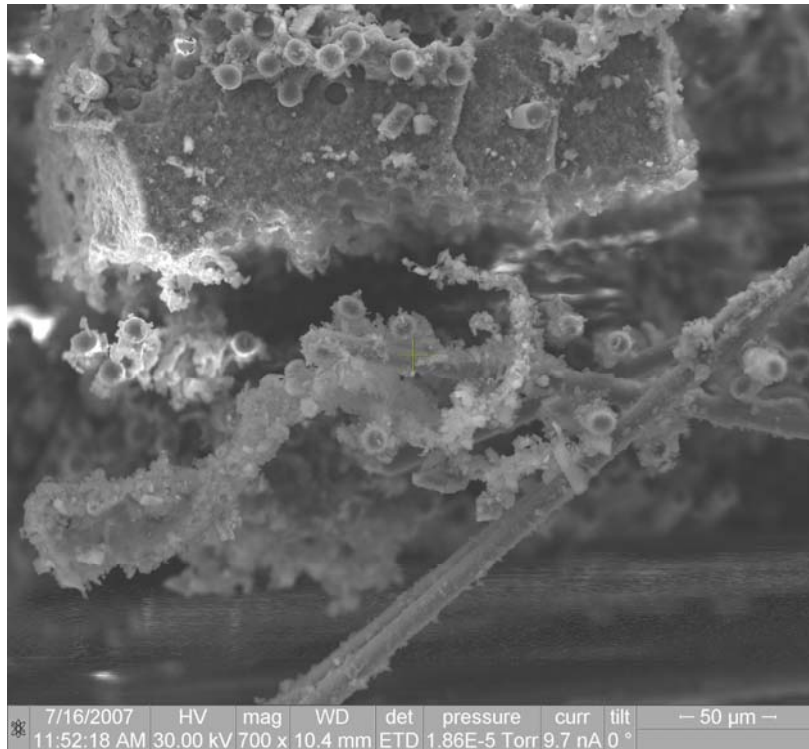
Figure 125. Fracture surface of N720/A specimen tested with cyclic creep-recovery with 1 hour hold times at 125 MPa in air at 1200 °C.
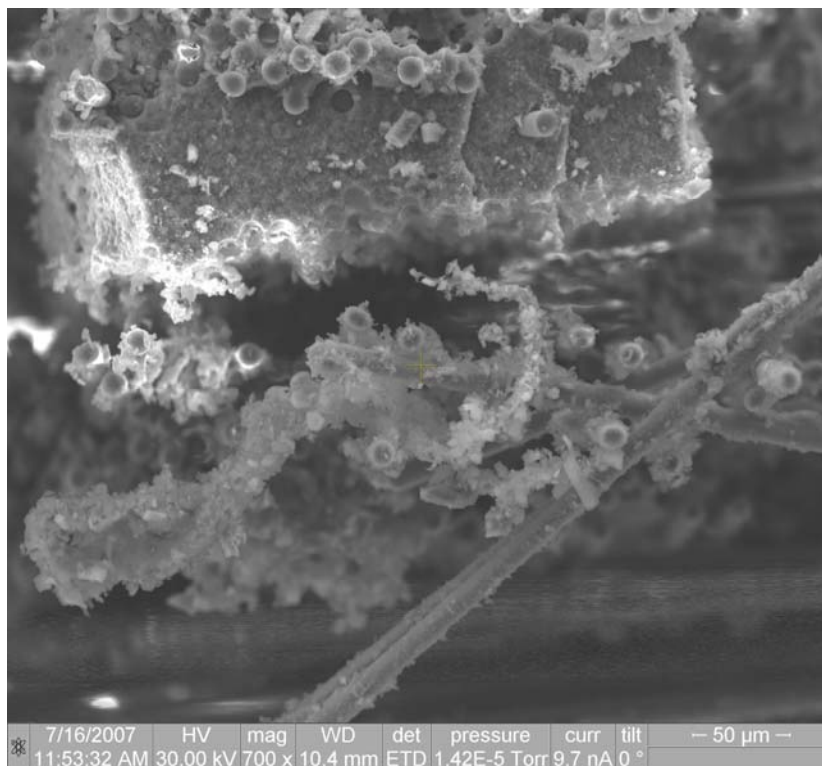

Figure 126. Fracture surface of N720/A specimen tested with cyclic creep-recovery with 1 hour hold times at 125 MPa in air at 1200 °C.

Figure 127. Fracture surface of N720/A specimen tested with cyclic creep-recovery with 1 hour hold times at 125 MPa in air at 1200 °C.
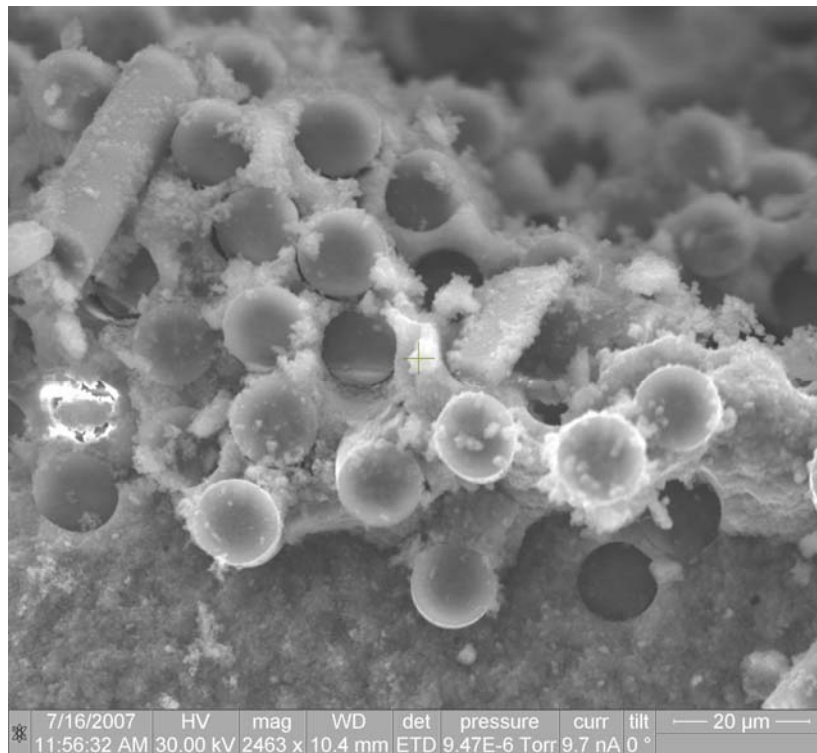
Figure 128. Fracture surface of N720/A specimen tested with cyclic creep-recovery with 1 hour hold times at 125 MPa in air at 1200 °C.
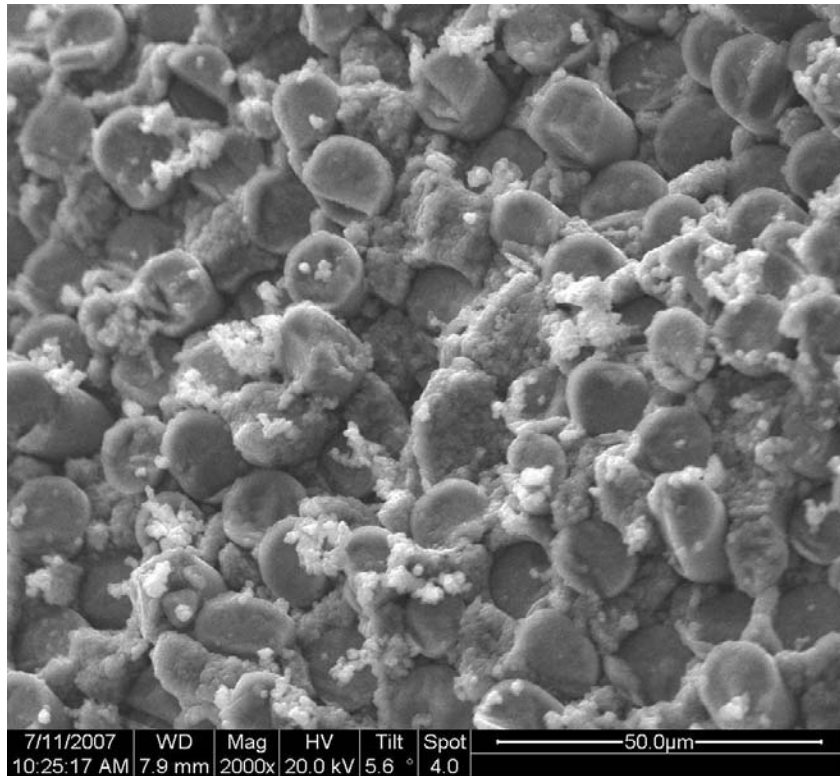
Figure 129. Fracture surface of N720/A specimen tested with cyclic creep-recovery with 1 hour hold times at 125 MPa in air at 1200 °C.


Figure 130. Fracture surface of N720/A specimen tested with cyclic creep-recovery with 1 hour hold times at 125 MPa in air at 1200 °C.
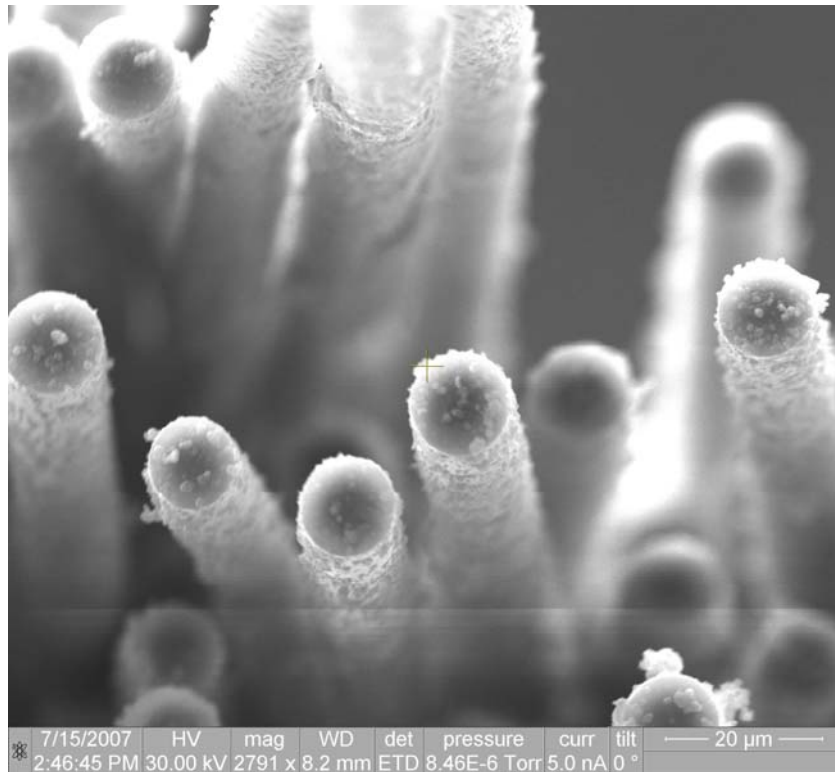
Figure 131. Fracture surface of N720/A specimen tested with cyclic creep-recovery with 1 hour hold times at 125 MPa in air at 1200 °C.
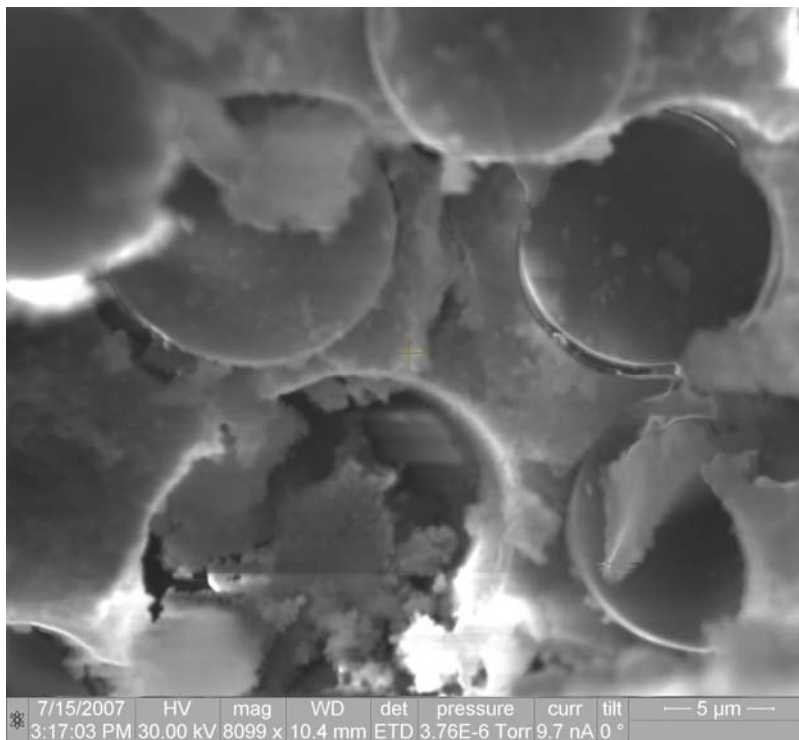
Figure 132. Fracture surface of N720/A specimen tested with cyclic creep-recovery with 1 hour hold times at 125 MPa in air at 1200 °C.
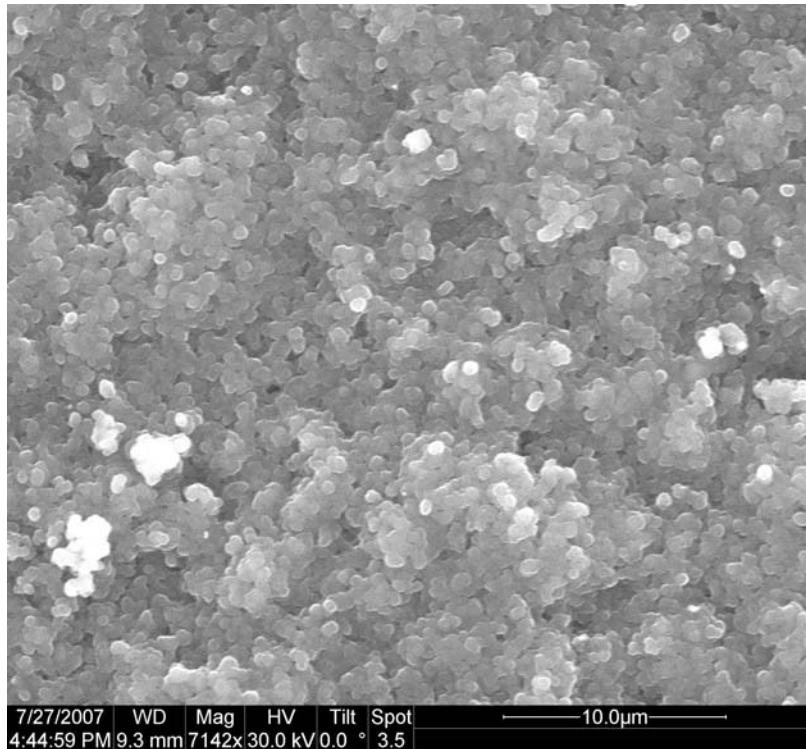
Figure 133. Fracture surface of N720/A specimen tested with cyclic creep-recovery with 1 hour hold times at 100 MPa in steam at 1200 °C.
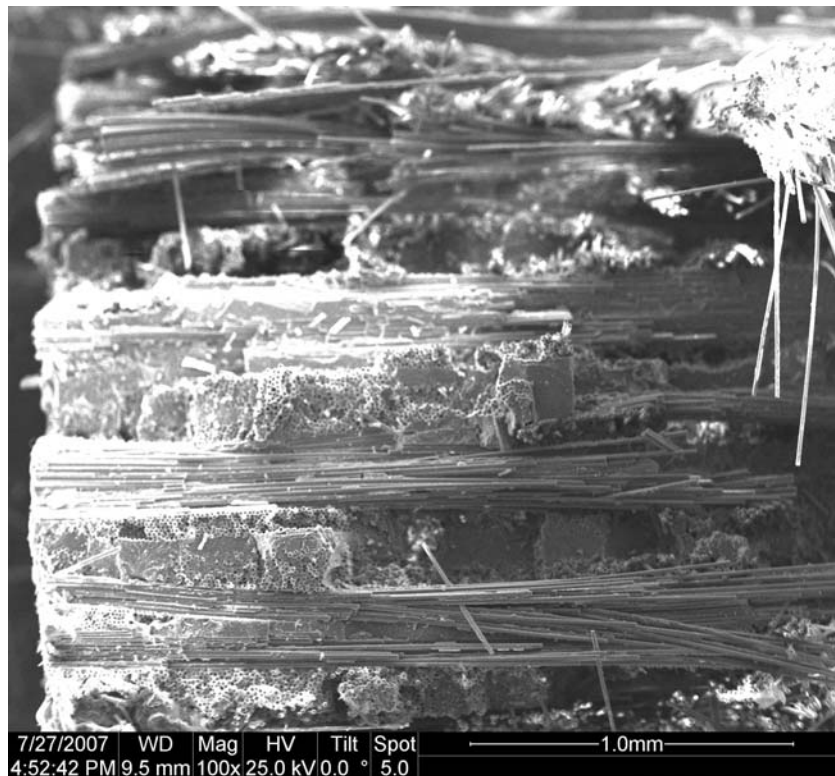
Figure 134. Fracture surface of N720/A specimen tested with cyclic creep-recovery with 1 hour hold times at 100 MPa in steam at 1200 °C.
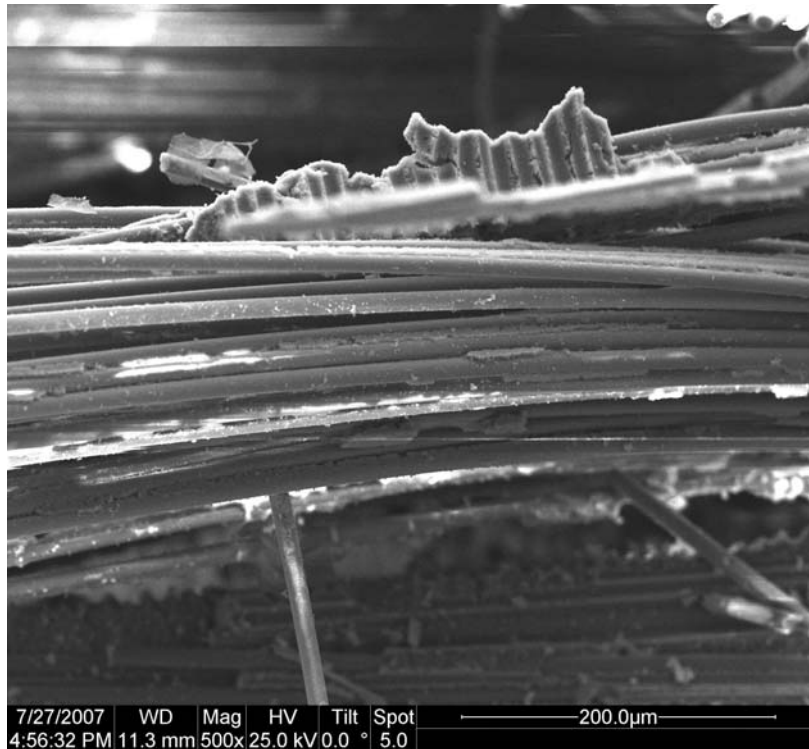
Figure 135. Fracture surface of N720/A specimen tested with cyclic creep-recovery with 1 hour hold times at 100 MPa in steam at 1200 °C.
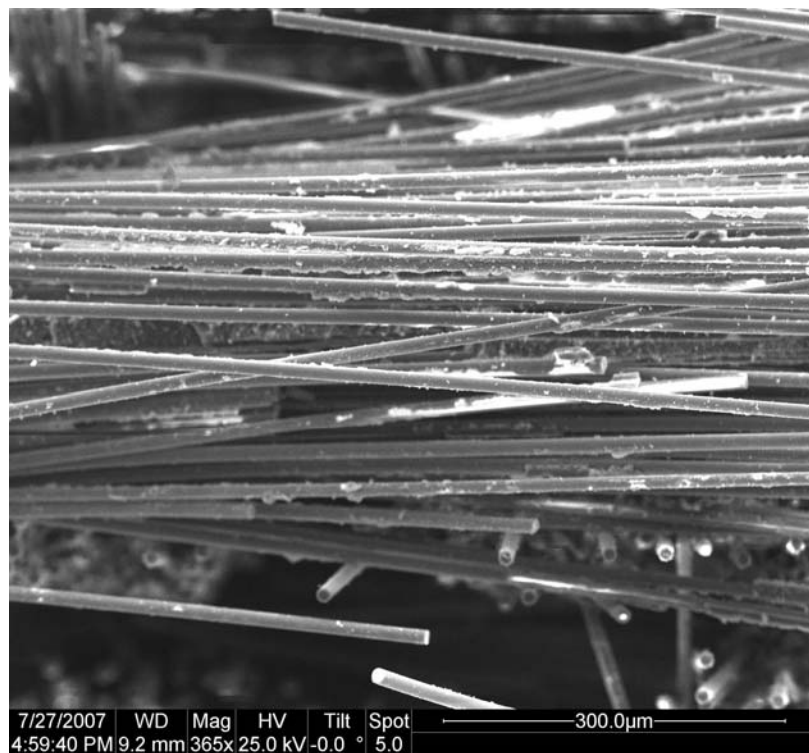
Figure 136. Fracture surface of N720/A specimen tested with cyclic creep-recovery with 1 hour hold times at 100 MPa in steam at 1200 °C.
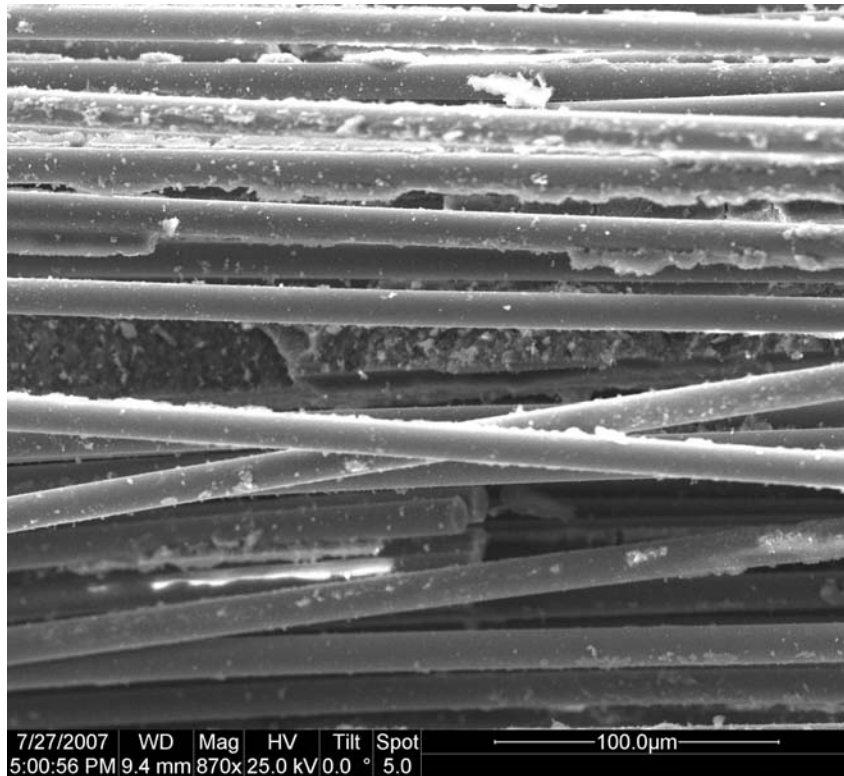
Figure 137. Fracture surface of N720/A specimen tested with cyclic creep-recovery with 1 hour hold times at 100 MPa in steam at 1200 °C.
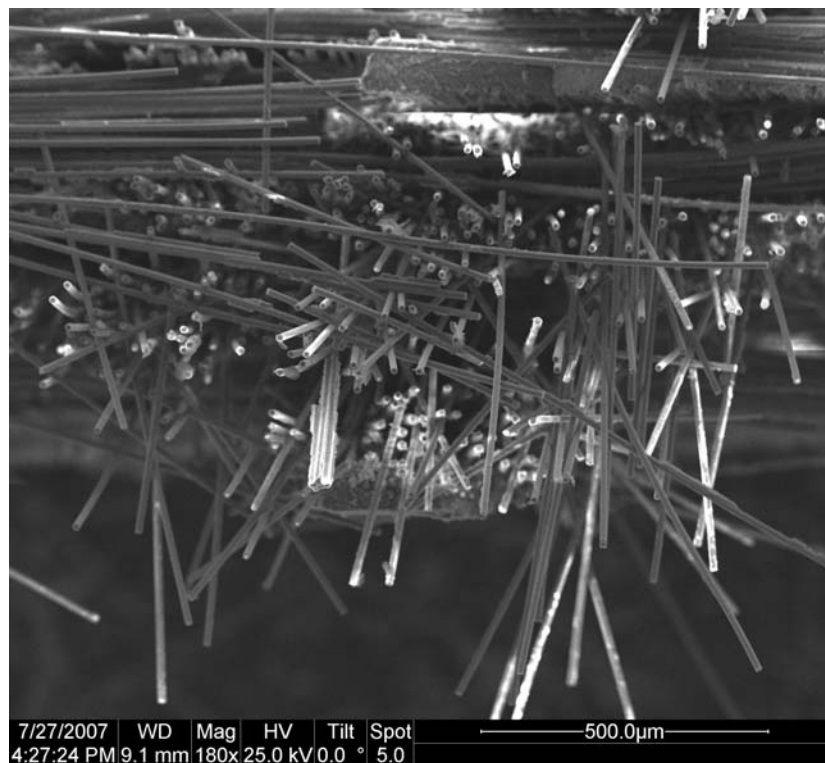

Figure 138. Fracture surface of N720/A specimen tested with cyclic creep-recovery with 1 hour hold times at 100 MPa in steam at 1200 °C.
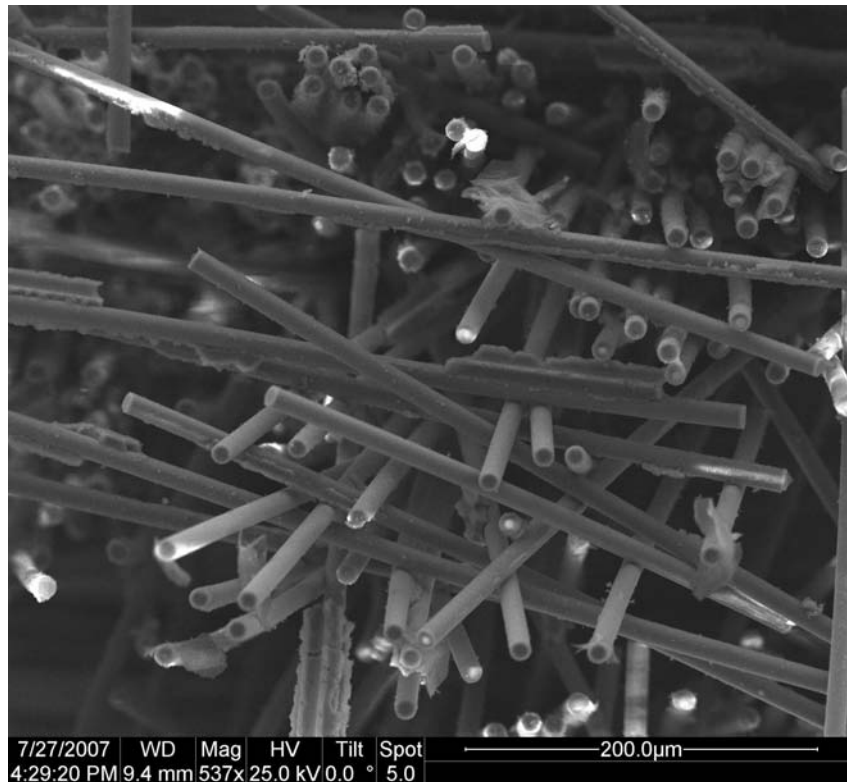
Figure 139. Fracture surface of N720/A specimen tested with cyclic creep-recovery with 1 hour hold times at 100 MPa in steam at 1200 °C.
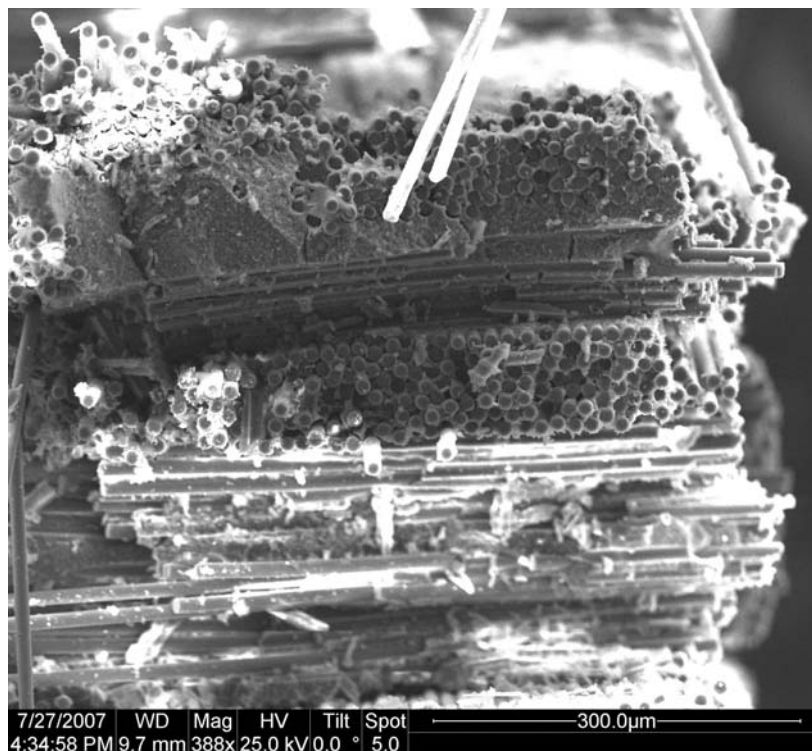

Figure 140. Fracture surface of N720/A specimen tested with cyclic creep-recovery with 1 hour hold times at 100 MPa in steam at 1200 °C.
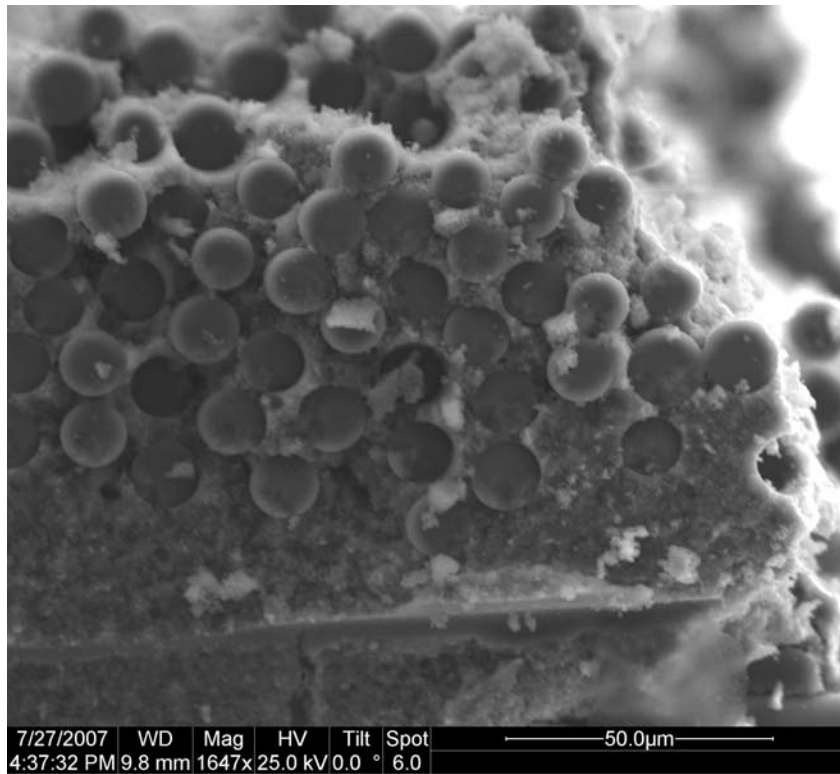
Figure 141 Fracture surface of N720/A specimen tested with cyclic creep-recovery with 1 hour hold times at 100 MPa in steam at 1200 °C.
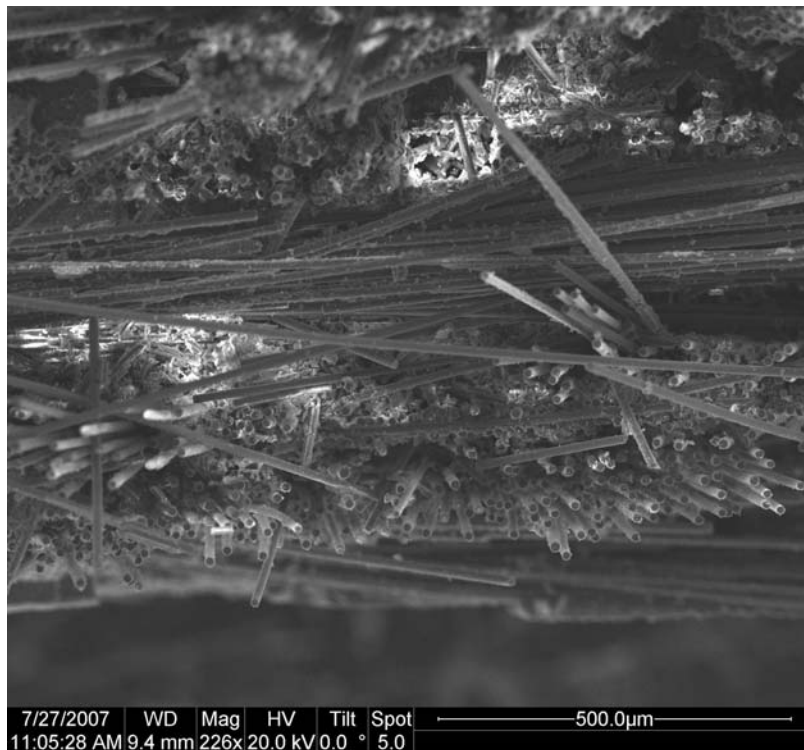
Figure 142. Fracture surface of N720/A specimen tested with cyclic creep-recovery with 1 hour hold times at 100 MPa in steam at 1200 °C, possible kinking.
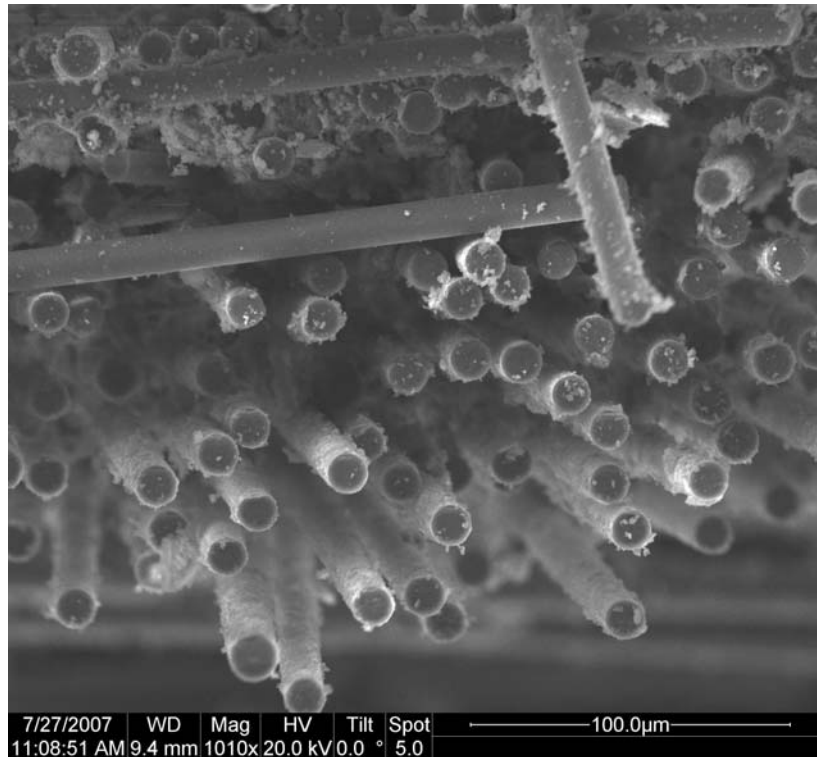
Figure 143. Fracture surface of N720/A specimen tested with cyclic creep-recovery with 1 hour hold times at 100 MPa in steam at 1200 °C, possible kinking.
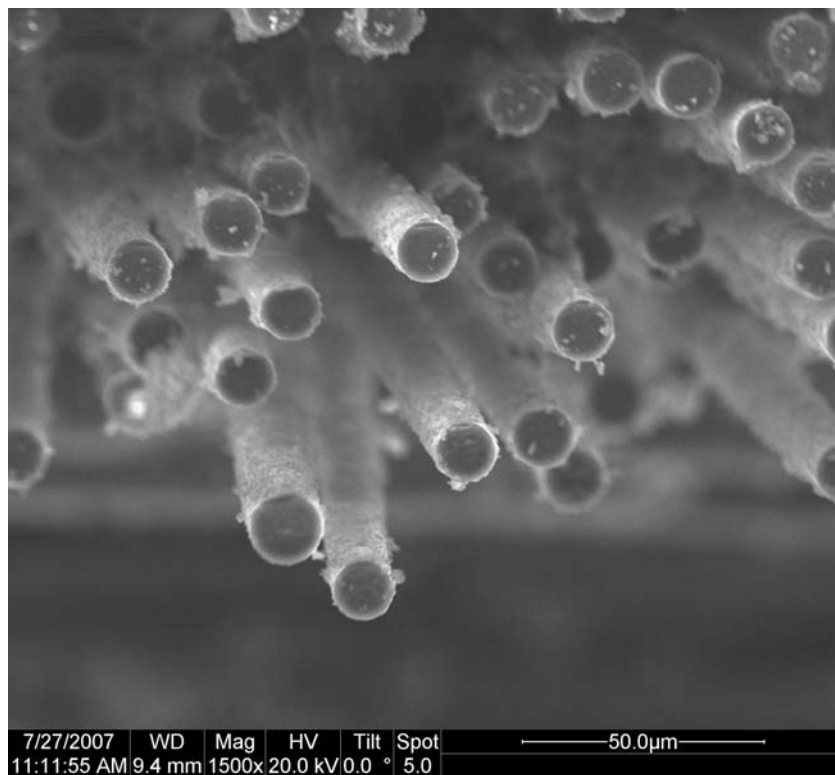
Figure 144. Fracture surface of N720/A specimen tested with cyclic creep-recovery with 1 hour hold times at 100 MPa in steam at 1200 °C, possible kinking.

**Figure 145. Fracture surface of N720/A specimen tested with cyclic creep-recovery with 1 hour hold times at 100 MPa in steam at 1200 °C, possible kinking.**
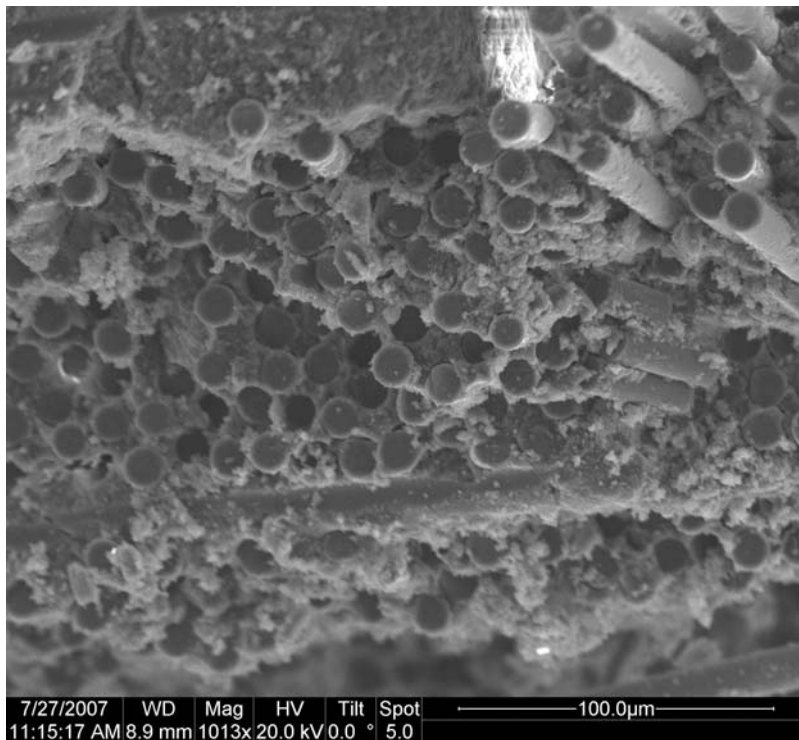
Figure 146. Fracture surface of N720/A specimen tested with cyclic creep-recovery with 1 hour hold times at 100 MPa in steam at 1200 °C, possible kinking.
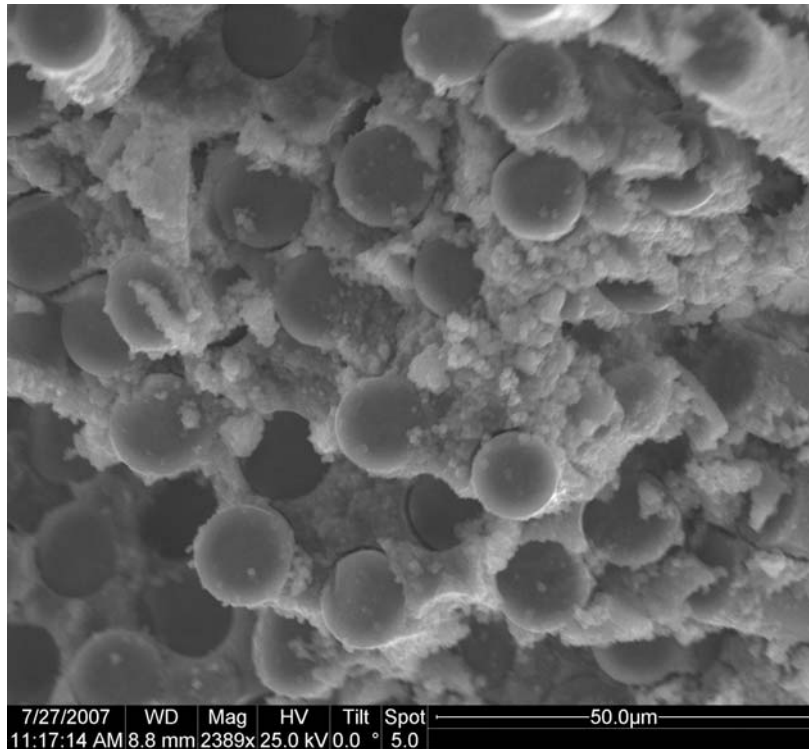
Figure 147. Fracture surface of N720/A specimen tested with cyclic creep-recovery with 1 hour hold times at 100 MPa in steam at 1200 °C, possible kinking.
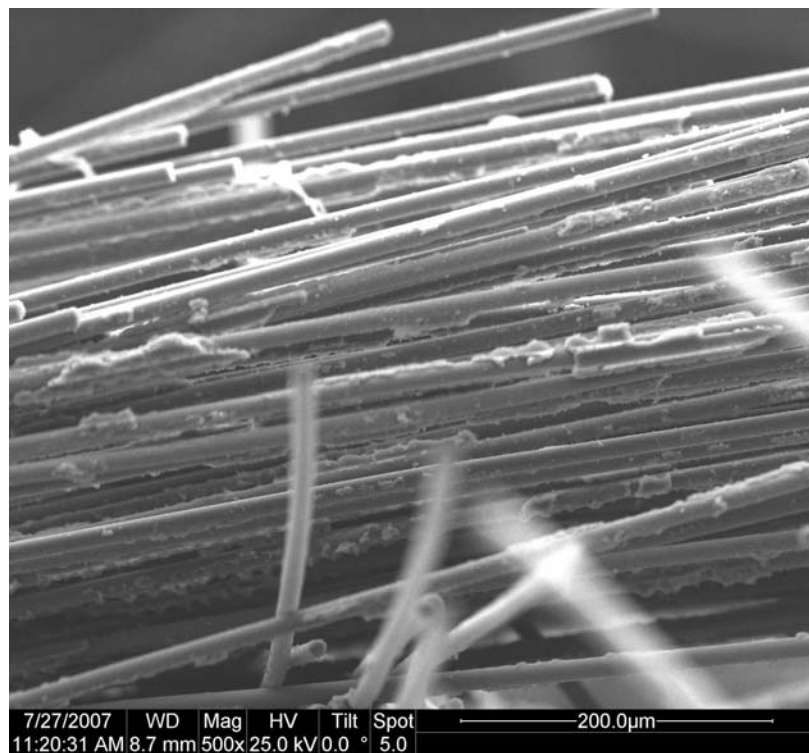
Figure 148. Fracture surface of N720/A specimen tested with cyclic creep-recovery with 1 hour hold times at 100 MPa in steam at 1200 °C, possible kinking.
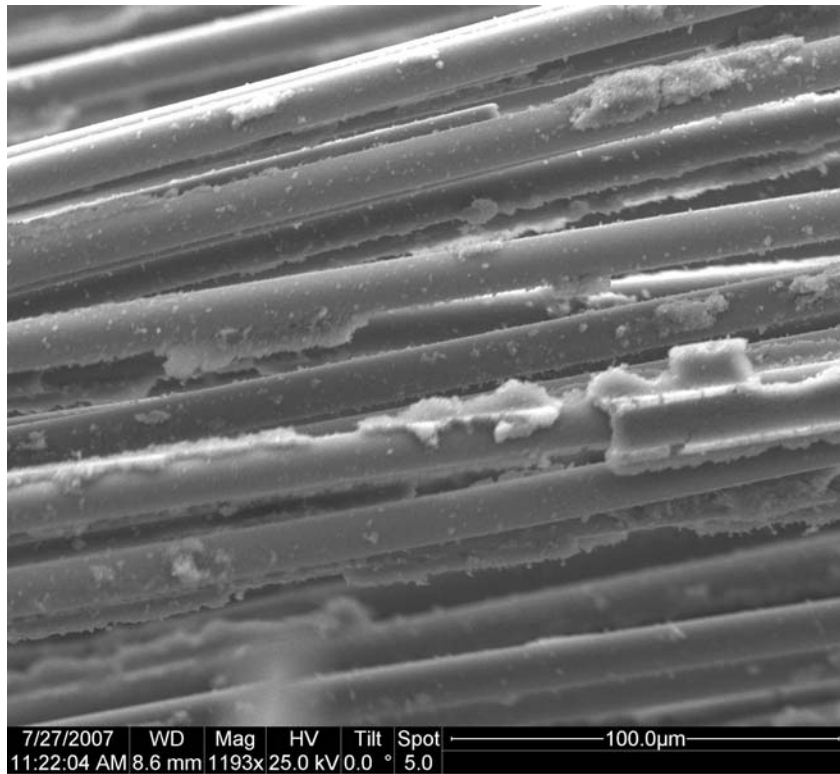
Figure 149. Fracture surface of N720/A specimen tested with cyclic creep-recovery with 1 hour hold times at 100 MPa in steam at 1200 °C, possible kinking.
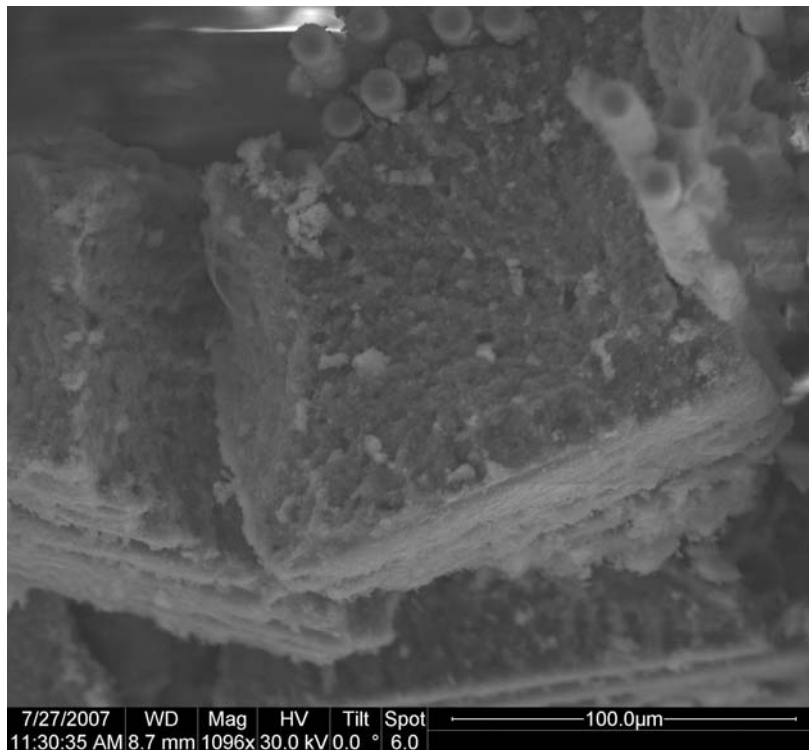
**Figure 150. Fracture surface of N720/A specimen tested with cyclic creep-recovery with 1 hour hold times at 100 MPa in steam at 1200 °C, possible kinking.**

**Figure 151. Fracture surface of N720/A specimen tested with cyclic creep-recovery with 1 hour hold times at 100 MPa in steam at 1200 °C, possible kinking.**
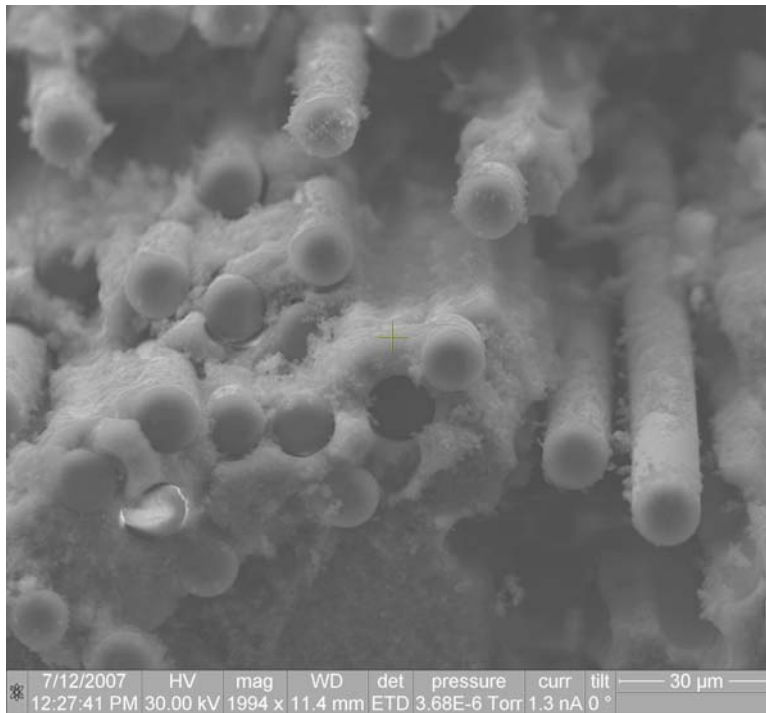
Figure 152. Fracture surface of N720/A specimen tested with cyclic creep-recovery with 1 hour hold times at 100 MPa in steam at 1200 °C, possible kinking.
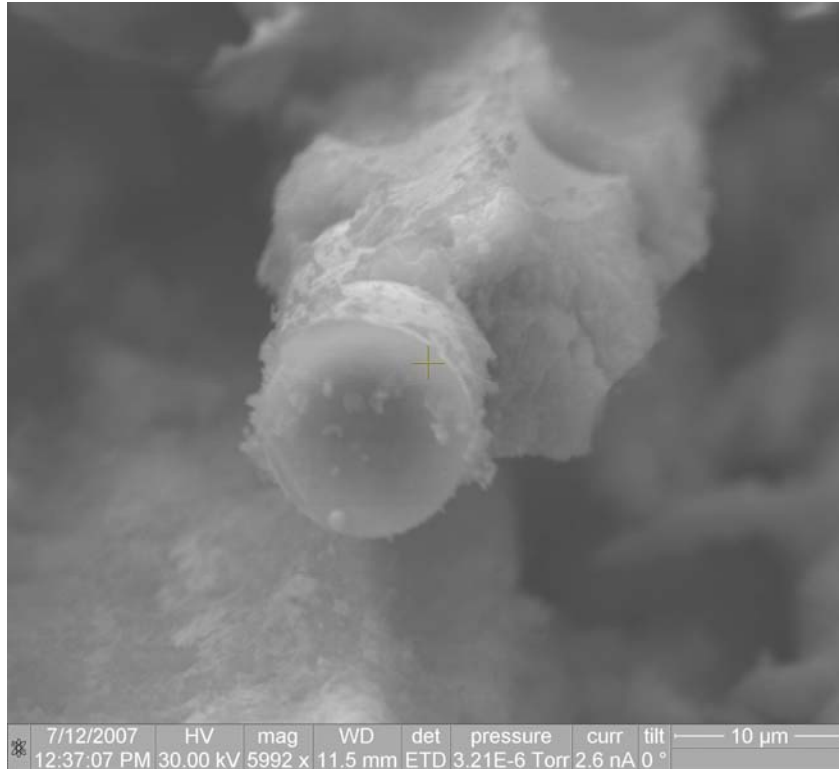
Figure 153. Fracture surface of N720/A specimen tested with cyclic creep-recovery with 1 hour hold times at 100 MPa in steam at 1200 °C, possible kinking.
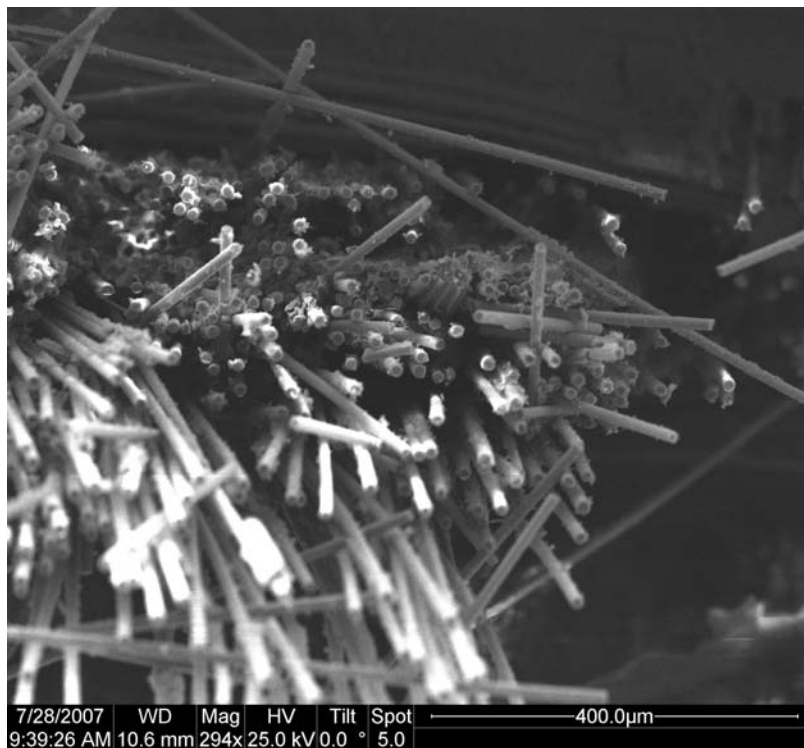

Figure 154. Fracture surface of N720/A specimen tested with cyclic creep-recovery with 0.05 hour hold times at 125 MPa in steam at 1200 °C.
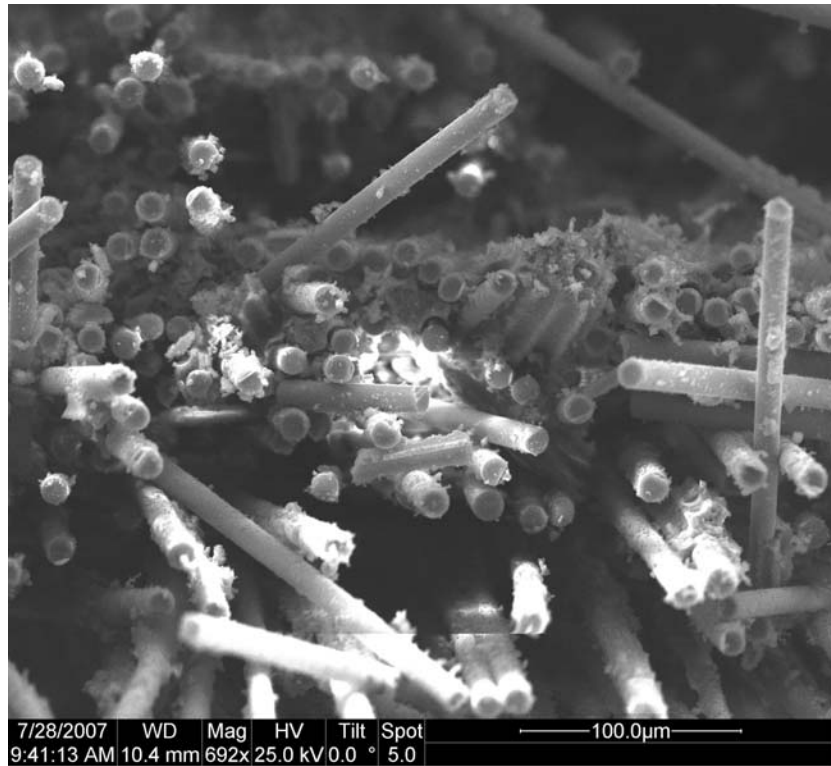
Figure 155. Fracture surface of N720/A specimen tested with cyclic creep-recovery with 0.05 hour hold times at 125 MPa in steam at 1200 °C.
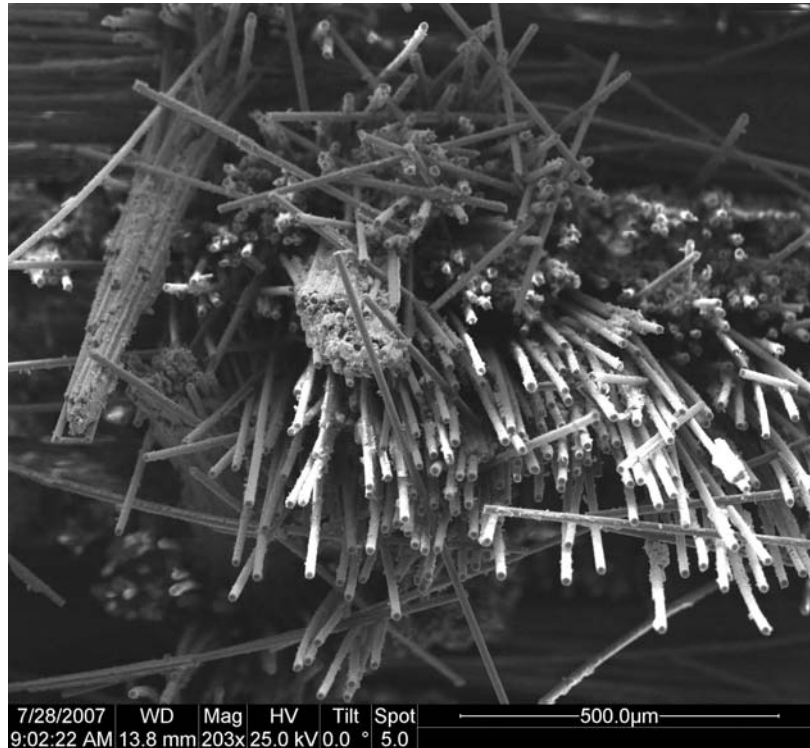

Figure 156. Fracture surface of N720/A specimen tested with cyclic creep-recovery with 0.05 hour hold times at 125 MPa in steam at 1200 °C.
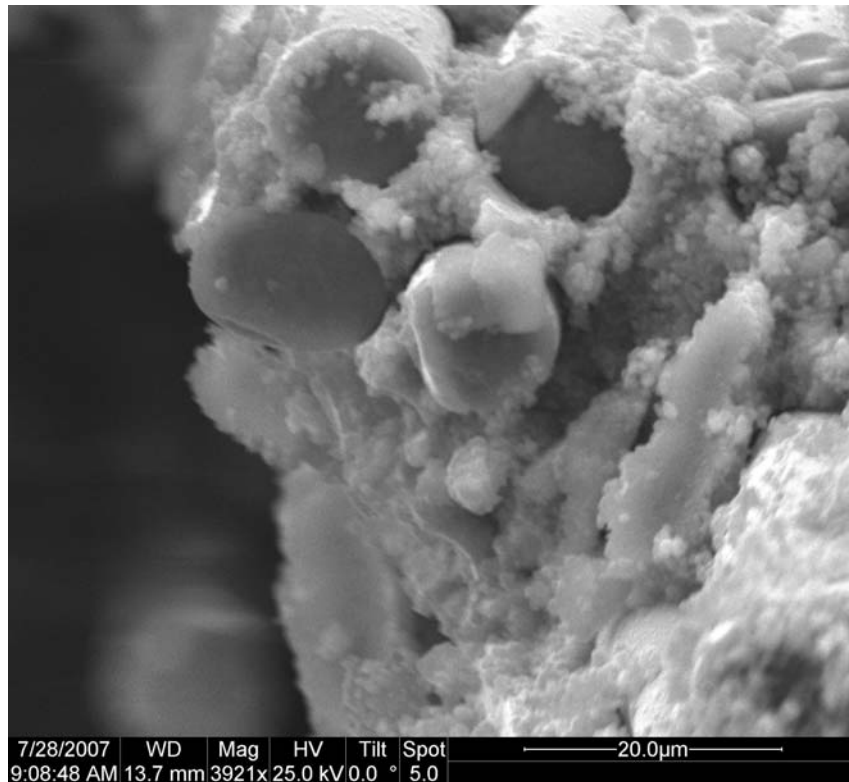
Figure 157. Fracture surface of N720/A specimen tested with cyclic creep-recovery with 0.05 hour hold times at 125 MPa in steam at 1200 °C.

Figure 158. Fracture surface of N720/A specimen tested with cyclic creep-recovery with 0.05 hour hold times at 125 MPa in steam at 1200 °C.
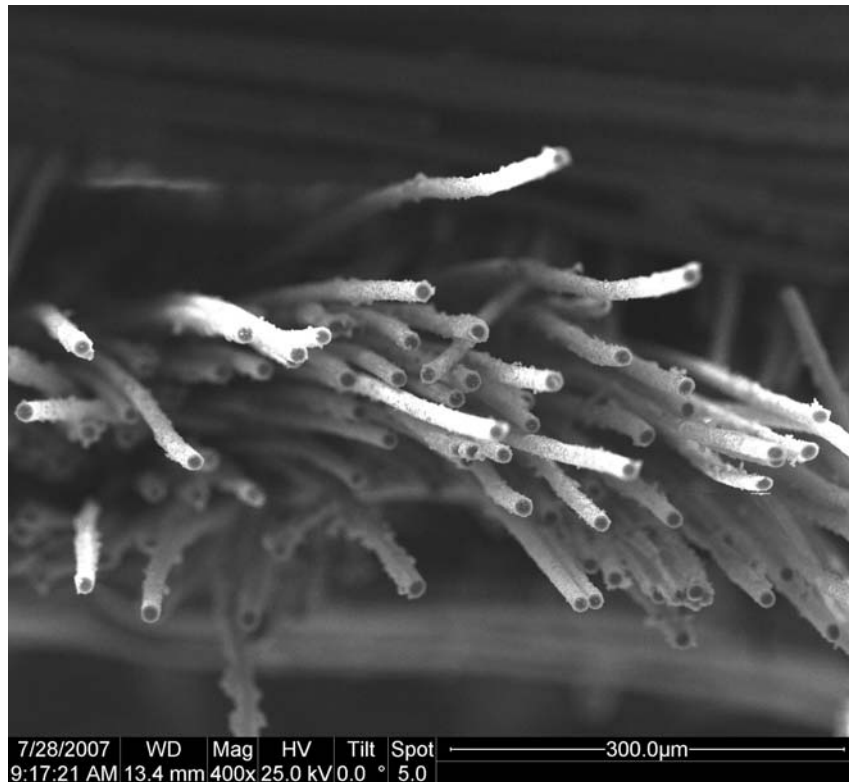
Figure 159. Fracture surface of N720/A specimen tested with cyclic creep-recovery with 0.05 hour hold times at 125 MPa in steam at 1200 °C.
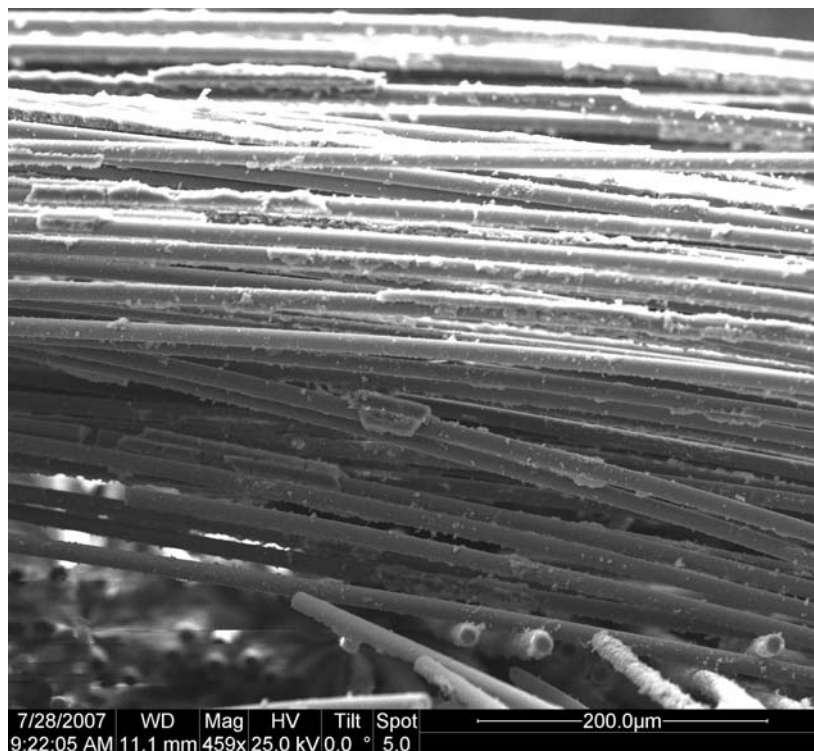

Figure 160. Fracture surface of N720/A specimen tested with cyclic creep-recovery with 0.05 hour hold times at 125 MPa in steam at 1200 °C.
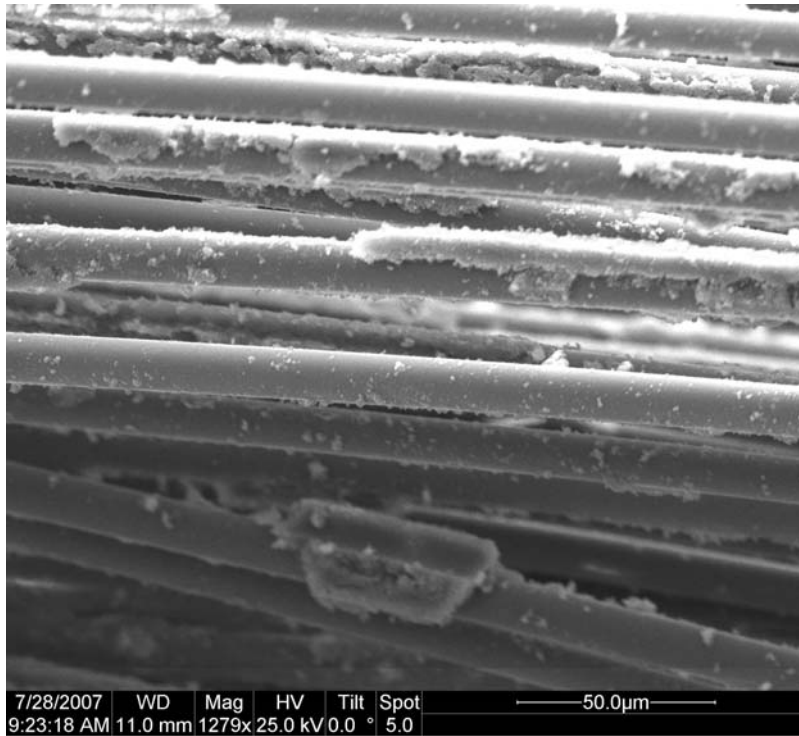
Figure 161. Fracture surface of N720/A specimen tested with cyclic creep-recovery with 0.05 hour hold times at 125 MPa in steam at 1200 °C.
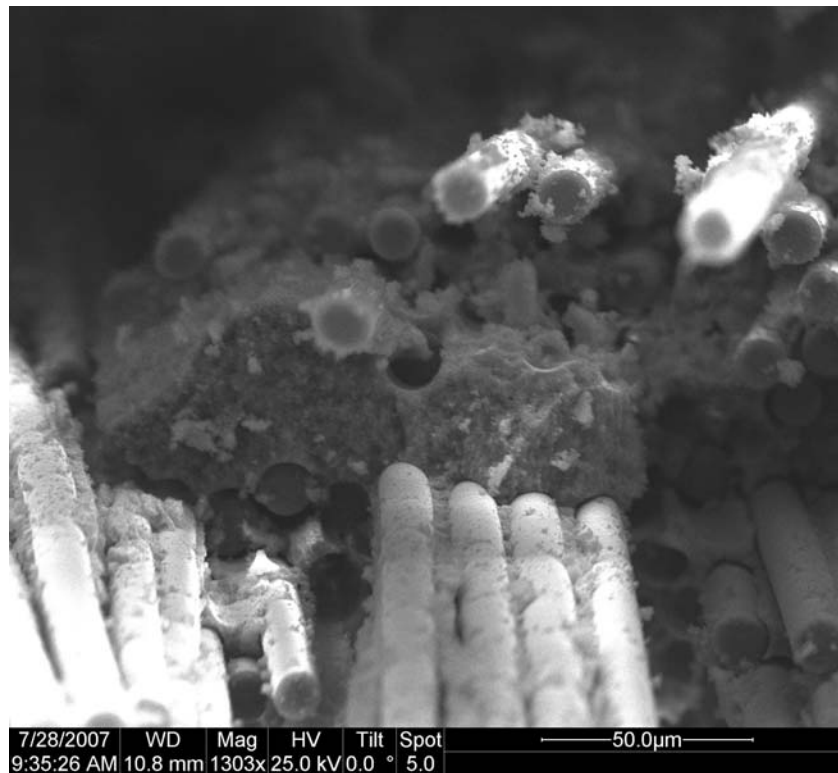
Figure 162. Fracture surface of N720/A specimen tested with cyclic creep-recovery with 0.05 hour hold times at 125 MPa in steam at 1200 °C.
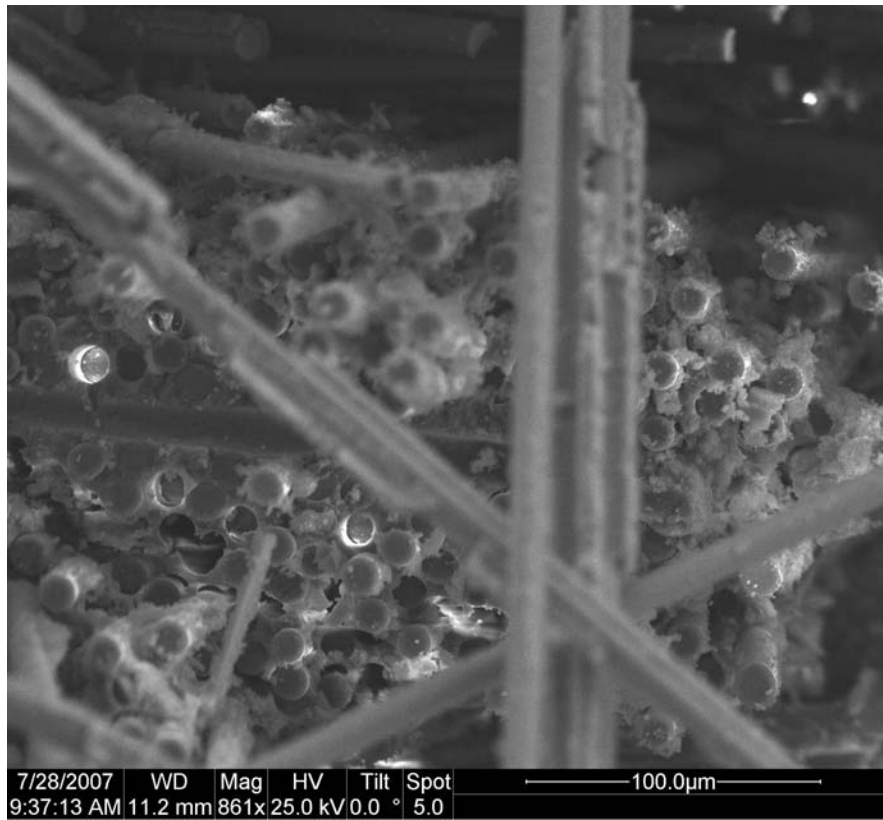
Figure 163. Fracture surface of N720/A specimen tested with cyclic creep-recovery with 0.05 hour hold times at 125 MPa in steam at 1200 °C.

Bibliography

1. "F-22 Raptor Materials and Processes." Globalsecurity.Org. http://www.globalsecurity.org/military/systems/aircraft/f-22-mp.htm. 19 Dec. 2005.

2. The Boeing Company, (Feb 2006), http://www.boeing.com.

3. Bolick, Ronnie L., Kelkar, Ajit D. and Taylor, Jeremy A. "Performance Evaluation of Unstitched, Stitched and Z-Pinned Textile Composites Under Static Loading," *Proceeding of International Mechanical Engineering Congress and Exposition,* 2005-81053: 1-5 (2005).

4. Baker, A., Dutton, S., Kelly, D. *Composite Materials for Aircraft Structures* (Second Edition). Virginia: AIAA, 2004.

5. Braun, Jason C. *Effects of Temperature and Envirnoment on Creep Behavior of an Oxide-Oxide Ceramic Matris Composite.* MS thesis, AFIT/GAE/ENY/07-M04. School of Engineering and Management, Air Force Institute of Technology (AU), Wright-Patterson AFB OH, March 2007.

6. Chawla, K. K. *Ceramic Matrix Composites* (Second Edition). Boston: Kluwer Academic Publishers, 2003.

7. COI Ceramics, Unpublished Data.

8. Daniel, Isaac M. and Ori Ishai. *Engineering Mechanics of Composite Materials*. New York, NY: Oxford University Press, 1994.

9. Davis, J. B., Marshall, D.B., and Morgan, P.E.D. "Oxide Composites of Al_2O_3 and $LaPO_4$," *Journal of the European Ceramic Society,* 19:2421-2426 (1999).

10. Fritsch, M., Klemm, H., Herrmann, M. and Schenk, B. "Corrosion of selected ceramic materials in hot gas environment," *Journal of the European Ceramic Society,* 26:3357-3656 (2006).

11. Jackson, Patrick R. *Characterization of compressive Creep Behavior of Oxide/Oxide Composite with Monazite Coating at Elevated Temperature.* MS thesis, AFIT/GA/ENY/06-M17. School of Engineering and Management, Air Force Institute of Technology (AU), Wright-Patterson AFB OH, March 2006.

12. Jackson, P.R., Ruggles-Wrenn M.B., Baek, S.S., and Keller, K.A. "Compressive creep behavior of an oxide-oxide ceramic composite with monazite fiber coating at elevated temperatures," *Materials Science and Engineering,* A 454: 590-601 (2007).

13. Jacobson, N.S. "Corrosion of Silicon-Based Ceramics in Combustion Environments," *Journal of the American Ceramic Society*, 76[1]:3-28 (1993).

14. Harlan, Lee B. *Creep-Rupture Behavior of an Oxide/Oxide Ceramic Matrix Composite at Elevated Temperatures in Air and Steam Environments.* MS thesis, AFIT/GA/ENY/05-M05. School of Engineering and Management, Air Force Institute of Technology (AU), Wright-Patterson AFB OH, March 2005.

15. Haslam, J.J., Berroth, K.E., and Lange, F.F. "Processing and Properties of an all oxide composite with a porous matrix," *Journal of the European Ceramic Society*, 20:607-618 (2000).

16. Hetrick, Griffin. *Effects of Frequency and Environment on Fatigue Behavior on an Oxide-Oxide Ceramic Matrix Composite at 1200° C.* MS thesis, AFIT/GAE/ENY/06-J05. School of Engineering and Management, Air Force Institute of Technology (AU), Wright-Patterson AFB OH, January 2006.

17. Holmes, John W., Park, Yong H., and Jones, J. W. "Tensile creep and creep-recovery behavior of SiC-fiber-Si_3N_4-matrix composite," *Journal of American Ceramic Society,* 76:1281-1293 (1993).

18. Kaya, C., Butler, E.G., Selcuk, A., Boccaccini, A.R., and Lewis, M.H. "Mullite (Nextel™ 720) fibre-reinforced mullite matrix composites exhibiting favourable thermomechanical properties," *Journal of the European Ceramic Society,* 22: 2333-2342 (2002).

19. Kelkar, A.D, and Tate, J.S. and Bolick, R. "Structural integrity of aerospace textile composite under fatigue loading," *Materials Science and Engineering,* B 132:79-84 (2006).

20. Kerans, R.J. and Parthasarathy, T.A. "Crack deflection in ceramic composites and fiber coating design criteria," *Composites: Part A,* 30:521-524 (1999).

21. Korinek, Sylvie L. and Castaing, Jacques. "Slip and twinning in polycrystalline alumina (Al_2O_3) deformed under hydrostatic pressure between 600° and 1000° C," *Journal of American Ceramic Society,* 86:566-573 (2003).

22. Kronenberg, A. K., Castaing, J., Mitchell, T.E. and Kirby, S.H. "Hydrogen defects in Al_2OH_3 and water weakening of sapphire and alumina ceramics between 600 and 1000°C-I. infarared characterization of defects," *Acta Materialia,* 48:1481-1494 (2000).

23. Lange, F.F., Tu, W.C., Evans, A.G. "Processing of damage-tolerant, oxidation resistant ceramic matrix composites by a precursor infiltration and pyrolysis method," *Materials Science and Engineering*, A195:145-150 (1995).

24. Levi, Carlos G., James Y. Yang, Brian J. Dalgleish, Frank W. Zok, and Anthony G. Evans. "Processing and Performance of an All-Oxide Ceramic Composite," *Journal of the American Ceramic Society*, 81[8]: 2077-86 (1998).

25. Mehrman, J.M. *Effect of Hold Times on Fatigue Behavior of Nextel™ 720/Alumina Ceramic Matrix Composite at 1200 °C in Air and in Steam Environment.* MS thesis, AFIT/GA/ENY/06-M23. School of Engineering and Management, Air Force Institute of Technology (AU), Wright-Patterson AFB, OH March 2006.

26. Mehrman, J.M., Ruggles-Wrenn, M.B., and Baek, S.S. "Influence of Hold Times on the Elevated-Temperature Fatigue Behavior of an Oxide-Oxide Ceramic Composite in Air and in Steam Environment", *Composites Science and Technology,* in press (2006).

27. *Minnesota Mining and Manufacturing Company (3M™).* "Nextel™ Ceramic Textiles Technical Notebook," Company produced technical notebook. No date

28. Morscher, Gregory N. "Modeling the stress strain behavior of woven ceramic matrix composites," *107th Annual American Ceramic Society Conference,* (2005).

29. Musil, Sean S. *Characterization of Creep Behavior of Oxide/Oxide Composite with Monazite Coating at Elevated Temperature.* MS thesis, AFIT/GAE/ENY/05-M14. School of Engineering and Management, Air Force Institute of Technology (AU), Wright-Patterson AFB OH, March 2005.

30. Ohnabe, H., Masaki, S., Onozuka, M., Miyahara, K., Sasa, T. "Potential application of ceramic matrix composites to aero-engine components," *Composites: Part A*, *Applied Science and Manufacturing* 30: 489-496 (1999).

31. Parlier, M. and Ritti, M.H. "State of the art and perspectives for oxide/oxide composites," *Aerospace Science and Technology*, 7: 211-221 (2003).

32. Ruggles-Wrenn, M. B., Hetrick, B., and Baek, S.S. "Effects of frequency and environment on fatigue behavior of an oxide-oxide ceramic composite at 1200° C," *International Journal of Fatigue,* (in press).

33. Ruggles-Wrenn, M.B., Mall, S., Eber, C.A., and Harlan, L.B. "Effects of Steam Environment on High-Temperature Mechanical Behavior of NextelTM720/Alumina (N720/A) Continuous Fiber Ceramic Composite**,** *Composites: Part A*, 37: 2029-2040 (2006).

34. Schmidt, S., Beyer, S., Knabe, H., Immich, H., Mestring, R., and Gessler, A. "Advanced ceramic matrix composite materials for current and future propulsion technology applications," *Acta Astronautica,* 55: 409-420 (2004).

35. Tu, W.C., Lange, F.F., Evans, A.G. "Concept for a Damage-Tolerant Ceramic Composite with Strong Interfaces," *Journal of the American Ceramic Society*, 79[2]: 417-424 (1996).

36. Wannaparhum, S., Seal, S., Desai, V. "Surface chemistry of Nextel-720, alumina and Nextel-720/alumina ceramic matrix composite (CMC) using XPS-A tool for nano-spectroscopy," *Applied Surface Science*, 185:183-196 (2002).

37. Wilson, D.M. and Visser, L.R. "High Performance Oxide Fibers for Metal and Ceramic Composites," *Composites: Part A*, 32[8]: 1143-1153 (2001).

38. Wilson, D.M., Lieder, S.L., and D.C. Luenegurg, "Microstructure and high temperature properties of Nextel 720 fibers," *Ceramic Engineering and Science Proceedings,* 16[5]: 1005–1014 (1995).

39. Wu, Xin, and Holmes John W. "Tensile creep and creep-strain recocvery behavior of silicon carbide fiber/calcium aluminosilicate matrix ceramic composites," *Journal of American Ceramic Society,* 76[10]:2695-2700 (1993).

40. Zawada, L.P. "Longitudinal and transthickness tensile behavior of several oxide/oxide composites," *Ceramic Science and Engineering Proceedings,* 19[3]: 327-340 (1998).

41. Zawada, L.P. and Staehler, J., Steel, S.G. "Consequence of Intermittent Exposure to Moisture and Salt Fog on the High-Temperature Fatigue Durability of Several Ceramic-Matrix Composites," *Journal of the American Ceramic Society*, 86 [8]: 1282-1291 (2003).

42. Zok, W. and Carlos G. Levi. "Mechanical Properties of Porous-Matrix Ceramic Composites," *Advanced Engineering Materials*, 3[1-2]: 15-23 (2001).

REPORT DOCUMENTATION PAGE

1. REPORT DATE *(DD-MM-YYYY)* 30-08-2007	2. REPORT TYPE **Master's Thesis**	3. DATES COVERED *(From – To)* Oct 2006 – Sept 2007

4. TITLE AND SUBTITLE	5a. CONTRACT NUMBER
Cyclic Creep and Recovery Behavior of Nextel[TM] 720/Alumina Ceramic Matrix Composite at 1200 °C in Air and in Steam Environments	5b. GRANT NUMBER
	5c. PROGRAM ELEMENT NUMBER

6. AUTHOR(S)	5d. PROJECT NUMBER 2006-097
Whiting, Bridgett A., 2nd Lieutenant, USAF	5e. TASK NUMBER
	5f. WORK UNIT NUMBER

7. PERFORMING ORGANIZATION NAMES(S) AND ADDRESS(S) Air Force Institute of Technology Graduate School of Engineering and Management (AFIT/EN) 2950 Hobson Way WPAFB OH 45433-7765	8. PERFORMING ORGANIZATION REPORT NUMBER AFIT/GAE/ENY/07-S05

9. SPONSORING/MONITORING AGENCY NAME(S) AND ADDRESS(ES) AFRL/PRTS Attn: Dr. Ruth Sikorski and Dr. Charles Cross 1950 5th Street WPAFB OH 45433-7251 DSN: 785-7268	10. SPONSOR/MONITOR'S ACRONYM(S)
	11. SPONSOR/MONITOR'S REPORT NUMBER(S)

12. DISTRIBUTION/AVAILABILITY STATEMENT
APPROVED FOR PUBLIC RELEASE; DISTRIBUTION UNLIMITED.

13. SUPPLEMENTARY NOTES

14. ABSTRACT

The cyclic creep and recovery behaviors of the $N720/Al_2O_3$ composite were investigated in this research. The ceramic matrix composite (CMC) contains a porous alumina matrix with laminated, woven mullite/alumina (Nextel[TM] 720) fibers. The composite does not have an interface between the fiber and matrix. The CMC relies on the porous nature for flaw tolerance. The objective of this study the influences of monotonic creep and cyclic creep loading histories on the creep lifetime, creep strain rate, accumulated creep strain as well as on the recovery of creep strain at near zero stress. The cyclic creep and recovery tests were performed at 1200 °C with maximum creep stress levels of 100 and 125 MPa in air and in steam. The creep and recovery periods were ranged from 3 min to 30 h. The laboratory air tests significantly exceeded the life of the monotonic creep tests. Introduction of intermittent periods of unloading and recovery at near zero stress into the monotonic creep history resulted in one to two orders of magnitude improvement in the creep life and rate. The presence of steam greatly reduced the performance of the material. The results in steam were similar to those of the monotonic creep. The composite microstructure, damage and failure mechanisms were also explored.

15. SUBJECT TERMS
Ceramic Matrix Composites, Composites, Scanning Electron Microscope, Microscopy, Cyclic Creep Recovery

16. SECURITY CLASSIFICATION OF:			17. LIMITATION OF ABSTRACT	18. NUMBER OF PAGES	19a. NAME OF RESPONSIBLE PERSON Marina B. Ruggles-Wrenn, AD-23, AFIT/ENY
REPORT U	ABSTRACT U	c. THIS PAGE U	UU	164	19b. TELEPHONE NUMBER *(Include area code)* (937) 255-3636, ext 4641; e-mail: Marina.Ruggles-Wrenn@afit.edu